

P-117

NASA CONTRACTOR REPORT 166582

Propfan Experimental Data Analysis

David F. Vernon
Gregory S. Page
H. Robert Welge

IN-05
DATE OVERRIDE
97696

(NASA-CR-166582) PROFFAN EXPERIMENTAL DATA
ANALYSIS (McDonnell-Douglas Corp.) 117 p
Avail: NTIS HC A06/MF A01 CSCL 01C

N87-28545

Unclas
G3/05 0097696

Date for general release JUNE 1987

CONTRACT NAS2-11672
August 1984



DATE OF GENERAL RELEASE JUNE 1987

NASA CONTRACTOR REPORT 166582

Propfan Experimental Data Analysis

David F. Vernon
Gregory S. Page
H. Robert Welge

McDonnell Douglas Corporation
Douglas Aircraft Company
Long Beach, California 90846

Prepared for
Ames Research Center
Under Contract NAS2-11672



National Aeronautics and
Space Administration

Ames Research Center
Moffett Field, California 94035

Date for general release June 1987

TABLE OF CONTENTS

| SECTION | PAGE |
|--|------|
| TABLE OF CONTENTS | i |
| NOMENCLATURE | iii |
| 1.0 SUMMARY | 1 |
| 2.0 INTRODUCTION | 2 |
| 3.0 TASK I. THRUST/DRAG BOOKKEEPING | 4 |
| 3.1 Thrust/Drag Bookkeeping Methods | 4 |
| 3.1.1 Current NASA Installed Performance Method | 4 |
| 3.1.2 DAC Isolated Performance Method | 6 |
| 3.2 Thrust/Drag Bookkeeping Method Comparison | 8 |
| 3.3 Results | 8 |
| 4.0 TASK II. DATA ANALYSIS, UNDERWING NACELLE | 10 |
| 4.1 Analysis of Straight Underwing Nacelle Data | 10 |
| 4.2 Comparison With Theory - Straight Underwing Nacelle | 12 |
| 5.0 TASK III. DATA ANALYSIS AND DESIGN, OVERWING NACELLE | 15 |
| 5.1 Analysis of Contoured Overwing Nacelle Data | 15 |
| 5.2 Comparison With Theory - Contoured Overwing Nacelle | 16 |
| 5.3 Design Modifications for Contoured Overwing Nacelle | 16 |
| 5.4 New Wing Design | 17 |
| 6.0 CONCLUSIONS | 19 |
| 7.0 TABLES | 20 |
| Table 1 Up-Outboard Propfan Rotation Wing Airfoil Geometry | 21 |
| Table 2 Up-Outboard Propfan Rotation Overwing Contoured Nacelle Geometry | 30 |

| | | PAGE | |
|------|------------|---|----|
| 8.0 | APPENDICES | 38 | |
| | Appendix A | Experimental SR-2C Isolated Propeller Performance Obtained at NASA Lewis | 39 |
| | Appendix B | Parasite Drag Summary | 44 |
| | Appendix C | Drag Polars | 46 |
| 9.0 | REFERENCES | 54 | |
| 10.0 | FIGURES | 55 | |

NOMENCLATURE

| | |
|---------------|--|
| A_E | cross sectional exhaust nozzle area |
| AR | aspect ratio |
| $C_{D_{BAL}}$ | balance drag coefficient |
| $C_{D_{EFF}}$ | thrust removed drag coefficient |
| C_L | lift coefficient |
| $C_{L_{EFF}}$ | thrust removed lift coefficient |
| C_{mac} | mean aerodynamic chord |
| C_P | power coefficient |
| c_p | pressure coefficient |
| $C_{T_{AP}}$ | apparent thrust coefficient |
| $C_{T_{AVG}}$ | jet thrust calibration factor |
| $C_{T_{JET}}$ | exhaust nozzle thrust coefficient |
| $C_{T_{NET}}$ | net propeller thrust coefficient |
| D | propeller diameter |
| DAC | Douglas Aircraft Company |
| DEL CXN | nacelle buoyancy coefficient |
| EPR | exhaust pressure ratio (P_{TE}/P_{SE}) |
| ETA | percent wing semispan |
| F | exhaust nozzle thrust |
| FRP | fuselage reference plane |
| J | propeller advance ratio (V/nD) |
| LEX | wing leading edge extension |
| M_L | local normal Mach number based on wing quarter chord sweep |

NOMENCLATURE

(continued)

| | |
|-----------------|---|
| M_0, M | freestream Mach number |
| NASA | National Aeronautics and Space Administration |
| NPR | nozzle pressure ratio (P_{TE}/P_{AMB}) |
| n | propeller speed (rev/sec) |
| P | turbine shaft power |
| P_{AMB} | ambient static pressure |
| P_{SE} | exhaust nozzle exit static pressure |
| P_{TE} | exhaust nozzle total pressure |
| PTR | propeller test rig |
| q_∞ | freestream dynamic pressure ($1/2 \rho V_\infty^2$) |
| R_{ec} | Reynold's number based on C_{mac} |
| RPM | revolutions per minute |
| S_{REF} | reference area |
| T | transition location |
| TIDEAL | ideal jet thrust |
| TJET1 | actual jet thrust |
| V_∞ | tunnel freestream velocity |
| V_{EFF} | effective velocity seen by propeller |
| x/c | fraction of local chord |
| α | angle of attack (deg) |
| β | propeller blade pitch angle |
| η | propeller efficiency |
| ρ_∞ | freestream density |
| $\Lambda_{C/4}$ | wing quarter chord sweep |

1.0 SUMMARY

The National Aeronautics and Space Administration (NASA) and Douglas Aircraft Company (DAC) have been working for several years to develop the installation aerodynamics technology for wing mounted turboprop propulsion system installations to the level required to assess the full potential of the propfan propulsion concepts. To meet this need, tests of several different wing/nacelle/power configurations have been made by NASA Ames. This report summarizes several design and data analysis tasks for these tests conducted by Douglas Aircraft Company in support of the NASA Ames installation aerodynamic program.

A data reduction thrust/drag bookkeeping method which is consistent with the performance prediction methods used for analysis of new aircraft designs is defined. Although numerous thrust/drag bookkeeping methods can be used, this method is compatible with data available to the engine, propeller and airframe manufacturers. When compared to the method used by NASA for analysis of Ames 11-foot transonic wind tunnel test data an 18 count (.0018) difference in interference drag results. This difference represents roughly 4% of the total configuration drag.

Powered data from the Ames high speed test for the underwing nacelle installation is reduced using the new thrust/drag accounting system, and a summary of the experimental performance is made. Pressure and flow visualization data from the test for both the straight underwing nacelle, and unpowered contoured overwing nacelle installations is used to determine the flow phenomena present for a wing mounted propfan installation. The test data is compared to analytic methods, showing the analytic methods to be suitable for design and analysis of new configurations. This analysis indicates that designs with zero interference drag levels are achievable with proper wing and nacelle tailoring.

The performance of an unpowered overwing countered nacelle with a solid body exhaust plume simulation is evaluated both with and without a wing leading edge extension (LEX). The effects of the LEX and of nacelle contouring are shown to be complimentary, but not strictly additive. Improvements in the wing flow obtained utilizing one modification, make additional large improvements by the complimenting modification more difficult to achieve. A new contoured overwing nacelle design as well as modifications to the existing contoured nacelle and wing leading edge extension wind tunnel model geometries are evaluated. Hardware constraints of the current model parts prevent obtaining any significant performance improvements due to the modified nacelle and LEX shapes.

A new, aspect ratio 11 wing design for an up outboard single rotation propfan installation is defined, and an advanced contoured nacelle is provided for this wing. The design shows a slight reduction in induced drag, when compared to the unpowered clean wing in lifting line analysis, and maintains good pressure characteristics for the power-on case.

2.0 INTRODUCTION

The reduction of aircraft fuel consumption has been a major goal of NASA and the Douglas Aircraft Company for many years. The Aircraft Energy Efficiency (ACEE) program has been a major part of this effort. One of the more recent areas of study for reduction of aircraft fuel consumption is the incorporation of advanced propeller (propfan) propulsion systems. The configurations under consideration consist of highly loaded eight to ten blade propellers, capable of high efficiency at cruise Mach numbers from 0.7 to 0.8.

The technology required to exploit the fuel savings offered by the propfan propulsion systems includes the development of an efficient propeller and nacelle design that minimizes the interference drag penalty when installed on supercritical wings. This is a much more severe design constraint than the installation of current turbofan propulsion systems, as not only the wing/nacelle interactions must be considered, but the wing/slipstream interactions must also be evaluated.

Initial testing used a wing developed for a turbofan concept, with a simulated propeller slipstream (reference 1). This test identified many of the critical issues affecting the turboprop installation including an increase in local stream velocity causing a change in shock location and strength, and large changes in the local wing upwash (or downwash) causing large changes in the leading edge suction pressure levels. A later test employed the same wing geometry definition, and added a straight, underwing nacelle and propeller system (reference 2). This test helped emphasize the importance of the nacelle to the understanding of the complete propulsion system installation picture. A test using a different wing geometry and several alternate nacelle geometries helped identify the significance of contouring the nacelle to account for the wing flow field. The results of this test are contained in unpublished NASA data. Both wing and nacelle design modifications based on the reference 2 test results were defined, and later tested.

This report describes an analysis performed for this latest test data. The test contained a baseline wing geometry (Table 1, reference 2), a modified wing geometry (Table 2, reference 2), a straight underwing nacelle and propeller installation, and a unpowered contoured overwing nacelle installation. The wind tunnel model installation for the straight underwing nacelle configuration is shown in figure 1.

Section 3.0(Task I) of this report details the development of a thrust/drag accounting method for turboprop installations. The thrust/drag accounting method is employed to assess the results of the wind tunnel tests utilizing isolated propeller performance to determine the installation or interference drag which is defined as the total configuration drag minus the clean wing and nacelle parasite drag. Isolated propeller performance can be obtained from the propeller manufacturer, allowing the analysis of many propeller designs on a given aircraft, without retesting each configuration.

Section 4.0(Task II) of the report uses the pressure and flow visualization data to describe the flow phenomenon producing the measured installation

interference drag. The experimental data is compared to suitable analysis methods for both the low ($0.6 M_0$) and high ($0.8 M_0$) Mach number data to verify the accuracy of the methods used to design the model geometry. The effects of the nacelle installation are considered both with and without the additional effects due to power. The wing leading edge extension (LEX) is analyzed to determine if it was successful in reducing the effects of power on the wing pressure distributions, and the resulting drag levels are presented.

Section 5.0(Task III) evaluates the effects of the nacelle contouring on reducing the installation interference drag. The contoured nacelle data does not contain any power effects, however, the model did include a solid body exhaust plume simulation to account for nacelle base drag effects. The combination of the contoured nacelle and the LEX is assessed to determine the extent to which the effects of the two modifications are additive. Using a more comprehensive nacelle contouring scheme, a new advanced contoured nacelle is designed. Enhancements to the existing contoured overwing nacelle and LEX geometries are explored. A new aspect ratio 11 wing is designed for an up outboard rotation turboprop propeller/nacelle installation. An advanced contoured nacelle is defined for integration with the up-outboard rotation wing design.

3.0 TASK I. THRUST/DRAG BOOKKEEPING

3.1 Thrust/Drag Bookkeeping Methods

In the design of a new aircraft configuration, the thrust required to overcome drag must be defined to allow for proper engine sizing, which in turn is needed to establish suitable aircraft takeoff, climb, and cruise performance. The purpose of performing thrust/drag bookkeeping analysis on wind tunnel test data is to quantify all of the measurable thrust and drag components acting on a model configuration and to ensure that these components are defined in a way that can be used by the engine, propeller, and aircraft manufacturers to predict aircraft performance. The primary point for this discussion is that the propeller and nozzle data must be based on isolated characteristics, as the isolated characteristics are all that the manufacturers of the components can supply. Any installed interferences, both on the aircraft and on the propulsion unit, are included in the polar for each specific configuration. For wind tunnel data analysis, these isolated characteristics are obtained by calibration of the wind tunnel propulsion hardware and the resulting forces are removed from the data. Then the thrust terms obtained from isolated propeller and engine tests can be combined with the resulting polars to predict aircraft performance.

In both the current NASA and DAC bookkeeping methods, propeller and engine exhaust nozzle thrust terms are removed from the drag balance measurements for a series of angles of attack at several different Mach numbers in the following manner:

$$C_{D_{EFF}} = C_{D_{BAL}} - C_{T_{NET}} - C_{T_{JET}} \quad (1)$$

The resulting thrust removed drag polars are used to find drag levels at a pre-defined lift coefficient for each Mach number. Parasite drag terms, which account for skin friction and propwash scrubbing, are calculated using standard procedures at the specified lift coefficient and subtracted out of the thrust-removed drag terms in order to obtain interference drag. What distinguishes the two methods from one another is the manner in which the propeller and engine exhaust nozzle thrust terms are calculated.

In the following sections both the NASA and DAC methods for determining propeller and exhaust nozzle thrust will be described. A comparison is made of results obtained from both methods for selected test conditions from the Ames test. As shown in figure 2 the powered conditions chosen for analysis are representative of normal cruise flight power settings at each Mach Number. Results, in the form of interference drag levels and lift curves, are given for each method. Finally, conclusions are drawn concerning the ramifications of the new analysis method.

3.1.1 Current NASA Installed Performance Method

In the force data reduction method currently used by NASA, the net propeller thrust is obtained from a rotating balance on the propeller drive shaft using the following relation:

$$C_{T_{NET}} = C_{T_{AP}} - DELCXN \quad (2)$$

where $C_{T_{AP}}$ is the apparent thrust coefficient, which accounts for hub base drag forces, and DELCXN is the nacelle buoyancy correction term which accounts for the opposing force generated on the propeller disk due to the presence of the nacelle. A brief outline of the installed procedure is shown in figure 3. Since the propeller thrust obtained in this manner is acting in the presence of the wing and nacelle, the value measured is configuration-dependent and, therefore, is not compatible with performance prediction techniques available to engine, propeller and airframe manufacturers. The performance data generated by engine and propeller manufacturers represents isolated performance predictions and are independent of any specific aircraft configuration.

The exhaust nozzle thrust coefficient ($C_{T_{JET}}$) is derived from a semi-empirical analysis which is developed in reference 3. The actual jet thrust term (TJET1) is the product of the ideal thrust (TIDEAL) and a jet thrust calibration factor ($C_{T_{AVG}}$) as shown below:

$$TJET1 = (C_{T_{AVG}})(TIDEAL) \quad (3)$$

$$\text{where: } TIDEAL = A_E \left(P_{SE} \left\{ \left(\frac{2q}{q-1} \right) \left[\left(\frac{P_{TE}}{P_{SE}} \right)^{\frac{\gamma-1}{\gamma}} - 1 \right] + 1 \right\} - P_{AMB} \right) \quad (4)$$

$$\text{and: } C_{T_{AVG}} = \text{ACTUAL THRUST/IDEAL THRUST} \quad (5)$$

Once TJET1 is known, the exhaust nozzle thrust coefficient is found using the following relation:

$$C_{T_{JET}} = TJET1/q_{\infty} S_{REF} \quad (6)$$

The results of an exhaust nozzle calibration study conducted by Tech Development were used to calculate $C_{T_{AVG}}$ over a range of exhaust nozzle pressure ratios from 1.08 through 1.91. The exhaust nozzle and associated instrumentation were removed from the air driven turbine motor and mounted in the Fluidyne static test stand which is located at the Fluid Dyne Engineering Corporation's Medicine Lake Laboratory. The resulting experimental datapoints, together with a fitted calibration curve, are shown in figure 4. As in the case of the propeller thrust, the exhaust nozzle thrust term obtained from this procedure is dependent on a specific configuration since the ideal thrust term is a function of the local exhaust nozzle static pressure, P_{SE} .

In order to account for nacelle pitch-down and toe-in as well as exhaust thrust orientation with respect to the FRP, the $C_{T_{NET}}$ and $C_{T_{JET}}$ terms obtained using the preceding equations are reduced into components acting in the axial and normal directions. A complete set of the equations used

to account for nacelle and exhaust nozzle orientation in the NASA method appears in reference 4.

3.1.2 DAC Isolated Performance Method

In the DAC bookkeeping method, both the propeller thrust and engine exhaust nozzle thrust are determined on an isolated basis; that is, they are calculated from propeller and engine manufacturers' experimental data which, as mentioned earlier, is independent of the specific aircraft configuration. An outline showing the proposed data reduction technique is given in figure 5.

The isolated propeller thrust term is found using propeller performance charts similar to the one shown in figure 6. The propeller charts used in the analysis of the Ames test data were generated at the NASA Lewis PTR for the Hamilton Standard SR-2C propeller. A set of these propeller charts appears in Appendix A.

For each test point a power coefficient (C_p) is calculated using the following equation:

$$C_p = \frac{P}{\rho_\infty \eta^3 D^5} \quad (7)$$

where P is the shaft horsepower calculated from the rotating balance torque and RPM and ρ_∞ is the freestream density at each test condition.

For each C_p at a given blade angle (β), a propeller efficiency (η) is found from the chart. C_p and β are used because they are directly related to fuel flow for an aircraft application and do not require the knowledge or assumption of a "velocity" as the Advance Ratio (J) does. Also, for normal operating conditions, C_p and β uniquely determine J, since any two parameters are all that is required to determine propeller performance. Once the propeller efficiency is found, the following relation is then used to determine the propeller thrust coefficient:

$$C_{T_{NET}} = \frac{\eta P}{q_\infty V_\infty S_{REF}} \quad (8)$$

The isolated exhaust nozzle calibration is the same data as previously discussed for the Tech Development motor, however, the data were analyzed in a different manor.

The equation used to calculate the actual exhaust nozzle thrust is developed from the ideal thrust relation. Assuming subsonic nozzle flow ($NPR \leq 1.893$), the ideal thrust equation can be written as:

$$\frac{F}{P_{AMB} A_E} = \frac{2\gamma}{\gamma-1} \left[\left(\frac{P_{TE}}{P_{AMB}} \right)^{\frac{\gamma-1}{\gamma}} - 1 \right] \quad (9)$$

This equation differs from Eq. 4, which is developed in reference 3, in that it does not contain a local static pressure term (P_{SE}).

For air, $\gamma = 1.4$, and Eq. 9 can be rewritten as:

$$\frac{F}{P_{AMB} A_E} = 7 \left[\left(\frac{P_{TE}}{P_{AMB}} \right)^{.2857} - 1 \right] \quad (10)$$

Equation 10, plotted together with the Fluidyne static test calibration data, is given in figure 7. The calibration data simply appears to "bend over" faster than the ideal thrust curve. If Eq. 10 is rearranged as follows:

$$\left(\frac{P_{TE}}{P_{AMB}} \right)^N = 1 + \frac{F}{7 P_{AMB} A_E} \quad (11)$$

and plotted in log-log format, then the exponent N is readily determined as the slope of the curve. Using this procedure, a curve-fit of the exhaust thrust calibration is established:

$$\frac{F}{P_{AMB} A_E} = 7 \left[\left(\frac{P_{TE}}{P_{AMB}} \right)^{.2682} - 1 \right] \quad (12)$$

Figure 8 shows the experimental calibration points together with the curve fit from Eq. 12. Equation 12 represents an exhaust nozzle thrust term which is based on isolated test data and is a function only of the nozzle total and ambient static pressures.

For each wind tunnel test point (i.e., each NPR), an exhaust nozzle thrust term is calculated using Eq. 12. The exhaust nozzle thrust coefficient can then be found using:

$$C_{T_{JET}} = \frac{F}{q_{\infty} S_{REF}} \quad (13)$$

Unlike the current NASA method, the $C_{T_{NET}}$ and $C_{T_{JET}}$ terms calculated using the isolated data are assumed to act in the freestream direction and are therefore added directly to the balance measurement in order to obtain the thrust removed drag. The thrust removed lift ($C_{L_{EFF}}$) is obtained by correcting the normal force balance reading for angle-of-attack. The thrust removed drag and lift terms are obtained in this manner because, although the geometric nacelle pitchdown and toe-in and exhaust nozzle toe-in angles are known relative to the FRP, the resultant directions in which these thrust forces actually act cannot be defined and are included in the lift and drag polars using this procedure.

Parasite drag terms have been calculated to account for skin friction, propeller scrubbing, and nacelle form drag using form factors and skin friction coefficients obtained at the appropriate Reynolds numbers. These

parasite drag terms were used in both bookkeeping methods. A summary of values obtained for the different parasite drag terms appears in Appendix B.

3.2 Thrust/Drag Bookkeeping Method Comparison

To illustrate the differences between the two force bookkeeping methods, a comparison of propeller and exhaust nozzle thrust terms, as well as the resulting thrust removed lift and drag values calculated using both methods, is presented in the Table below. The selected test point for this comparison is the wing/nacelle/power case at 0.8M. A force data summary of the interference drag levels for all of the test points analyzed will be presented in the following section.

METHOD COMPARISON

| α° | C_{TNET} | | C_{TJET} | | C_{DEFF} | | C_{LEFF} | |
|----------------|------------|--------|------------|--------|------------|--------|------------|--------|
| | DAC | NASA | DAC | NASA | DAC | NASA | DAC | NASA |
| 1.0 | .02780 | .03087 | .01779 | .01800 | .04490 | .04689 | .37800 | .37700 |
| 2.0 | .02740 | .03009 | .01754 | .01742 | .05280 | .05461 | .49600 | .49440 |
| 3.0 | .02482 | .02691 | .01459 | .01450 | .06180 | .06326 | .60100 | .59950 |

A comparison between the drag polars constructed using the above data is given in figure 9. A complete set of all drag polars used in the analysis appears in Appendix C. The tabulated data above shows that most of the differences in drag levels can be attributed to the difference in the net propeller thrust values (C_{TNET}). At a C_L of .5, the drag level for the NASA method is 18 counts higher than that for the isolated thrust method. These 18 counts can be attributed mainly to the influence of the wing and nacelle installation on the propeller.

3.3 RESULTS

The results of the force data analysis are presented in figure 10, which shows interference drag levels as a function of Mach Number for both bookkeeping methods. For the wing nacelle combination without the LEX, the interference drag levels obtained from the isolated thrust data are less than the installed method by 10 counts at $.75M_0$ and 18 counts at $.8M_0$. For the wing nacelle combination including the LEX, there is no difference in interference levels at $.75M_0$ while at $.8M_0$ the isolated thrust data level is roughly 8 counts less than the installed thrust data level. Both of these configurations exhibit a similar trend in that as Mach Number is increased above .75 the difference between the interference drag levels increases. For the fillet configuration the trend seen in the first two configurations seems to be reversed. At $.78M_0$ the interference drag level for the fillet configuration is roughly 13 counts higher for the isolated thrust method while at $.8M$ both methods show essentially no interference drag. This reversal may be due to the fact that the positioning of the fillet, which is only .25 blade diameters downstream of the prop-plane, may have a significant influence on the installed prop thrust.

Figure 11 shows a comparison between the thrust removed lift curves generated using both force data reduction methods. There is a slight

increase in the level of the lift curves for the isolated thrust method as compared to the installed thrust method. This shift can be considered negligible since, at the most, it results in a C_L increase of only .005.

One way of determining the inflow velocity to the propeller is from the isolated propeller charts. Each test point has a unique power coefficient which is calculated using Eq. 7. For a given blade angle, a value for J can be found for each power coefficient using the propeller charts at the freestream Mach number. The J obtained in this manner is based on isolated prop data, therefore, the associated velocity is the local propeller onset velocity. Figure 12 shows two propeller curves, one based on isolated propeller data and the other based on tunnel freestream velocity. These results are similar to the results obtained in Reference 4. This shift in the propeller curve for the 0.8 tunnel freestream Mach number condition has an effect on propeller performance since propeller efficiency levels are a function of J . This difference in propeller performance shows up in the interference drag levels shown in Figure 10.

4.0 TASK II. DATA ANALYSIS, UNDERWING NACELLE

Section 3.0 of this contract presented a discussion and suggested approach for assessing the propulsion system interference drag levels in such a way that they are comparable with data supplied by the propeller manufacturer. Having established these drag levels, an analysis of the surface pressure and oil flow photographs is necessary to gain an understanding of the aerodynamics features of the propulsion system installation. In addition, comparisons of the surface pressure data with theoretical methods is required to establish the accuracy of these methods for future design.

4.1 Analysis of Straight Underwing Nacelle Data

The test conditions chosen for the experimental wing pressure summary presented in this section correspond to the same test conditions used in determining the interference drag levels shown in figure 10. The DAC isolated interference drag buildup results for the wing-nacelle configuration shown in figure 13 and 14, with and without power, are shown in figure 15. The corresponding pressure data obtained for freestream Mach numbers of 0.6, 0.75, and 0.8 appears in figures 16, 17, and 18 respectively. (Force and pressure data for the wing-nacelle-power case at $0.6M_0$ was not obtained during the Ames test and, as a result, interference drag levels are not available at this condition; however, suitable powered wing pressure data was obtained during the previous Ames test in the 14-foot transonic wind tunnel and is included in figure 16.)

At $0.6 M_0$, the 20 count interference drag level due to the nacelle presented in figure 15 can most likely be attributed to the increased wing suction peak levels inboard of the nacelle. At the $ETA = .418$ pressure row, the presence of the nacelle results in suction peak normal Mach numbers based on wing $c/4$ sweep (M_L) of just over 1.1. The significance of this result is that even at this relatively low Mach number, the wing is experiencing regions of transonic flow due to the presence of the straight underwing nacelle. Previous analysis of installation effects for varying nacelle shapes (reference 2) has shown that proper tailoring or contouring of the nacelle shape can help alleviate these localized regions of highly accelerated flow.

As Mach number is increased from 0.6 to 0.8 the nacelle interference drag increases roughly 15 counts. This rise in the interference drag level can be attributed to increased wing compressibility effects. These compressibility effects are most clearly illustrated in the pressure distributions immediately inboard of the nacelle at the $ETA = .418$ pressure row (figures 17 and 18). The local suction peak Mach numbers just inboard of the nacelle at 0.75 and $0.80M_0$ are roughly 1.4 and 1.6, respectively, as compared to 1.1 for the $0.6M_0$ condition. These higher local Mach numbers result in stronger wing shocks. The flow visualization pictures presented in figures 19 and 20 for the windmilling test condition indicate a stronger more unswept shock at the $0.8M_0$ condition as compared to the $0.75M_0$ condition.

Comparison of the flow visualization for the clean wing (figure 21) and the unpowered nacelle configuration presented in figure 20 indicates the change in upper surface spanwise flow due to the presence of the nacelle.

As shown in figure 15, the addition of power (up-inboard propeller rotation) leads to a further increase in the interference drag values at all Mach numbers analyzed. Figures 17 and 18 show that at the $ETA = .365$ pressure row, where the effects of power are most pronounced, the onset of power increases the suction peak local Mach numbers from 1.2 to 1.6 at $0.75M_0$ and from 1.3 to 1.5 at $0.8M_0$. These higher inboard peak levels are due to an increase in the local wing angle-of-attack resulting from propeller upwash. For the area of the wing just outboard of the nacelle the effect of the propeller onset flow is reversed with a propeller downwash component producing a lower local angle-of-attack and, as a result, more positive wing pressures. At the $ETA = .418$ pressure row the effect of power has no appreciable effect on the wing suction peaks but rather a "bubbling" effect on the wing upper surface pressure recovery which may be due to a laminar bubble or local separated flow. The flow visualization pictures presented in figures 22 and 23 both appear to show an area of local separated flow in the region where this "bubbling" effect occurs in the pressure distributions.

Interference drag results for the wing leading edge extension (LEX) configuration (shown in Figure 24 and 25) with and without the inboard nacelle/wing fillet, are shown in Figure 26. The corresponding wing pressure data appears in figures 27, 28, and 29. At $0.6M_0$ the presence of the LEX results in a 10 count drag benefit when compared with the same unpowered nacelle configuration without the LEX (figure 15). Comparison of the $0.6M_0$ pressure data presented in figure 27 with the unmodified baseline wing-nacelle data previously shown in figure 16 demonstrates the effectiveness of the LEX in reducing the wing leading-edge peak local Mach numbers. At the pressure row just inboard of the nacelle ($ETA = .418$) the LEX reduces the wing local Mach numbers from 1.1 to a subsonic value. The drag benefit due to the LEX increases at higher Mach numbers; at $0.8M_0$ a 20 count benefit, relative to the unmodified wing, is realized. Comparing the $0.8M_0$ LEX pressure data (figure 29) with the baseline wing-nacelle data (figure 18) indicates a similar trend in the local Mach number reduction seen for the $0.6M_0$ test condition.

The interference drag increment due to power for the LEX configuration is approximately 10 counts at $0.6M_0$; however, as Mach number is increased the interference drag increment due to power decreases to a point where at $0.8M_0$, a 10 drag count favorable interference, relative to the unpowered LEX configuration, is seen. Examination of the $0.6M_0$ chordwise pressure distributions (figure 27) indicates that even with the LEX installed noticeable adverse effects due to power still exist. However, at the flow condition for which the LEX was designed, $0.8M_0$, the LEX does a better job of suppressing the inboard pressure peak levels (figure 29). The advantage of the LEX can be clearly seen in figure 30 which shows the powered conditions with and without LEX compared with the clean wing at $0.8M_0$. At $ETA = .365$ the LEX returns the pressure distributions close to the original clean wing levels. At the $ETA = .418$ station the LEX did not improve the upper surface suction peak levels compared to those for the unmodified wing, although there is some improvement seen on the lower wing surface pressures at this station. The flow visualization picture given in figure 31 shows the wing with LEX and power at $0.8M_0$.

To help improve the upper surface pressures just inboard of the nacelle a leading-edge fillet section, which is shown in figures 32 and 33, was fabricated at the wing/nacelle intersection. The fillet shape was defined by NASA during the test based on preliminary analysis of selected wind tunnel data without the benefit of any theoretical analysis. As shown in figure 26, the addition of the fillet improved the interference drag at $0.8M_0$. Figure 34 shows the resulting pressure distribution just inboard of the nacelle due to the addition of the fillet. When compared with the wing-LEX configuration, the addition of the fillet lowers the upper surface local Mach number by roughly 0.2.

4.2 Comparison With Theory, Straight Underwing Nacelle

Presently, the three theoretical methods used at DAC to analyze and design wings operating in the presence of a wing mounted propfan are the DAC lifting-line program (Ref.5), the DAC-Neumann panel program (modification of Ref. 6), and the DAC-Jameson 3-D transonic program (modification of Ref. 7).

The lifting-line program has been utilized to evaluate the effects of non-uniform onset flows on the wing induced drag characteristics. This method has been very useful in developing the optimum wing span loading for a particular propeller flow field. The DAC-Neumann program with its capability to handle complex 3-D geometries, as well as simulate propeller onset flows, has been used extensively to develop the engine nacelle and wing geometry at subsonic conditions. The DAC-Jameson program coupled with propeller onset flow effects and empirical transonic nacelle installation effects has been employed to develop the wing transonic flow characteristics.

The usefulness of these design methods is dependent on how well they can actually predict the effects of the nacelle installation and propeller onset flow. The series of comparisons that follow have been assembled in such a manner as to allow a one-to-one comparison between the actual nacelle and power effects as measured in the Ames test and the predicted effects obtained from the theoretical methods described above. For the three configurations on which the majority of the testing was performed (i.e., clean wing, wing-nacelle, and wing-LEX-nacelle) $0.6M_0$ data is compared with results from the DAC-Neumann program and $0.8M_0$ test data is compared with the DAC-Jameson results.

Presently, because of mathematical formulation difficulties, the DAC-Neumann program must be run at zero Mach number when the propfan onset flow is being simulated. In addition, to facilitate the use of the method, particularly when the nacelle is incorporated with the wing geometry, the Neumann solutions have been obtained without considering any viscous corrections to the wing geometry. Based on the above operational constraints and the fact that at low subsonic Mach numbers changes to the flow characteristics over the upper surface and forward position of the wing, due to the addition of a nacelle and power are the most important to predict all DAC-Neumann to experimental correlations have been made at a constant angle-of-attack. Since Mach number and viscous effects are accounted for in the present transonic nacelle and power simulation procedures, the DAC-Jameson correlations with experimental data are shown at constant C_L .

The comparison of the experimental and DAC-Neumann theoretical wing chordwise pressure distributions at $0.6M_0$ for the clean wing configuration is presented in Figure 35. As can be seen, the correlation is very good on the wing upper surface which supports the approach of making comparison at a constant angle-of-attack. For comparison, figure 36, a DAC-Jameson solution is compared to the above $0.6M_0$ data at a constant C_L . The DAC-Jameson calculated pressures are in very close agreement with the experiment data over the entire wing surface. A similar clean wing comparison at $0.8M_0$ is presented in figure 37. In general the DAC-Jameson calculated pressure distribution is in reasonable agreement with the experimental data.

Figure 38 shows the DAC-Neumann and experimental nacelle installation effects on the wing's chordwise pressure distributions just inboard and outboard of the nacelle at $0.6M_0$. As can be seen, the changes to the wing's surface pressure distributions due to the nacelle installation are predicted well by the DAC-Neumann program. Figure 39 presents, at the same wing semispan stations, the comparison of DAC-Jameson and experimental wing chordwise pressure distribution for the wing/nacelle configuration at $0.8M_0$. In general the DAC-Jameson/empirical transonic nacelle simulation procedure correlates well with the experimental data.

The comparison of the DAC-Neumann and experimental propeller slipstream (power) effects on the wing chordwise pressure distributions at $0.6M_0$ is presented in figure 40. The propeller swirl and total pressure ratio characteristics used in the DAC-Neumann power simulation are given in figure 15 of reference 2. These results indicate that the propeller onset flow simulation incorporated in the DAC-Neumann program is properly predicting the experimental power effects. The comparison of the DAC-Jameson and experimental wing chordwise pressure distributions for the powered wing/nacelle configuration at $0.8M_0$ is shown in figure 41. Again, the correlation is quite good except at the 42 percent semispan station where the experimental data is indicating separated flow as shown in the oil flow visualization picture (figure 23). The quality of the above correlation supports the present scheme used in the DAC-Jameson program to simulate propeller power effects.

Figure 42 presents, for the LEX configuration, the nacelle installation effects at $0.6M_0$ measured experimentally and predicted by the DAC-Neumann program. Again, the wing chordwise pressure distribution changes due to installing the nacelle are accurately predicted by the DAC-Neumann program. The DAC-Jameson/experimental comparisons for the straight underwing nacelle and LEX configuration at $0.8M_0$ appear in figure 43. With the exception of the slight over prediction of the suction peak level at $ETA = .365$ the theory is generally in good agreement with the experimental results.

Figure 44 compares the DAC-Neumann and experimental propeller power effects on the wing chordwise pressure distributions for the LEX configuration at $0.6M_0$. Again, as seen on the baseline wing configuration, the DAC-Neumann power effects simulation technique predicts the experimental results quite accurately, except at the 42 percent wing semispan station where the experimental flow is indicating a separation bubble downstream of its suction peak. Comparison of the DAC-Jameson and experimental chordwise pressure distribution at $0.8M_0$ for the LEX configuration with power is shown in figure 45. Again, the above comparison generally supports the present power effect technique employed in the DAC-Jameson program. As was

the case for the baseline wing, the experimental pressures at the 42 percent semispan span station appear separated as indicated in the flow visualization photograph (figure 31).

Figures 46 through 49 present the changes to the wing span loading due to propeller power effects as measured experimentally and predicted by DAC's current analysis methods. In all cases (i.e., independent of Mach number and wing configuration) the theoretical programs underestimate the increase in the experimental wing span loading in the region inboard of the nacelle. Whereas, in general, the correlation is quite good in the wing region outboard of the nacelle. The poor correlation in the wing region inboard of the nacelle may possibly be attributed to the fact that the experimental flow appears to separate in this region of the wing when power is applied to the propeller and/or due to the chordwise summation of small pressure differences between the theory and experimental data.

5.0 TASK III DATA ANALYSIS AND DESIGN, OVERWING NACELLE

This section describes the interference drag increments and wing chordwise pressure distribution changes due to the overwing contoured nacelle installation. Data is presented for the baseline wing, baseline wing plus leading edge extension (LEX), and the LEX wing configuration with an inboard nacelle/wing leading-edge fillet developed by NASA personnel during the wind tunnel test. The complete configuration with the LEX and fillet installed is shown in figures 50, 51, and 52. Only unpowered (i.e., propeller off) data was acquired for this configuration, however, a solid body exhaust plume simulation was included in the model geometry. These experimental results are presented in a format similar to that used in the straight underwing nacelle data analysis (Section 4.0). A new contoured overwing nacelle design and a modification to the LEX for the current wind tunnel model design are evaluated. A new $AR = 11$ wing design for an up-outboard rotation turboprop installation is defined, and an advanced contoured nacelle is provided

5.1 Analysis of Contoured Overwing Nacelle Data

The interference drag increments for the overwing contoured nacelle at $0.5C_L$ are shown in figure 53. Examination of the 0.6 and $0.8M_0$ wing pressure data, presented in figures 54 and 55 respectively, suggests this level of interference drag is due to the increase in wing suction pressure levels inboard of the nacelle, as was the situation for the underwing nacelle installation. The oil flow photograph for the contoured nacelle configuration at $0.8M_0$ (figure 56) shows that the high leading-edge suction peak seen in the pressure distributions is producing a local shock, accounting for the increase in drag.

The addition of the LEX wing modification produced essentially no change to the contoured overwing nacelle interference drag levels (except at $0.7M_0$). The inboard wing surface pressure distributions do not fully explain this drag increment since the pressure distribution increments due to the addition of the LEX are very similar for both the contoured nacelle and straight underwing nacelle configurations and, as seen in figures 15 and 26, the LEX reduced the underwing nacelle interference drag level by 10 counts at $0.8M$. Figures 54, 55, 57, and 58 present the effect of the LEX on the wing chordwise pressure for both nacelle configurations at 0.6 and $0.8M_0$. The small improvement in drag with the addition of the LEX for the contoured nacelle may be attributed to the complimentary effect of the nacelle contouring and the LEX. Both modifications were designed to reduce the leading edge suction peaks. Since either component by itself will reduce the suction peak there is a less severe condition for the other component to improve. It is therefore appropriate that the effects are not strictly additive.

The addition of the inboard nacelle/wing fillet reduced the nacelle interference drag approximately 10 drag counts relative to the LEX only configuration. This reduction in interference drag occurs because the fillet affects the wing pressures and shock in the region just inboard of the nacelle, as seen in figure 59 for $0.6M_0$ and $0.8M_0$.

PRECEDING PAGE BLANK NOT FILMED

5.2 Comparison With Theory, Contoured Overwing Nacelle

The DAC-Neumann and DAC-Jameson analysis methods have been utilized at 0.6 and 0.8 Mach numbers, respectively, to obtain comparisons with the experimental data for the contoured overwing nacelle configurations in a manner similar to the comparisons made for the straight underwing nacelle installations.

Figure 60 presents the DAC-Neumann and $0.6M_0$ experimental effects of the contoured overwing nacelle on the wing chordwise pressure distribution just inboard and outboard of the nacelle. The changes due to the nacelle installation on the wing surface pressure distributions are generally predicted well by the DAC-Neumann program. The increase in wing leading edge suction peaks just inboard of the nacelle are slightly underestimated by the DAC-Neumann program. Figure 61 presents, at the same wing semispan stations, the comparison of the DAC-Jameson and experimental wing chordwise pressure distributions for the wing/nacelle configuration at $0.8M$. As was the case for the underwing nacelle configuration, the DAC-Jameson/emperical transonic nacelle simulation procedure correlates well with the experimental data.

Nacelle installation effects for the LEX wing configuration, as predicted by DAC-Neumann and measured experimentally, are shown in figure 62. Again, the changes to the wing chordwise pressure distribution are adequately predicted by the DAC-Neumann program. The comparison of DAC-Jameson and experimental chordwise pressure distribution at 0.8 Mach number for the LEX/contoured overwing nacelle configuration is presented in figure 63. The correlation for this wing configuration, compared to that for the baseline wing and nacelle (figure 61) is slightly worse in the region inboard of the nacelle; but is acceptable outboard of the nacelle.

5.3 Design Modifications for Overwing Contoured Nacelle

Since the overwing contoured nacelle was not designed for the wing with the LEX, a study was conducted to determine if a better nacelle contouring, including a refined contouring procedure, could be developed that would reduce the wing/lex/nacelle installation drag and would meet constraints imposed by the current model hardware.

Two modified nacelle shapes were defined and analyzed using the DAC Neumann code. These nacelle shapes together with the existing wind tunnel model (baseline) geometry appear in figure 64. The modified baseline nacelle shape was designed subject to constraints of the existing internal hardware and, as a result, appears the same in the side view as the baseline nacelle. The fully contoured nacelle shape was designed using current design technology without any hardware constraints and therefore represents a more optimum design. Figure 65 shows the Neumann pressure comparisons for all three nacelle shapes at the two pressure rows just inboard of the nacelle. While the modified baseline nacelle pressures do not show much improvement over the baseline case, the unconstrained, fully contoured nacelle resulted in a significant reduction in the upper surface suction peaks. The modifications allowable with the physical constraints imposed by the internal hardware did not yield any major improvement in the pressure distributions. Therefore, nacelle modifications for the Ames model are not recommended.

Based on the interference drag level results of the powered testing of the straight underwing nacelle geometry, a modification to the LEX in the area just inboard of the nacelle was investigated. The transonic design and analysis method of reference 5 was used to modify the LEX geometry with the objective of reducing the suction pressure peaks in this region by 0.2. This value is the same decrease obtained with the addition of the fillet to the contoured nacelle LEX geometry which resulted in a 10 count drag reduction. The resulting geometry and corresponding chordwise pressure distributions appear in figures 66 and 67. Wing rework would be required aft of $.15x/c$ to match these shapes to the existing wing.

5.4 New Wing Design

The purpose of the wing design effort was to design a wing which is tailored to minimize the interference drag increments associated with wing mounted up-outboard rotation propfan configurations. This wing would then be complementary to up-inboard work already completed. An existing supercritical wing geometry (Douglas Aircraft Co. Wing W1) with an AR of 11.1, $\Lambda_c/4$ of 26 degrees, and taper ratio of .275 was used as a baseline (figure 68). An overwing full chord engine nacelle was specified which is compatible with current installation requirements for a typical low wing airplane application.

As discussed previously, the wing design method currently employed at DAC utilizes a lifting-line program to evaluate the wing induced drag characteristics in the presence of nonuniform onset flows; a 3-D inverse Henne/Jameson program to generate the wing geometry to meet specified chordwise pressure distributions; and a 3-D Neumann program to determine the subsonic nacelle installation effects.

Initially the lifting line program was used to determine the span loading for the wing W1 planform which results in the minimum induced drag with both up-inboard and up-outboard propfan rotation onset flows. As was the case for the data-theory comparisons the propeller characteristics used to determine the onset flow were taken from results of a NASA Lewis PTR test on an isolated Hamilton Standard SR 2 propfan (Appendix A). The resulting drag polars are presented in Figure 69. It was found that the minimum attainable induced drag polar for up-outboard propfan rotation was roughly equal to the baseline W1 wing unpowered value. The 10 count benefit seen for the up-inboard rotation configuration is consistent with results seen in reference 8. From an induced drag standpoint, an up-inboard rotation configuration would appear preferable to the up-outboard rotation design. However, if interference and viscous effects discussed previously in this report, and wing thickness and shape are taken into account, the up-outboard rotation configuration may result in an overall improvement in the installed drag values.

The Henne/Jameson inverse design routine was employed to obtain pressure distributions for the wing operating in the presence of the propeller onset flow which are similar to the unpowered clean wing pressures. The resulting geometry for two of the modified airfoil geometries which lie within the propfan slipstream are shown in figure 70 together with the corresponding camber and thickness distributions. Coordinates for the complete wing defining airfoil sections are given in Table 1. The two airfoil sections are located to be downstream of the 70% installed propfan blade radius

spanwise location. The outboard airfoil section has significantly more camber than the section inboard of the nacelle. This increase in camber helps alleviate the adverse flow effects due to the added propfan upwash outboard of the nacelle. These airfoil modifications outboard of the nacelle are similar to the wing geometry resulting from the addition of the LEX to the wing W4 geometry for the Ames 11-foot test.

Wing thickness distributions for both the modified and baseline wing geometries appear in figure 71. The change in thickness made to the original W1 wing extends from roughly 20 to 70 percent semispan. Inboard and outboard of this section the W1 geometry is maintained.

A contoured nacelle shape was designed to eliminate adverse flow characteristics in the area of the wing-nacelle intersection while at the same time maintaining the internal lines necessary to contain a proposed flight propulsion system. Contouring of the nacelle was accomplished by first tracing several flow streamlines over the clean wing surface with the aid of the 3-D potential flow DAC Neumann code. A single streamline was selected to act as the centerline for the contoured nacelle. An in-house nacelle geometry generation routine was employed to modify a series of predefined nacelle cross sections to follow the selected streamline path. These cross sections are defined to clear the internal drive system and related equipment. Figures 72 and 73 show the resulting contoured nacelle shape compared with the initial straight overwing nacelle geometry. Coordinates for the nacelle defining cross sections are given in Table 2. A top view of the modified wing and contoured overwing nacelle geometry appears in figure 74.

Figures 75 and 76 show the resulting pressure distributions and span loadings for the modified wing geometry with power, compared to the baseline wing W1 with and without power at a configuration C_L of .55. For the wing W1 geometry, the addition of power increases the wing suction pressure peak levels outboard of the nacelle and offloads the leading edge area of the wing inboard of the nacelle. These changes are due to the effect of the up-outboard propfan rotation which increases local angle-of-attack outboard of the nacelle and decreases local angle-of-attack inboard of the nacelle. The resulting pressure distributions for the modified wing with power show that, with proper tailoring of airfoil shape and incidence, the adverse effects due to the propeller onset flow have been eliminated. In addition, the wing leading-edge pressures are off-loaded in the area of the nacelle to add a design margin.

Results of a lifting line induced drag analysis conducted on the modified wing geometry appear in figure 77. The new wing design shows a slight improvement, in induced drag, from both the unpowered and powered baseline wing.

6.0 CONCLUSIONS

- o A thrust/drag bookkeeping method is described which is compatible with data available to the engine, propeller and airframe manufacturers, and is recommended for data reduction during future testing. The results of the thrust/drag bookkeeping method comparison show that the difference in the interference drag levels obtained using both methods is, at the most, 18 drag counts at the higher Mach numbers and represents roughly 4% of the total configuration drag.
- o The propeller experiences a 13% shift in advance ratio when installed on the aircraft. This shift is due to the differences between the freestream and local(propfan diskplane) flowfield environments.
- o Propfan propulsion system interference drag levels near zero are achievable by properly designing the wing to account for the nacelle and power. Modified designs to eliminate remaining flow problem areas can result in additional drag improvements.
- o Theoretical methods agree very well with experimental pressure distributions at all Mach numbers and these methods are adequate for design purposes.
- o Incremental span loads are adequately predicted outboard of the nacelle, however, discrepancies between data and theory were found inboard of the nacelle. The inboard separated flow regions which are apparent in the chordwise pressure distributions are probably causing this poor correlation. To confirm this assumption additional study is required.
- o Analysis of the unpowered contoured overwing nacelle shows that contouring reduces the increase of nacelle interference drag as a function of Mach number.
- o The benefits seen for the LEX with the contoured nacelle did not meet the level expected from analysis of the underwing nacelle. This can be explained by the complimentary nature of the two modifications.
- o A modified nacelle contouring was evaluated, but hardware constraints prevent attaining any significant improvements.
- o A new wing was designed with up-outboard prop rotation. This was selected based on considerations of viscous effects and wing thickness. An advanced, full chord, contoured nacelle was designed for use with the new wing.

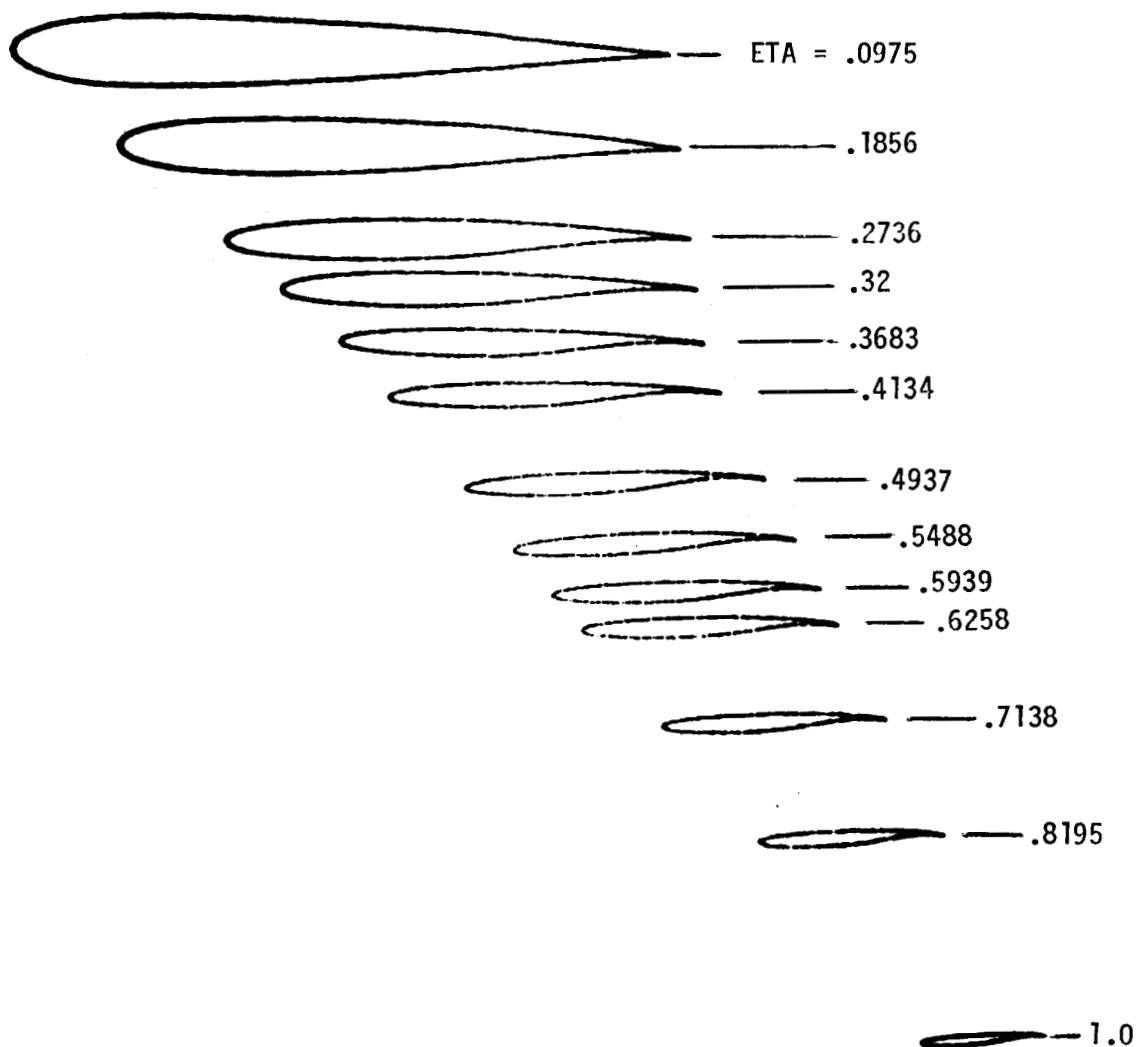
7.0 TABLES

PRECEDING PAGE BLANK NOT FILMED

TABLE 1
UP-OUTBOARD PROPFAN ROTATION
WING AIRFOIL GEOMETRY

PRECEDING PAGE BLANK NOT FILMED

ORIGINAL PAGE IS
OF POOR QUALITY



UP-OUTBOARD PROPFAN ROTATION WING AIRFOIL GEOMETRY

PRECEDING PAGE BLANK NOT FILMED

ORIGINAL PAGE IS
OF POOR QUALITY

ETA = .0975

ETA = .1856

| X | Y | Z | X | Y | Z |
|----------|---------|----------|----------|----------|----------|
| 290.1074 | 56.4494 | -12.3343 | 292.8545 | 107.3989 | -9.7807 |
| 288.6584 | 56.4494 | -12.0928 | 291.6306 | 107.3989 | -9.4372 |
| 284.3528 | 56.4494 | -11.2776 | 287.9871 | 107.3989 | -8.4580 |
| 277.3018 | 56.4494 | -9.8036 | 282.0146 | 107.3989 | -6.8477 |
| 267.6731 | 56.4494 | -7.8234 | 273.8516 | 107.3989 | -4.8291 |
| 255.7011 | 56.4494 | -5.4408 | 263.6890 | 107.3989 | -2.6424 |
| 241.6803 | 56.4494 | -2.7159 | 251.7800 | 107.3989 | -0.2897 |
| 225.9520 | 56.4494 | 0.2076 | 238.4165 | 107.3989 | 2.1481 |
| 208.8969 | 56.4494 | 3.1276 | 223.9207 | 107.3989 | 4.4697 |
| 190.9298 | 56.4494 | 5.8724 | 208.6448 | 107.3989 | 6.5254 |
| 172.4897 | 56.4494 | 8.3093 | 192.9653 | 107.3989 | 8.2702 |
| 154.0333 | 56.4494 | 10.4307 | 177.2711 | 107.3989 | 9.7187 |
| 136.0184 | 56.4494 | 12.2469 | 161.9488 | 107.3989 | 10.8390 |
| 118.8861 | 56.4494 | 13.6673 | 147.3722 | 107.3989 | 11.5331 |
| 103.0497 | 56.4494 | 14.4912 | 133.8963 | 107.3989 | 11.7030 |
| 88.8903 | 56.4494 | 14.5243 | 121.8498 | 107.3989 | 11.2854 |
| 76.7445 | 56.4494 | 13.5312 | 111.5267 | 107.3989 | 10.2351 |
| 66.9021 | 56.4494 | 11.3577 | 103.1798 | 107.3989 | 8.5473 |
| 59.6057 | 56.4494 | 8.0636 | 97.0116 | 107.3989 | 6.2068 |
| 55.0565 | 56.4494 | 4.1445 | 93.1743 | 107.3989 | 3.2772 |
| 53.3670 | 56.4494 | -0.2916 | 91.7756 | 107.3989 | 0.0936 |
| 54.6011 | 56.4494 | -4.7015 | 92.8300 | 107.3989 | -3.6650 |
| 58.7137 | 56.4494 | -9.2647 | 96.3598 | 107.3989 | -6.9332 |
| 65.6170 | 56.4494 | -13.6050 | 102.2656 | 107.3989 | -9.8828 |
| 75.1635 | 56.4494 | -17.1793 | 110.4064 | 107.3989 | -12.3508 |
| 87.1331 | 56.4494 | -19.6084 | 120.5818 | 107.3989 | -14.2771 |
| 101.2252 | 56.4494 | -20.9494 | 132.5382 | 107.3989 | -15.6760 |
| 117.0732 | 56.4494 | -21.5472 | 145.9773 | 107.3989 | -16.5887 |
| 134.2759 | 56.4494 | -21.5997 | 160.5659 | 107.3989 | -17.0410 |
| 152.4050 | 56.4494 | -21.1975 | 175.9438 | 107.3989 | -17.0388 |
| 171.0078 | 56.4494 | -20.4762 | 191.7323 | 107.3989 | -16.5857 |
| 189.6231 | 56.4494 | -19.5093 | 207.5430 | 107.3989 | -15.6873 |
| 207.7918 | 56.4494 | -18.3396 | 222.9810 | 107.3989 | -14.4738 |
| 225.0616 | 56.4494 | -17.0886 | 237.6571 | 107.3989 | -13.1633 |
| 241.0034 | 56.4494 | -15.8640 | 251.2017 | 107.3989 | -11.9497 |
| 255.2234 | 56.4494 | -14.7205 | 263.2756 | 107.3989 | -10.9758 |
| 267.3665 | 56.4494 | -13.7830 | 273.5791 | 107.3989 | -10.3232 |
| 277.1309 | 56.4494 | -13.1259 | 281.8601 | 107.3989 | -9.9662 |
| 284.2773 | 56.4494 | -12.7442 | 287.9182 | 107.3989 | -9.8478 |
| 288.6311 | 56.4494 | -12.6237 | 291.6072 | 107.3989 | -9.9100 |
| 290.0925 | 56.4494 | -12.6235 | 292.8447 | 107.3989 | -9.9800 |

ORIGINAL PAGE IS
OF POOR QUALITY

ETA = .2736

ETA = .32

| X | Y | Z | X | Y | Z |
|----------|----------|----------|----------|----------|---------|
| 295.4822 | 158.3481 | -5.4909 | 297.4685 | 185.1767 | -4.7442 |
| 294.4729 | 158.3481 | -5.2182 | 296.5674 | 185.1767 | -4.5055 |
| 291.4670 | 158.3481 | -4.4871 | 293.8838 | 185.1767 | -3.8748 |
| 286.5371 | 158.3481 | -3.3746 | 289.4805 | 185.1767 | -2.9390 |
| 279.8040 | 158.3481 | -1.9102 | 283.4678 | 185.1767 | -1.6883 |
| 271.4297 | 158.3481 | -0.2379 | 275.9893 | 185.1767 | -0.2525 |
| 261.6187 | 158.3481 | 1.5457 | 267.2271 | 185.1767 | 1.2656 |
| 250.6103 | 158.3481 | 3.3286 | 257.3940 | 185.1767 | 2.7624 |
| 238.6716 | 158.3481 | 4.9616 | 246.7293 | 185.1767 | 4.1170 |
| 226.0946 | 158.3481 | 6.3407 | 235.4940 | 185.1767 | 5.2641 |
| 213.1875 | 158.3481 | 7.3961 | 223.9639 | 185.1767 | 6.1517 |
| 200.2706 | 158.3481 | 8.1670 | 212.4257 | 185.1767 | 6.8316 |
| 187.6646 | 158.3481 | 8.7136 | 201.1666 | 185.1767 | 7.3646 |
| 175.6777 | 158.3481 | 8.9580 | 190.4609 | 185.1767 | 7.6603 |
| 164.6023 | 158.3481 | 8.8197 | 180.5694 | 185.1767 | 7.6411 |
| 154.7091 | 158.3481 | 8.2389 | 171.7341 | 185.1767 | 7.2676 |
| 146.2419 | 158.3481 | 7.2336 | 164.1726 | 185.1767 | 6.5489 |
| 139.4101 | 158.3481 | 5.8608 | 158.0717 | 185.1767 | 5.5178 |
| 134.3850 | 158.3481 | 4.2411 | 153.5839 | 185.1767 | 4.2591 |
| 131.2854 | 158.3481 | 2.2699 | 150.8140 | 185.1767 | 2.6565 |
| 130.1899 | 158.3481 | 0.0609 | 149.8286 | 185.1767 | 0.7062 |
| 131.1157 | 158.3481 | -2.6088 | 150.6551 | 185.1767 | -1.4594 |
| 134.0748 | 158.3481 | -4.6772 | 153.2969 | 185.1767 | -3.1737 |
| 138.9817 | 158.3481 | -6.4528 | 157.6802 | 185.1767 | -4.6222 |
| 145.7092 | 158.3481 | -8.0784 | 163.6875 | 185.1767 | -6.0159 |
| 154.0913 | 158.3481 | -9.5206 | 171.1715 | 185.1767 | -7.3030 |
| 163.9224 | 158.3481 | -10.7256 | 179.9493 | 185.1767 | -8.4176 |
| 174.9617 | 158.3481 | -11.6236 | 189.8066 | 185.1767 | -9.2863 |
| 186.9394 | 158.3481 | -12.1340 | 200.5028 | 185.1767 | -9.8286 |
| 199.5630 | 158.3481 | -12.1752 | 211.7769 | 185.1767 | -9.9707 |
| 212.5249 | 158.3481 | -11.6517 | 223.3557 | 185.1767 | -9.5991 |
| 225.5074 | 158.3481 | -10.5376 | 234.9566 | 185.1767 | -8.6527 |
| 238.1847 | 158.3481 | -9.0364 | 246.2889 | 185.1767 | -7.2905 |
| 250.2334 | 158.3481 | -7.5060 | 257.0603 | 185.1767 | -5.8850 |
| 261.3469 | 158.3481 | -6.2642 | 266.9932 | 185.1767 | -4.7905 |
| 271.2476 | 158.3481 | -5.4759 | 275.8376 | 185.1767 | -4.1795 |
| 279.6907 | 158.3481 | -5.1662 | 283.3760 | 185.1767 | -4.0665 |
| 286.4731 | 158.3481 | -5.2075 | 289.4280 | 185.1767 | -4.2994 |
| 291.4336 | 158.3481 | -5.4489 | 293.8521 | 185.1767 | -4.6937 |
| 294.4546 | 158.3481 | -5.7394 | 296.5457 | 185.1767 | -5.0710 |
| 295.4683 | 158.3481 | -5.8868 | 297.4492 | 185.1767 | -5.2442 |

ORIGINAL PAGE IS
OF POOR QUALITY.

ETA = .3683

ETA = .4134

| X | Y | Z | X | Y | Z |
|----------|----------|---------|----------|----------|---------|
| 299.5388 | 213.1270 | -3.9665 | 304.8037 | 239.2250 | -2.7197 |
| 298.7507 | 213.1270 | -3.7632 | 304.0823 | 239.2250 | -2.5266 |
| 296.4021 | 213.1270 | -3.2370 | 301.9338 | 239.2250 | -2.0274 |
| 292.5471 | 213.1270 | -2.4852 | 298.4099 | 239.2250 | -1.3360 |
| 287.2839 | 213.1270 | -1.4571 | 293.5979 | 239.2250 | -0.4241 |
| 280.7383 | 213.1270 | -0.2673 | 287.6147 | 239.2250 | 0.5873 |
| 273.0676 | 213.1270 | 0.9742 | 280.6060 | 239.2250 | 1.5921 |
| 264.4583 | 213.1270 | 2.1731 | 272.7432 | 239.2250 | 2.5099 |
| 255.1194 | 213.1270 | 3.2376 | 264.2195 | 239.2250 | 3.2715 |
| 245.2808 | 213.1270 | 4.1430 | 255.2447 | 239.2250 | 3.8699 |
| 235.1844 | 213.1270 | 4.8557 | 246.0395 | 239.2250 | 4.2771 |
| 225.0824 | 213.1270 | 5.4406 | 236.8319 | 239.2250 | 4.5454 |
| 215.2270 | 213.1270 | 5.9594 | 227.8493 | 239.2250 | 4.7171 |
| 205.8567 | 213.1270 | 6.3089 | 219.3116 | 239.2250 | 4.7136 |
| 197.1994 | 213.1270 | 6.4135 | 211.4283 | 239.2250 | 4.4945 |
| 189.4676 | 213.1270 | 6.2556 | 204.3933 | 239.2250 | 4.0493 |
| 182.8516 | 213.1270 | 5.8357 | 198.3798 | 239.2250 | 3.3941 |
| 177.5141 | 213.1270 | 5.1612 | 193.5361 | 239.2250 | 2.5531 |
| 173.5879 | 213.1270 | 4.2787 | 189.9821 | 239.2250 | 1.5830 |
| 171.1633 | 213.1270 | 3.0661 | 187.8039 | 239.2250 | 0.4283 |
| 170.2925 | 213.1270 | 1.3788 | 187.0548 | 239.2250 | -0.8970 |
| 171.0172 | 213.1270 | -0.2756 | 187.7534 | 239.2250 | -2.3553 |
| 173.3306 | 213.1270 | -1.6065 | 189.8925 | 239.2250 | -3.3595 |
| 177.1696 | 213.1270 | -2.7192 | 193.4143 | 239.2250 | -4.1657 |
| 182.4274 | 213.1270 | -3.8691 | 198.2279 | 239.2250 | -4.9819 |
| 188.9758 | 213.1270 | -4.9942 | 204.2155 | 239.2250 | -5.7558 |
| 196.6561 | 213.1270 | -6.0143 | 211.2301 | 239.2250 | -6.4368 |
| 205.2814 | 213.1270 | -6.8517 | 219.0998 | 239.2250 | -6.9657 |
| 214.6417 | 213.1270 | -7.4281 | 227.6320 | 239.2250 | -7.2671 |
| 224.5091 | 213.1270 | -7.6742 | 236.6178 | 239.2250 | -7.2603 |
| 234.6460 | 213.1270 | -7.4595 | 245.8381 | 239.2250 | -6.8309 |
| 244.8073 | 213.1270 | -6.6886 | 255.0677 | 239.2250 | -5.8914 |
| 254.7387 | 213.1270 | -5.4708 | 264.0779 | 239.2250 | -4.5376 |
| 264.1799 | 213.1270 | -4.1950 | 272.6406 | 239.2250 | -3.1444 |
| 272.8828 | 213.1270 | -3.2544 | 280.5391 | 239.2250 | -2.1020 |
| 280.6262 | 213.1270 | -2.8339 | 287.5750 | 239.2250 | -1.6003 |
| 287.2202 | 213.1270 | -2.9194 | 293.5757 | 239.2250 | -1.6537 |
| 292.5093 | 213.1270 | -3.3542 | 298.3962 | 239.2250 | -2.0913 |
| 296.3728 | 213.1270 | -3.9071 | 301.9224 | 239.2250 | -2.6646 |
| 298.7239 | 213.1270 | -4.3747 | 304.0710 | 239.2250 | -3.1427 |
| 299.5125 | 213.1270 | -4.5746 | 304.7925 | 239.2250 | -3.3440 |

ORIGINAL PAGE IS
OF POOR QUALITY

ETA = .4937

ETA = .5488

| X | Y | Z | X | Y | Z |
|----------|----------|---------|----------|----------|---------|
| 319.6018 | 285.7209 | -0.0330 | 329.9924 | 317.5776 | -0.2747 |
| 318.9441 | 285.7209 | 0.1507 | 329.3752 | 317.5776 | -0.0629 |
| 316.9878 | 285.7209 | 0.6158 | 327.5398 | 317.5776 | 0.4694 |
| 313.7822 | 285.7209 | 1.2027 | 324.5334 | 317.5776 | 1.1367 |
| 309.4062 | 285.7209 | 1.9398 | 320.4299 | 317.5776 | 1.9359 |
| 303.9680 | 285.7209 | 2.7481 | 315.3315 | 317.5776 | 2.7829 |
| 297.6021 | 285.7209 | 3.5266 | 309.3643 | 317.5776 | 3.5706 |
| 290.4656 | 285.7209 | 4.2009 | 302.6760 | 317.5776 | 4.2245 |
| 282.7344 | 285.7209 | 4.7141 | 295.4316 | 317.5776 | 4.7074 |
| 274.5994 | 285.7209 | 5.0614 | 287.8093 | 317.5776 | 5.0260 |
| 266.2603 | 285.7209 | 5.2351 | 279.9971 | 317.5776 | 5.1558 |
| 257.9226 | 285.7209 | 5.2264 | 272.1873 | 317.5776 | 5.0730 |
| 249.7919 | 285.7209 | 5.0531 | 264.5720 | 317.5776 | 4.7966 |
| 242.0677 | 285.7209 | 4.7363 | 257.3389 | 317.5776 | 4.3584 |
| 234.9405 | 285.7209 | 4.2811 | 250.6656 | 317.5776 | 3.7599 |
| 228.5858 | 285.7209 | 3.6846 | 244.7167 | 317.5776 | 3.0172 |
| 223.1604 | 285.7209 | 2.9236 | 239.6387 | 317.5776 | 2.1494 |
| 218.7982 | 285.7209 | 1.9933 | 235.5564 | 317.5776 | 1.1840 |
| 215.6061 | 285.7209 | 0.9609 | 232.5705 | 317.5776 | 0.1420 |
| 213.6624 | 285.7209 | -0.0978 | 230.7536 | 317.5776 | -0.8707 |
| 213.0153 | 285.7209 | -1.1971 | 230.1492 | 317.5776 | -1.7362 |
| 213.6811 | 285.7209 | -2.3687 | 230.7786 | 317.5776 | -2.9724 |
| 215.6401 | 285.7209 | -3.1803 | 232.6161 | 317.5776 | -3.6820 |
| 218.8460 | 285.7209 | -3.8292 | 235.6210 | 317.5776 | -4.2292 |
| 223.2210 | 285.7209 | -4.4513 | 239.7206 | 317.5776 | -4.7211 |
| 228.6571 | 285.7209 | -4.9933 | 244.8137 | 317.5776 | -5.1151 |
| 235.0203 | 285.7209 | -5.4288 | 250.7749 | 317.5776 | -5.4009 |
| 242.1536 | 285.7209 | -5.7158 | 257.4570 | 317.5776 | -5.5499 |
| 249.8810 | 285.7209 | -5.7840 | 264.6951 | 317.5776 | -5.5105 |
| 258.0112 | 285.7209 | -5.5590 | 272.3101 | 317.5776 | -5.2173 |
| 266.3440 | 285.7209 | -4.9500 | 280.1135 | 317.5776 | -4.6066 |
| 274.6726 | 285.7209 | -3.8493 | 287.9121 | 317.5776 | -3.5856 |
| 282.7925 | 285.7209 | -2.3327 | 295.5144 | 317.5776 | -2.2211 |
| 290.5063 | 285.7209 | -0.7720 | 302.7363 | 317.5776 | -0.8315 |
| 297.6274 | 285.7209 | 0.4326 | 309.4041 | 317.5776 | 0.2295 |
| 303.9817 | 285.7209 | 1.0771 | 315.3555 | 317.5776 | 0.7783 |
| 309.4133 | 285.7209 | 1.0817 | 320.4438 | 317.5776 | 0.7638 |
| 313.7869 | 285.7209 | 0.6533 | 324.5425 | 317.5776 | 0.3604 |
| 316.9922 | 285.7209 | 0.0694 | 327.5476 | 317.5776 | -0.1855 |
| 318.9487 | 285.7209 | -0.4106 | 329.3818 | 317.5776 | -0.6327 |
| 319.6067 | 285.7209 | -0.6092 | 329.9990 | 317.5776 | -0.8159 |

ORIGINAL PAGE IS
OF POOR QUALITY

ETA = .5939

ETA = .6258

| X | Y | Z | X | Y | Z |
|----------|----------|---------|----------|----------|---------|
| 338.6877 | 343.6768 | 0.0671 | 344.6692 | 362.1445 | -0.3359 |
| 338.1067 | 343.6768 | 0.2660 | 344.1128 | 362.1445 | -0.1341 |
| 336.3772 | 343.6768 | 0.7708 | 342.4565 | 362.1445 | 0.3810 |
| 333.5413 | 343.6768 | 1.4113 | 339.7402 | 362.1445 | 1.0470 |
| 329.6689 | 343.6768 | 2.1740 | 336.0303 | 362.1445 | 1.8296 |
| 324.8550 | 343.6768 | 2.9894 | 331.4180 | 362.1445 | 2.6579 |
| 319.2175 | 343.6768 | 3.7627 | 326.0159 | 362.1445 | 3.4381 |
| 312.8953 | 343.6768 | 4.4299 | 319.9570 | 362.1445 | 4.1091 |
| 306.0442 | 343.6768 | 4.9594 | 313.3901 | 362.1445 | 4.6443 |
| 298.8325 | 343.6768 | 5.3496 | 306.4775 | 362.1445 | 5.0435 |
| 291.4377 | 343.6768 | 5.5732 | 299.3887 | 362.1445 | 5.2772 |
| 284.0422 | 343.6768 | 5.6197 | 292.2986 | 362.1445 | 5.3351 |
| 276.8281 | 343.6768 | 5.5172 | 285.3816 | 362.1445 | 5.2452 |
| 269.9731 | 343.6768 | 5.2904 | 278.8088 | 362.1445 | 5.0379 |
| 263.6460 | 343.6768 | 4.9395 | 272.7415 | 362.1445 | 4.7139 |
| 258.0024 | 343.6768 | 4.4637 | 267.3293 | 362.1445 | 4.2644 |
| 253.1816 | 343.6768 | 3.8549 | 262.7051 | 362.1445 | 3.6809 |
| 249.3017 | 343.6768 | 3.1103 | 258.9829 | 362.1445 | 2.9724 |
| 246.4584 | 343.6768 | 2.2449 | 256.2542 | 362.1445 | 2.1561 |
| 244.7218 | 343.6768 | 1.2857 | 254.5859 | 362.1445 | 1.2024 |
| 244.1348 | 343.6768 | 0.2778 | 254.0192 | 362.1445 | 0.1714 |
| 244.7114 | 343.6768 | -0.8070 | 254.5679 | 362.1445 | -0.9575 |
| 246.4390 | 343.6768 | -1.6752 | 256.2207 | 362.1445 | -1.8650 |
| 249.2745 | 343.6768 | -2.3827 | 258.9363 | 362.1445 | -2.5988 |
| 253.1474 | 343.6768 | -3.0469 | 262.6472 | 362.1445 | -3.2723 |
| 257.9624 | 343.6768 | -3.6263 | 267.2615 | 362.1445 | -3.8522 |
| 263.6013 | 343.6768 | -4.1008 | 272.6663 | 362.1445 | -4.3211 |
| 269.9250 | 343.6768 | -4.4409 | 278.7280 | 362.1445 | -4.6551 |
| 276.7781 | 343.6768 | -4.5863 | 285.2979 | 362.1445 | -4.8045 |
| 283.9924 | 343.6768 | -4.4693 | 292.2148 | 362.1445 | -4.6987 |
| 291.3904 | 343.6768 | -4.0029 | 299.3093 | 362.1445 | -4.2476 |
| 298.7905 | 343.6768 | -3.1029 | 306.4072 | 362.1445 | -3.3851 |
| 306.0105 | 343.6768 | -1.8422 | 313.3333 | 362.1445 | -2.1937 |
| 312.8708 | 343.6768 | -0.5290 | 319.9148 | 362.1445 | -0.9562 |
| 319.2012 | 343.6768 | 0.4883 | 325.9873 | 362.1445 | 0.0020 |
| 324.8452 | 343.6768 | 1.0200 | 331.3999 | 362.1445 | 0.5014 |
| 329.6631 | 343.6768 | 1.0152 | 336.0193 | 362.1445 | 0.5055 |
| 333.5376 | 343.6768 | 0.6395 | 339.7329 | 362.1445 | 0.1657 |
| 336.3740 | 343.6768 | 0.1293 | 342.4509 | 362.1445 | -0.3051 |
| 338.1040 | 343.6768 | -0.2831 | 344.1082 | 362.1445 | -0.6838 |
| 338.6853 | 343.6768 | -0.4483 | 344.6650 | 362.1445 | -0.8329 |

ORIGINAL PAGE IS
OF POOR QUALITY

ETA = .7138

ETA = .8195

| X | Y | Z | X | Y | Z |
|----------|----------|---------|----------|----------|---------|
| 361.4495 | 413.0933 | 0.7638 | 381.1624 | 474.2329 | 1.4374 |
| 360.9570 | 413.0933 | 0.9207 | 380.7522 | 474.2329 | 1.5443 |
| 359.4924 | 413.0933 | 1.3350 | 379.5327 | 474.2329 | 1.8440 |
| 357.0920 | 413.0933 | 1.8976 | 377.5339 | 474.2329 | 2.3097 |
| 353.8157 | 413.0933 | 2.5535 | 374.8066 | 474.2329 | 2.8473 |
| 349.7444 | 413.0933 | 3.2214 | 371.4197 | 474.2329 | 3.3653 |
| 344.9785 | 413.0933 | 3.8210 | 367.4570 | 474.2329 | 3.8048 |
| 339.6357 | 413.0933 | 4.3070 | 363.0168 | 474.2329 | 4.1398 |
| 333.8479 | 413.0933 | 4.6644 | 358.2083 | 474.2329 | 4.3652 |
| 327.7573 | 413.0933 | 4.8949 | 353.1492 | 474.2329 | 4.4869 |
| 321.5137 | 413.0933 | 4.9842 | 347.9646 | 474.2329 | 4.5062 |
| 315.2710 | 413.0933 | 4.9401 | 342.7815 | 474.2329 | 4.4322 |
| 309.1831 | 413.0933 | 4.7743 | 337.7278 | 474.2329 | 4.2687 |
| 303.3992 | 413.0933 | 4.5080 | 332.9280 | 474.2329 | 4.0199 |
| 298.0620 | 413.0933 | 4.1538 | 328.5000 | 474.2329 | 3.6908 |
| 293.3032 | 413.0933 | 3.7153 | 324.5530 | 474.2329 | 3.2884 |
| 289.2397 | 413.0933 | 3.1863 | 321.1843 | 474.2329 | 2.8189 |
| 285.9717 | 413.0933 | 2.5660 | 318.4771 | 474.2329 | 2.2781 |
| 283.5801 | 413.0933 | 1.8579 | 316.4985 | 474.2329 | 1.6498 |
| 282.1238 | 413.0933 | 0.9977 | 315.2988 | 474.2329 | 0.8798 |
| 281.6392 | 413.0933 | 0.0034 | 314.9072 | 474.2329 | 0.0002 |
| 282.1370 | 413.0933 | -0.9837 | 315.3313 | 474.2329 | -0.8690 |
| 283.6042 | 413.0933 | -1.8095 | 316.5583 | 474.2329 | -1.5839 |
| 286.0049 | 413.0933 | -2.4480 | 318.5583 | 474.2329 | -2.1127 |
| 289.2805 | 413.0933 | -2.9881 | 321.2832 | 474.2329 | -2.5238 |
| 293.3503 | 413.0933 | -3.4244 | 324.6663 | 474.2329 | -2.8309 |
| 298.1145 | 413.0933 | -3.7485 | 328.6245 | 474.2329 | -3.0329 |
| 303.4551 | 413.0933 | -3.9390 | 333.0601 | 474.2329 | -3.1123 |
| 309.2407 | 413.0933 | -3.9639 | 337.8633 | 474.2329 | -3.0506 |
| 315.3286 | 413.0933 | -3.7559 | 342.9153 | 474.2329 | -2.7977 |
| 321.5681 | 413.0933 | -3.2390 | 348.0906 | 474.2329 | -2.2978 |
| 327.8052 | 413.0933 | -2.3645 | 353.2603 | 474.2329 | -1.5119 |
| 333.8867 | 413.0933 | -1.2096 | 358.2983 | 474.2329 | -0.5013 |
| 339.6646 | 413.0933 | -0.0247 | 363.0837 | 474.2329 | 0.5289 |
| 344.9978 | 413.0933 | 0.8955 | 367.5029 | 474.2329 | 1.3319 |
| 349.7563 | 413.0933 | 1.3888 | 371.4492 | 474.2329 | 1.7731 |
| 353.8232 | 413.0933 | 1.4165 | 374.8257 | 474.2329 | 1.8253 |
| 357.0972 | 413.0933 | 1.1360 | 377.5464 | 474.2329 | 1.6318 |
| 359.4963 | 413.0933 | 0.7348 | 379.5420 | 474.2329 | 1.3337 |
| 360.9604 | 413.0933 | 0.4174 | 380.7605 | 474.2329 | 1.0986 |
| 361.4526 | 413.0933 | 0.2988 | 381.1702 | 474.2329 | 1.0162 |

ORIGINAL PAGE IS
OF POOR QUALITY

ETA = 1.0

| X | Y | Z |
|----------|----------|---------|
| 416.1240 | 578.6787 | 2.6707 |
| 415.8425 | 578.6787 | 2.7350 |
| 415.0063 | 578.6787 | 2.9097 |
| 413.6370 | 578.6787 | 3.1718 |
| 411.7708 | 578.6787 | 3.4643 |
| 409.4568 | 578.6787 | 3.7281 |
| 406.7539 | 578.6787 | 3.9254 |
| 403.7290 | 578.6787 | 4.0398 |
| 400.4568 | 578.6787 | 4.0712 |
| 397.0171 | 578.6787 | 4.0244 |
| 393.4949 | 578.6787 | 3.9036 |
| 389.9763 | 578.6787 | 3.7163 |
| 386.5479 | 578.6787 | 3.4715 |
| 383.2939 | 578.6787 | 3.1761 |
| 380.2947 | 578.6787 | 2.8369 |
| 377.6240 | 578.6787 | 2.4617 |
| 375.3477 | 578.6787 | 2.0563 |
| 373.5225 | 578.6787 | 1.6210 |
| 372.1943 | 578.6787 | 1.1481 |
| 371.3989 | 578.6787 | 0.5997 |
| 371.1550 | 578.6787 | -0.0004 |
| 371.4648 | 578.6787 | -0.5722 |
| 372.3164 | 578.6787 | -1.0192 |
| 373.6882 | 578.6787 | -1.3240 |
| 375.5496 | 578.6787 | -1.5328 |
| 377.8557 | 578.6787 | -1.6554 |
| 380.5496 | 578.6787 | -1.6925 |
| 383.5647 | 578.6787 | -1.6365 |
| 386.8262 | 578.6787 | -1.4744 |
| 390.2517 | 578.6787 | -1.1765 |
| 393.7542 | 578.6787 | -0.7064 |
| 397.2458 | 578.6787 | -0.0415 |
| 400.6423 | 578.6787 | 0.7734 |
| 403.8665 | 578.6787 | 1.5957 |
| 406.8479 | 578.6787 | 2.2556 |
| 409.5171 | 578.6787 | 2.6569 |
| 411.8093 | 578.6787 | 2.7799 |
| 413.6624 | 578.6787 | 2.7188 |
| 415.0256 | 578.6787 | 2.5659 |
| 415.8594 | 578.6787 | 2.4360 |
| 416.1399 | 578.6787 | 2.3895 |

TABLE 2
UP-OUTBOARD PROPFAN ROTATION OVERWING
CONTOURED NACELLE GEOMETRY

ORIGINAL PAGE IS
OF POOR QUALITY

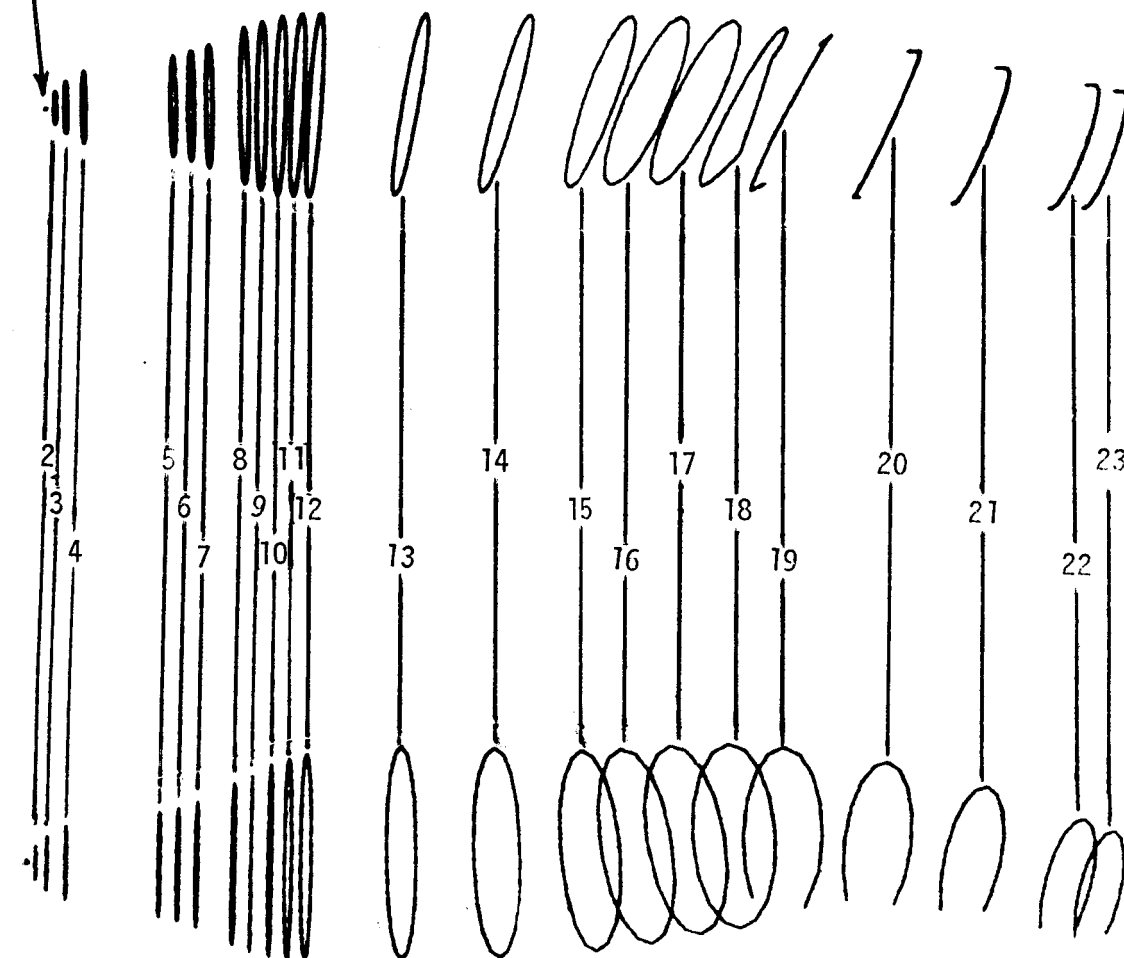
SPINNER POINT:

X = -9.218

Y = 266.6243

Z = -1.7109

TOP VIEW



SIDE VIEW

UP-OUTBOARD PROPFAN ROTATION OVERWING CONTOURED NACELLE GEOMETRY

PRECEDING PAGE BLANK NOT FILMED

ORIGINAL PAGE IS
OF POOR QUALITY

2

| X | Y | Z |
|---------|----------|---------|
| -7.2039 | 266.6660 | 3.3132 |
| -7.2212 | 268.5410 | 2.9408 |
| -7.1929 | 270.1313 | 1.8804 |
| -7.1234 | 271.1953 | 0.2934 |
| -7.0233 | 271.5706 | -1.5787 |
| -6.9079 | 271.1997 | -3.4507 |
| -6.7945 | 270.1396 | -5.0378 |
| -6.7007 | 268.5518 | -6.0982 |
| -6.6406 | 266.6775 | -6.4706 |
| -6.6233 | 264.8022 | -6.0982 |
| -6.6516 | 263.2117 | -5.0378 |
| -6.7211 | 262.1477 | -3.4507 |
| -6.8212 | 261.7727 | -1.5787 |
| -6.9367 | 262.1433 | 0.2934 |
| -7.0500 | 263.2036 | 1.8804 |
| -7.1438 | 264.7915 | 2.9408 |
| -7.2039 | 266.6660 | 3.3132 |

3

| X | Y | Z |
|---------|----------|---------|
| -4.1824 | 266.7283 | 6.4923 |
| -4.2102 | 269.7515 | 5.8919 |
| -4.1646 | 272.3157 | 4.1822 |
| -4.0526 | 274.0310 | 1.6235 |
| -3.8912 | 274.6357 | -1.3947 |
| -3.7050 | 274.0383 | -4.4129 |
| -3.5223 | 272.3289 | -6.9716 |
| -3.3710 | 269.7688 | -8.6813 |
| -3.2741 | 266.7471 | -9.2816 |
| -3.2463 | 263.7236 | -8.6813 |
| -3.2919 | 261.1592 | -6.9716 |
| -3.4039 | 259.4438 | -4.4129 |
| -3.5653 | 258.8391 | -1.3947 |
| -3.7515 | 259.4368 | 1.6235 |
| -3.9341 | 261.1460 | 4.1822 |
| -4.0354 | 263.7063 | 5.8919 |
| -4.1824 | 266.7283 | 6.4923 |

4

| X | Y | Z |
|--------|----------|----------|
| 1.1464 | 266.8381 | 9.6039 |
| 1.1088 | 270.9329 | 8.7907 |
| 1.1705 | 274.4062 | 6.4751 |
| 1.3222 | 276.7295 | 3.0095 |
| 1.5408 | 277.5486 | -1.0784 |
| 1.7930 | 276.7390 | -5.1664 |
| 2.0404 | 274.4241 | -8.6320 |
| 2.2453 | 270.9563 | -10.9476 |
| 2.3766 | 266.8635 | -11.7607 |
| 2.4143 | 262.7688 | -10.9476 |
| 2.3525 | 259.2954 | -8.6320 |
| 2.2008 | 256.9724 | -5.1664 |
| 1.9822 | 256.1531 | -1.0784 |
| 1.7301 | 256.9626 | 3.0095 |
| 1.4827 | 259.2773 | 6.4751 |
| 1.2777 | 262.7454 | 8.7907 |
| 1.1464 | 266.8381 | 9.6039 |

5

| X | Y | Z |
|---------|----------|----------|
| 28.0427 | 267.3931 | 15.5605 |
| 27.9895 | 273.1716 | 14.4130 |
| 28.0767 | 278.0732 | 11.1452 |
| 28.2908 | 281.3516 | 6.2545 |
| 28.5992 | 282.5076 | 0.4855 |
| 28.9551 | 281.3655 | -5.2834 |
| 29.3043 | 278.0986 | -10.1741 |
| 29.5935 | 273.2046 | -13.4419 |
| 29.7788 | 267.4290 | -14.5895 |
| 29.8319 | 261.6501 | -13.4419 |
| 29.7448 | 256.7485 | -10.1741 |
| 29.5307 | 253.4704 | -5.2834 |
| 29.2222 | 252.3144 | 0.4855 |
| 28.8663 | 253.4567 | 6.2545 |
| 28.5172 | 256.7231 | 11.1452 |
| 28.2279 | 261.6172 | 14.4130 |
| 28.0427 | 267.3931 | 15.5605 |

ORIGINAL PRICE
OF FOOD QUALITY

| 6 | | | 7 | | |
|---------|----------|----------|---------|----------|----------|
| X | Y | Z | X | Y | Z |
| 33.3636 | 267.5029 | 17.0690 | 38.8382 | 267.6160 | 19.3877 |
| 33.3063 | 273.7407 | 15.8303 | 38.7741 | 274.5806 | 18.0046 |
| 33.4003 | 279.0317 | 12.3028 | 38.8791 | 280.4885 | 14.0659 |
| 33.6314 | 282.5708 | 7.0235 | 39.1372 | 284.4399 | 8.1712 |
| 33.9644 | 283.8186 | 0.7960 | 39.5090 | 285.8335 | 1.2179 |
| 34.3486 | 282.5854 | -5.4314 | 39.9437 | 284.4568 | -5.8353 |
| 34.7254 | 279.0591 | -10.7107 | 40.3645 | 280.5193 | -11.7300 |
| 35.0376 | 273.7764 | -14.2383 | 40.7131 | 274.6206 | -15.6687 |
| 35.2377 | 267.5415 | -15.4770 | 40.9364 | 267.6592 | -17.0518 |
| 35.2950 | 261.3037 | -14.2383 | 41.0004 | 260.6941 | -15.6687 |
| 35.2010 | 256.0125 | -10.7107 | 40.8954 | 254.7864 | -11.7300 |
| 34.9699 | 252.4737 | -5.4314 | 40.6374 | 250.8349 | -5.8353 |
| 34.6369 | 251.2258 | 0.7960 | 40.2656 | 249.4416 | 1.1180 |
| 34.2527 | 252.4589 | 7.0235 | 39.8309 | 250.8183 | 8.1712 |
| 33.8758 | 255.9853 | 12.3028 | 39.4100 | 254.7557 | 14.0659 |
| 33.5636 | 261.2678 | 15.8303 | 39.0614 | 260.6541 | 18.0046 |
| 33.3636 | 267.5029 | 17.0690 | 38.8382 | 267.6160 | 19.3877 |

| 8 | | | 9 | | |
|---------|----------|----------|---------|----------|----------|
| X | Y | Z | X | Y | Z |
| 49.3076 | 267.8318 | 25.3997 | 54.3491 | 267.9687 | 27.7972 |
| 49.2266 | 276.6335 | 23.6519 | 54.4464 | 277.4592 | 25.9118 |
| 49.3593 | 284.0999 | 18.6744 | 54.7515 | 285.5046 | 20.5446 |
| 49.6854 | 289.0933 | 11.2250 | 55.2179 | 290.8806 | 12.5124 |
| 50.1553 | 290.8542 | 2.4379 | 55.7746 | 292.7683 | 3.0382 |
| 50.7376 | 289.1150 | -7.0481 | 55.8335 | 292.7683 | 2.0400 |
| 51.2694 | 284.1392 | -14.4975 | 56.3958 | 290.8806 | -7.4339 |
| 51.7100 | 276.6848 | -19.4750 | 56.8779 | 285.5046 | -15.4651 |
| 51.9922 | 267.8872 | -21.2229 | 57.2067 | 277.4592 | -20.8310 |
| 52.0731 | 259.0852 | -19.4750 | 57.3319 | 267.9687 | -22.7147 |
| 51.9404 | 251.6194 | -14.4975 | 57.2346 | 258.4783 | -20.8294 |
| 51.6143 | 246.6259 | -7.0481 | 56.9295 | 250.4326 | -15.4621 |
| 51.1444 | 244.8650 | 1.7390 | 56.4631 | 245.0567 | -7.4299 |
| 50.5621 | 246.6042 | 11.2250 | 55.9064 | 243.1690 | 2.0443 |
| 50.0303 | 251.5800 | 18.6744 | 55.8475 | 243.1690 | 3.0425 |
| 49.5898 | 259.0342 | 23.6519 | 55.2852 | 245.0567 | 12.5164 |
| 49.3076 | 267.8318 | 25.3997 | 54.8031 | 250.4326 | 20.5476 |
| | | | 54.4743 | 258.4783 | 25.9135 |
| | | | 54.3491 | 267.9687 | 27.7972 |

ORIGINAL PAGE IS
OF POOR QUALITY

| 10 | | | 11 | | |
|---------|----------|----------|---------|----------|----------|
| X | Y | Z | X | Y | Z |
| 59.6975 | 268.0894 | 31.5240 | 64.8300 | 268.2068 | 33.6941 |
| 60.0101 | 278.1135 | 29.5450 | 65.3507 | 278.4165 | 31.6903 |
| 60.5173 | 286.6121 | 23.8859 | 66.0461 | 287.0723 | 25.9347 |
| 61.1417 | 292.2903 | 15.4083 | 66.8104 | 292.8557 | 17.3035 |
| 61.7885 | 294.2844 | 5.4028 | 67.5271 | 294.8867 | 7.1108 |
| 61.9706 | 294.2844 | 2.4084 | 67.7989 | 294.8867 | 2.7692 |
| 62.5411 | 292.2903 | -7.6018 | 68.3590 | 292.8557 | -7.4334 |
| 62.9485 | 286.6121 | -16.0926 | 68.6771 | 287.0723 | -16.0925 |
| 63.1309 | 278.1135 | -21.7714 | 68.7050 | 278.4165 | -21.8899 |
| 63.0604 | 268.0894 | -23.7737 | 68.4382 | 268.2068 | -23.9430 |
| 62.7477 | 258.0649 | -21.7947 | 67.9175 | 257.9968 | -21.9392 |
| 62.2406 | 249.5666 | -16.1356 | 67.2220 | 249.3412 | -16.1835 |
| 61.6161 | 243.8882 | -7.6580 | 66.4578 | 243.5577 | -7.5524 |
| 60.9694 | 241.8942 | 2.3475 | 65.7411 | 241.5267 | 2.6404 |
| 60.7873 | 241.8942 | 5.3420 | 65.4693 | 241.5267 | 6.9819 |
| 60.2168 | 243.8882 | 15.3521 | 64.9092 | 243.5577 | 17.1845 |
| 59.8093 | 249.5666 | 23.8428 | 64.5910 | 249.3412 | 25.8436 |
| 59.6270 | 258.0649 | 29.5217 | 64.5632 | 257.9968 | 31.6410 |
| 59.6975 | 268.0894 | 31.5240 | 64.8300 | 268.2068 | 33.6941 |

| 12 | | | 13 | | |
|---------|----------|----------|----------|----------|----------|
| X | Y | Z | X | Y | Z |
| 69.8849 | 268.3254 | 35.3682 | 97.1578 | 269.0217 | 39.6049 |
| 70.6062 | 278.5642 | 33.3704 | 98.9257 | 279.1108 | 37.7048 |
| 71.4803 | 287.2441 | 27.6052 | 100.7421 | 287.6643 | 32.0417 |
| 72.3741 | 293.0439 | 18.9503 | 102.3306 | 293.3794 | 23.4776 |
| 73.1515 | 295.0806 | 8.7232 | 103.4493 | 295.3865 | 13.3163 |
| 73.5119 | 295.0806 | 3.1348 | 104.0746 | 295.3865 | 5.3407 |
| 74.0546 | 293.0439 | -7.1074 | 104.5531 | 293.3794 | -4.8707 |
| 74.2799 | 287.2441 | -15.8054 | 104.3187 | 287.6643 | -13.5778 |
| 74.1535 | 278.5642 | -21.6351 | 103.4070 | 279.1108 | -19.4548 |
| 73.6947 | 268.3254 | -23.7090 | 101.9569 | 269.0217 | -21.6072 |
| 72.9734 | 258.0864 | -21.7112 | 100.1890 | 258.9324 | -19.7071 |
| 72.0992 | 249.4065 | -15.9461 | 98.3726 | 250.3791 | -14.0439 |
| 71.2054 | 243.6069 | -7.2911 | 96.7841 | 244.6639 | -5.4798 |
| 70.4280 | 241.5702 | 2.9360 | 95.6654 | 242.6570 | 4.6815 |
| 70.0676 | 241.5702 | 8.5244 | 95.0401 | 242.6570 | 12.6570 |
| 69.5250 | 243.6069 | 18.7666 | 94.5616 | 244.6639 | 22.8685 |
| 69.2997 | 249.4065 | 27.4646 | 94.7960 | 250.3791 | 31.5755 |
| 69.4261 | 258.0864 | 33.2943 | 95.7076 | 258.9324 | 37.4525 |
| 69.8849 | 268.3254 | 35.3682 | 97.1578 | 269.0217 | 39.6049 |

ORIGINAL PAGE IS
OF POOR QUALITY

| 14 | | | 15 | | |
|----------|----------|----------|----------|----------|----------|
| X | Y | Z | X | Y | Z |
| 124.2681 | 269.8396 | 41.1261 | 150.3350 | 270.7959 | 42.2876 |
| 127.0502 | 279.7246 | 39.3725 | 154.1013 | 280.4033 | 40.8594 |
| 129.8298 | 288.1047 | 33.8428 | 157.9676 | 288.5483 | 35.6400 |
| 132.1839 | 293.7043 | 25.3791 | 161.3453 | 293.9905 | 27.4239 |
| 133.7540 | 295.6707 | 15.2698 | 163.7202 | 295.9016 | 17.4621 |
| 134.4896 | 295.6707 | 8.2080 | 164.5319 | 295.9016 | 12.6298 |
| 135.0367 | 293.7043 | -2.0080 | 165.5424 | 293.9905 | 2.4387 |
| 134.4775 | 288.1047 | -10.7752 | 165.0347 | 288.5483 | -6.4300 |
| 132.8972 | 279.7246 | -16.7589 | 163.0860 | 280.4033 | -12.6263 |
| 130.5363 | 269.8396 | -19.0483 | 159.9932 | 270.7959 | -15.2067 |
| 127.7542 | 259.9543 | -17.2946 | 156.2269 | 261.1882 | -13.7785 |
| 124.9745 | 251.5743 | -11.7651 | 152.3606 | 253.0434 | -8.5591 |
| 122.6205 | 245.9749 | -3.3013 | 148.9829 | 247.6012 | -0.3430 |
| 121.0504 | 244.0085 | 6.8081 | 146.6080 | 245.6900 | 9.6188 |
| 120.3148 | 244.0085 | 13.8699 | 145.7962 | 245.6900 | 14.4511 |
| 119.7677 | 245.9749 | 24.0858 | 144.7857 | 247.6012 | 24.6422 |
| 120.3268 | 251.5743 | 32.8530 | 145.2935 | 253.0434 | 33.5109 |
| 121.9072 | 259.9543 | 38.8367 | 147.2421 | 261.1882 | 39.7072 |
| 124.2681 | 269.8396 | 41.1261 | 150.3350 | 270.7959 | 42.2876 |

| 16 | | | 17 | | |
|----------|----------|----------|----------|----------|---------|
| X | Y | Z | X | Y | Z |
| 162.3763 | 271.1868 | 43.4952 | 176.4236 | 270.9456 | 45.5252 |
| 166.6197 | 280.5981 | 42.4312 | 181.0272 | 280.1130 | 44.5949 |
| 171.1621 | 288.5771 | 37.5914 | 185.8961 | 287.8850 | 39.9049 |
| 175.3120 | 293.9084 | 29.7127 | 190.2889 | 293.0781 | 32.1693 |
| 178.4374 | 295.7805 | 19.9943 | 193.5369 | 294.9016 | 22.5656 |
| 179.3241 | 295.7805 | 16.2992 | 194.1378 | 294.9016 | 20.1388 |
| 180.9494 | 293.9084 | 6.2209 | 195.7465 | 293.0781 | 10.1292 |
| 180.8269 | 288.5771 | -2.6832 | 195.4709 | 287.8850 | 1.2375 |
| 178.9755 | 280.5981 | -9.0573 | 193.3531 | 280.1130 | -5.1825 |
| 175.6770 | 271.1868 | -11.9312 | 189.7155 | 270.9456 | -8.1535 |
| 171.4335 | 261.7751 | -10.8672 | 185.1118 | 261.7778 | -7.2232 |
| 166.8911 | 253.7964 | -6.0274 | 180.2430 | 254.0060 | -2.5332 |
| 162.7412 | 248.4649 | 1.8514 | 175.8501 | 248.8129 | 5.2025 |
| 159.6158 | 246.5929 | 11.5698 | 172.6022 | 246.9893 | 14.8062 |
| 158.7291 | 246.5929 | 15.2649 | 172.0013 | 246.9893 | 17.2329 |
| 157.1038 | 248.4649 | 25.3432 | 170.3926 | 248.8129 | 27.2425 |
| 157.2264 | 253.7964 | 34.2472 | 170.6682 | 254.0060 | 36.1342 |
| 159.0778 | 261.7751 | 40.6214 | 172.7859 | 261.7778 | 42.5542 |
| 162.3763 | 271.1868 | 43.4952 | 176.4236 | 270.9456 | 45.5252 |

ORIGINAL PAGE IS
OF POOR QUALITY

18

| X | Y | Z |
|----------|----------|---------|
| 193.2558 | 269.8447 | 47.2171 |
| 198.0875 | 278.7566 | 45.9019 |
| 202.7557 | 286.3123 | 40.8395 |
| 206.5494 | 291.3606 | 32.8005 |
| 208.8912 | 293.1333 | 23.0088 |
| 209.0489 | 293.1333 | 21.9201 |
| 209.5822 | 291.9526 | 11.8664 |
| 208.2259 | 288.5906 | 3.0813 |
| 205.1863 | 283.5581 | -3.0978 |
| 200.9265 | 269.8447 | -5.7301 |
| 196.0947 | 256.1309 | -4.4149 |
| 191.4265 | 251.0988 | 0.6475 |
| 187.6328 | 247.7366 | 8.6865 |
| 185.2910 | 246.5560 | 18.4782 |
| 185.1333 | 246.5560 | 19.5669 |
| 184.6000 | 248.3287 | 29.6206 |
| 185.9564 | 253.3771 | 38.4057 |
| 188.9959 | 260.9326 | 44.5848 |
| 193.2558 | 269.8447 | 47.2171 |

19

| X | Y | Z |
|----------|----------|---------|
| 203.7980 | 247.6231 | 3.3964 |
| 201.0166 | 246.0843 | 11.1786 |
| 199.5693 | 245.5047 | 20.9073 |
| 199.8554 | 247.2450 | 31.0380 |
| 201.8637 | 252.2007 | 39.4748 |
| 205.2708 | 259.6172 | 45.2329 |
| 209.5582 | 268.3660 | 47.4356 |
| 214.0730 | 277.1145 | 45.7476 |
| 218.1280 | 284.5312 | 40.4258 |
| 221.1058 | 289.4868 | 32.2805 |
| 222.5706 | 291.2271 | 22.2522 |
| 222.2670 | 290.6475 | 12.4211 |
| 218.9035 | 288.1243 | 1.5566 |

20

| X | Y | Z |
|----------|----------|---------|
| 231.2213 | 243.7296 | 4.6902 |
| 229.5094 | 243.7258 | 13.0536 |
| 229.1831 | 243.7258 | 22.1098 |
| 230.3605 | 245.3600 | 31.3965 |
| 232.8371 | 250.0143 | 38.9462 |
| 236.2493 | 256.9795 | 43.9092 |
| 240.0778 | 265.1958 | 45.5300 |
| 243.7398 | 273.4119 | 43.5617 |
| 246.6778 | 280.3772 | 38.3040 |
| 248.4445 | 285.0315 | 30.5574 |
| 248.7569 | 286.6658 | 21.2016 |
| 247.5933 | 286.6658 | 12.2145 |
| 244.9967 | 286.6809 | 4.5332 |

21

| X | Y | Z |
|----------|----------|---------|
| 258.7842 | 242.0561 | 3.8350 |
| 258.2595 | 242.0341 | 11.9376 |
| 258.7646 | 242.0341 | 20.2116 |
| 260.5046 | 243.5559 | 28.3264 |
| 263.2129 | 247.8893 | 35.0284 |
| 266.4778 | 254.3748 | 39.3071 |
| 269.8027 | 262.0249 | 40.5112 |
| 272.6809 | 269.6748 | 38.4573 |
| 274.6748 | 276.1604 | 33.4582 |
| 275.4807 | 280.4937 | 26.2748 |
| 274.9746 | 282.0156 | 17.9908 |
| 273.2356 | 282.0156 | 9.8859 |
| 271.4307 | 281.9805 | 4.6505 |

ORIGINAL PAGE IS
OF POOR QUALITY

| 22 | | | 23 | | |
|----------|----------|---------|----------|----------|---------|
| X | Y | Z | X | Y | Z |
| 287.9004 | 241.1779 | 0.6556 | 298.1560 | 241.4208 | -1.1110 |
| 287.6294 | 241.1805 | 8.1048 | 297.7847 | 241.4403 | 6.5725 |
| 288.5056 | 241.1805 | 15.4556 | 298.4824 | 241.4403 | 13.5172 |
| 290.3704 | 242.5616 | 22.6504 | 300.0767 | 242.7492 | 20.3123 |
| 292.9314 | 246.4949 | 28.5394 | 302.3242 | 246.4763 | 25.9235 |
| 295.8035 | 252.3811 | 32.2555 | 304.8833 | 252.0542 | 29.4963 |
| 298.5493 | 259.3247 | 33.2331 | 307.3645 | 258.6338 | 30.4870 |
| 300.7510 | 266.2681 | 31.3232 | 309.3892 | 265.2131 | 28.7447 |
| 302.0735 | 272.1545 | 26.8166 | 310.6499 | 270.7910 | 24.5346 |
| 302.3152 | 276.0876 | 20.3995 | 310.9548 | 274.5183 | 18.4977 |
| 301.4341 | 277.4687 | 13.0193 | 310.2568 | 275.8271 | 11.5530 |
| 299.5742 | 277.4687 | 5.8539 | 308.6628 | 275.8271 | 4.7579 |
| 298.4993 | 277.3857 | 1.9943 | 306.9634 | 275.8218 | 0.4535 |

8.0 APPENDICES

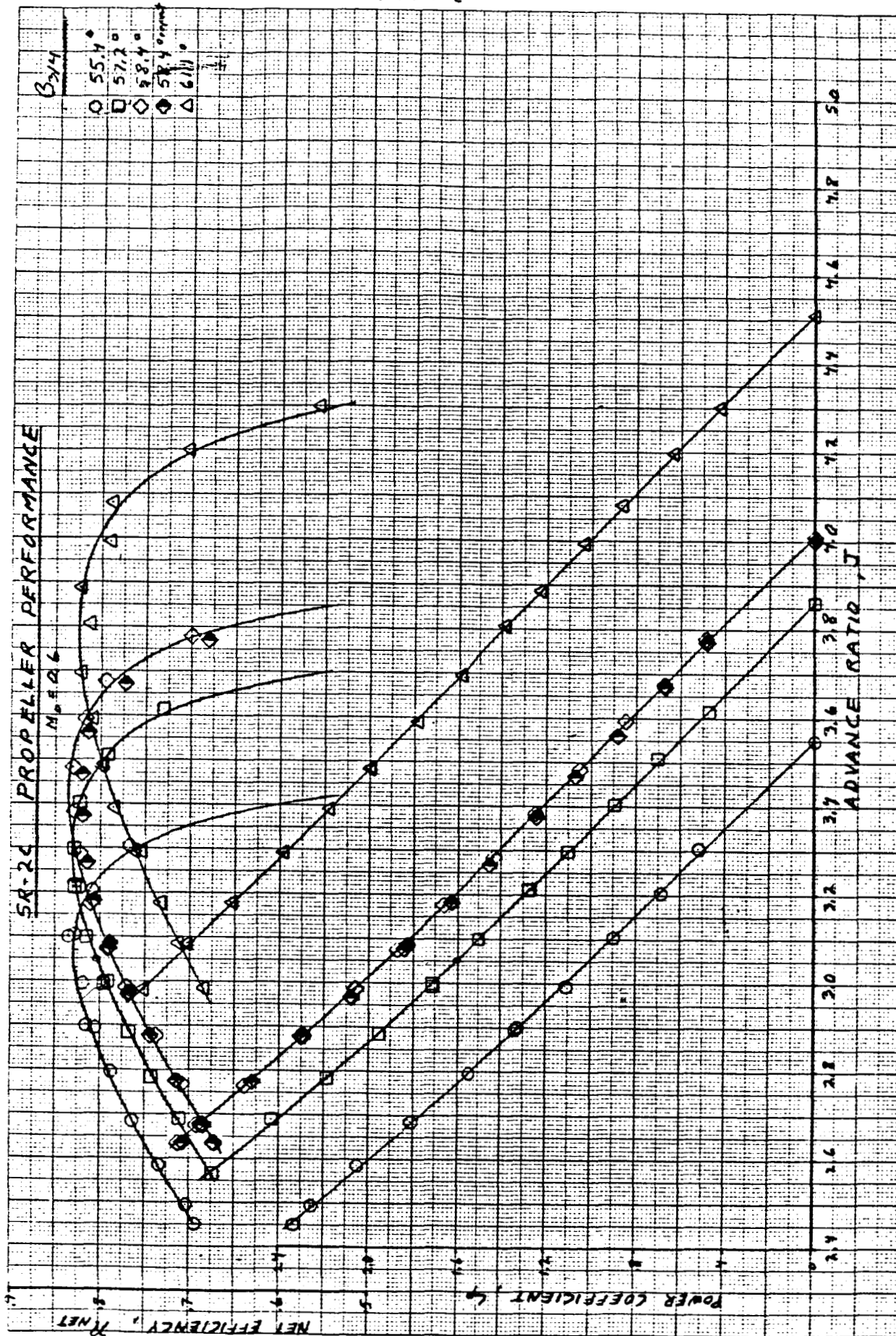
PRECEDING PAGE BLANK NOT FILMED

PAGE 44 INTENTIONALLY BLANK

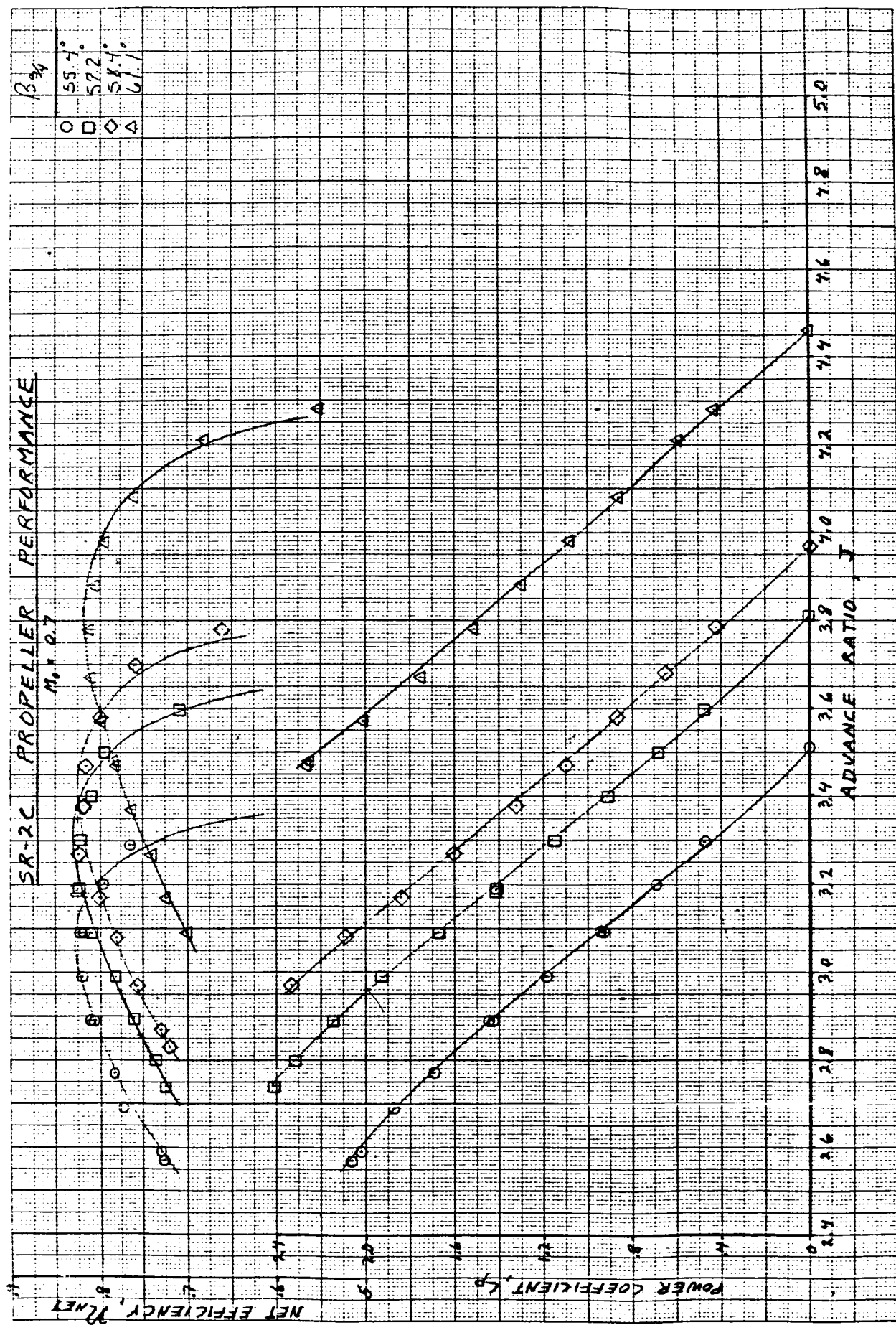
APPENDIX A
EXPERIMENTAL SR-2C
ISOLATED PROPELLER PERFORMANCE
OBTAINED AT NASA LEWIS

PRECEDING PAGE BLANK NOT FILMED

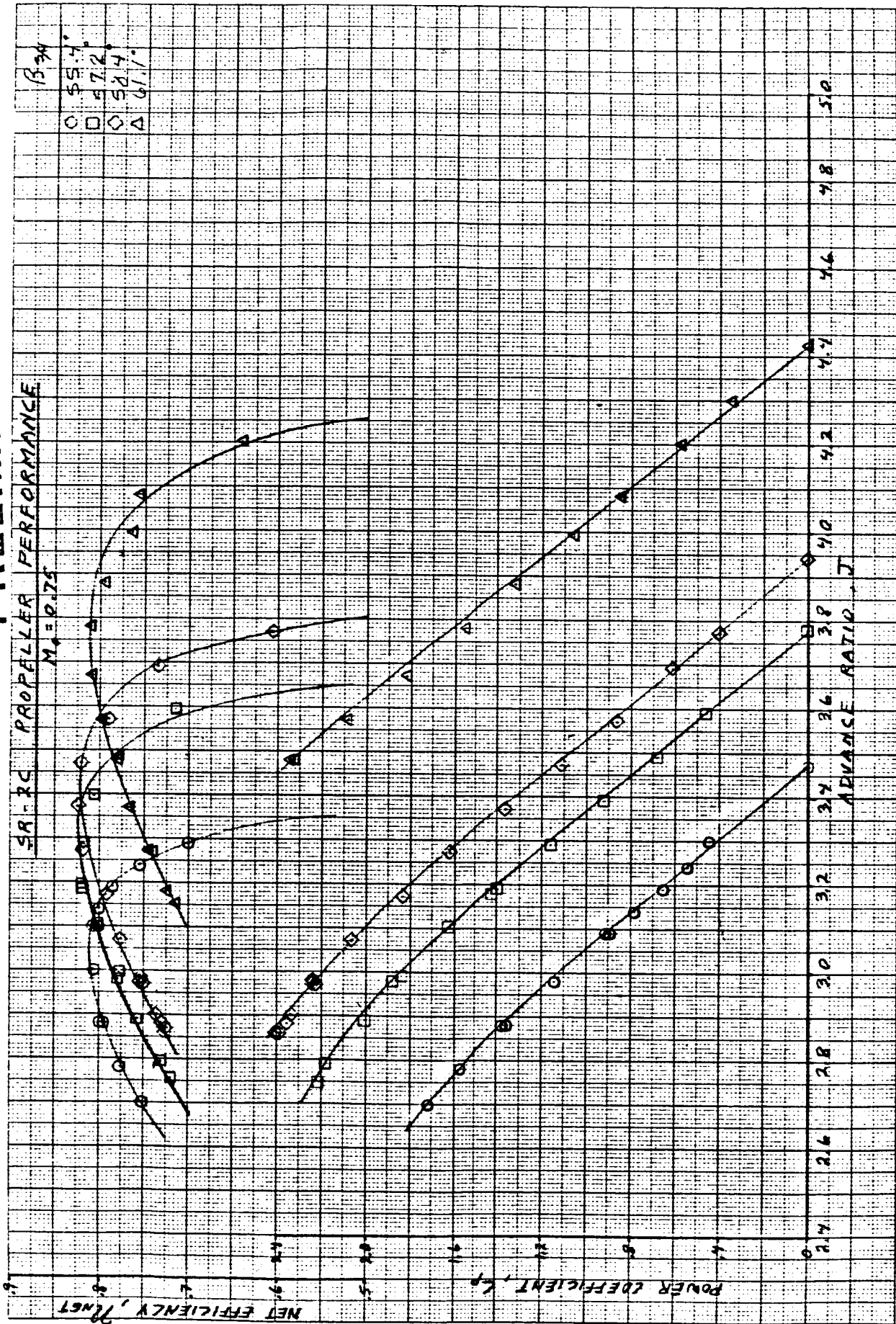
PRELIMINARY DATA



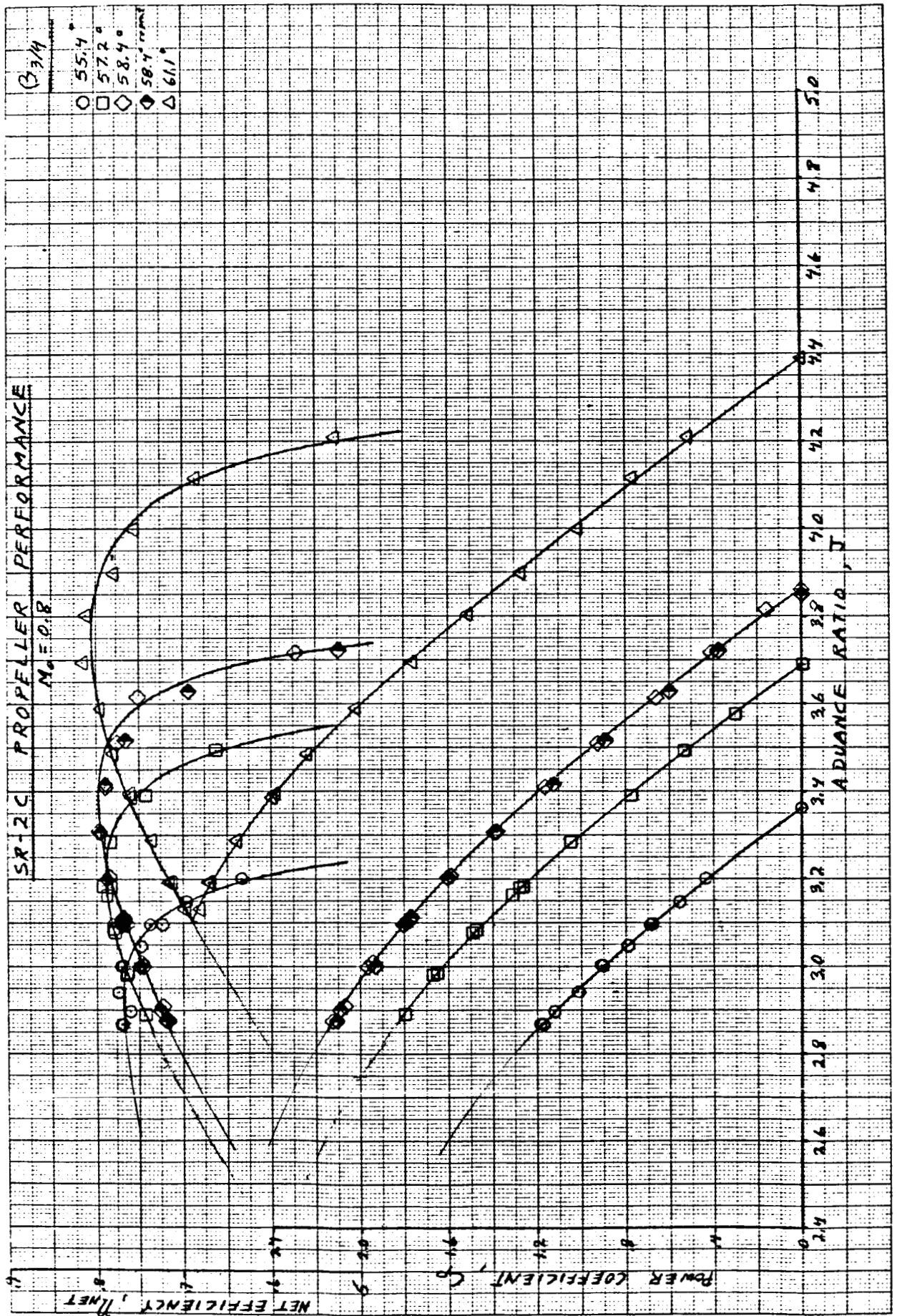
PRELIMINARY DATA



PRELIMINARY DATA



PRELIMINARY DATA



APPENDIX B
PARASITE DRAG SUMMARY
WING MOUNTED PROPFAN NACELLE

PARASITE DRAG SUMMARY:

| | | <u>DRAG COUNTS</u> |
|------------------|----------------------------------|------------------------|
| ΔC_{D_1} | due to LEX skin friction | 6 |
| ΔC_{D_2} | due to nacelle footprint on wing | -1 |
| ΔC_{D_3} | due to scrubbing drag on wing* | 3 |
| ΔC_{D_4} | due to wing footprint on nacelle | -1.2 |
| ΔC_{D_5} | due to scrubbing drag on nacelle | 1.1 |
| ΔC_{D_6} | due to nacelle skin friction | 7.3 |

*Did not include scrub drag increment on LEX (rough Calc. showed it to be only 0.1 count)

NOTE: 1 Drag Count = .0001

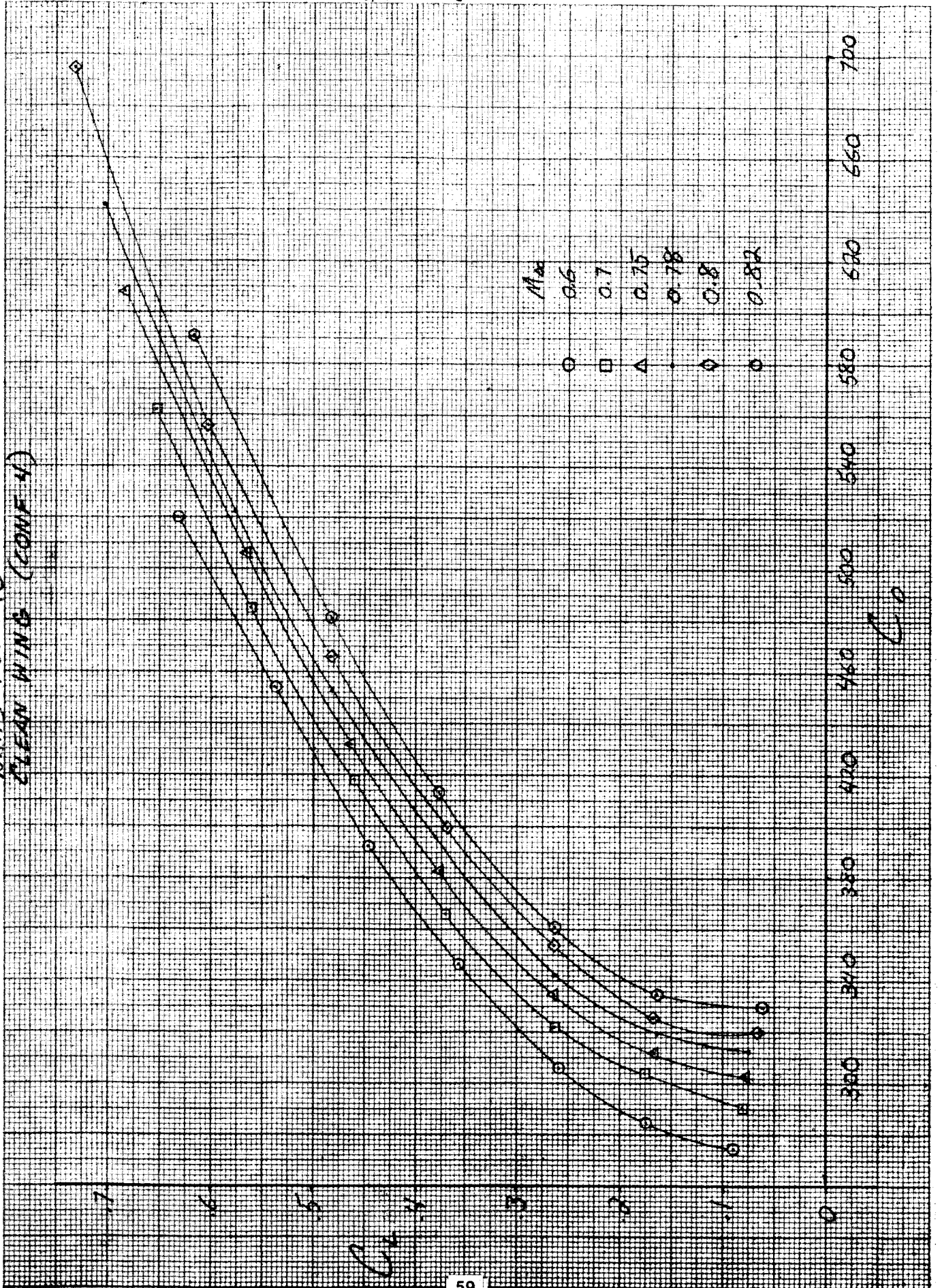
PRECEDING PAGE BLANK NOT FILMED

PAGE 54 INTENTIONALLY BLANK

APPENDIX C
DRAG POLARS
WING MOUNTED PROPFAN NACELLE

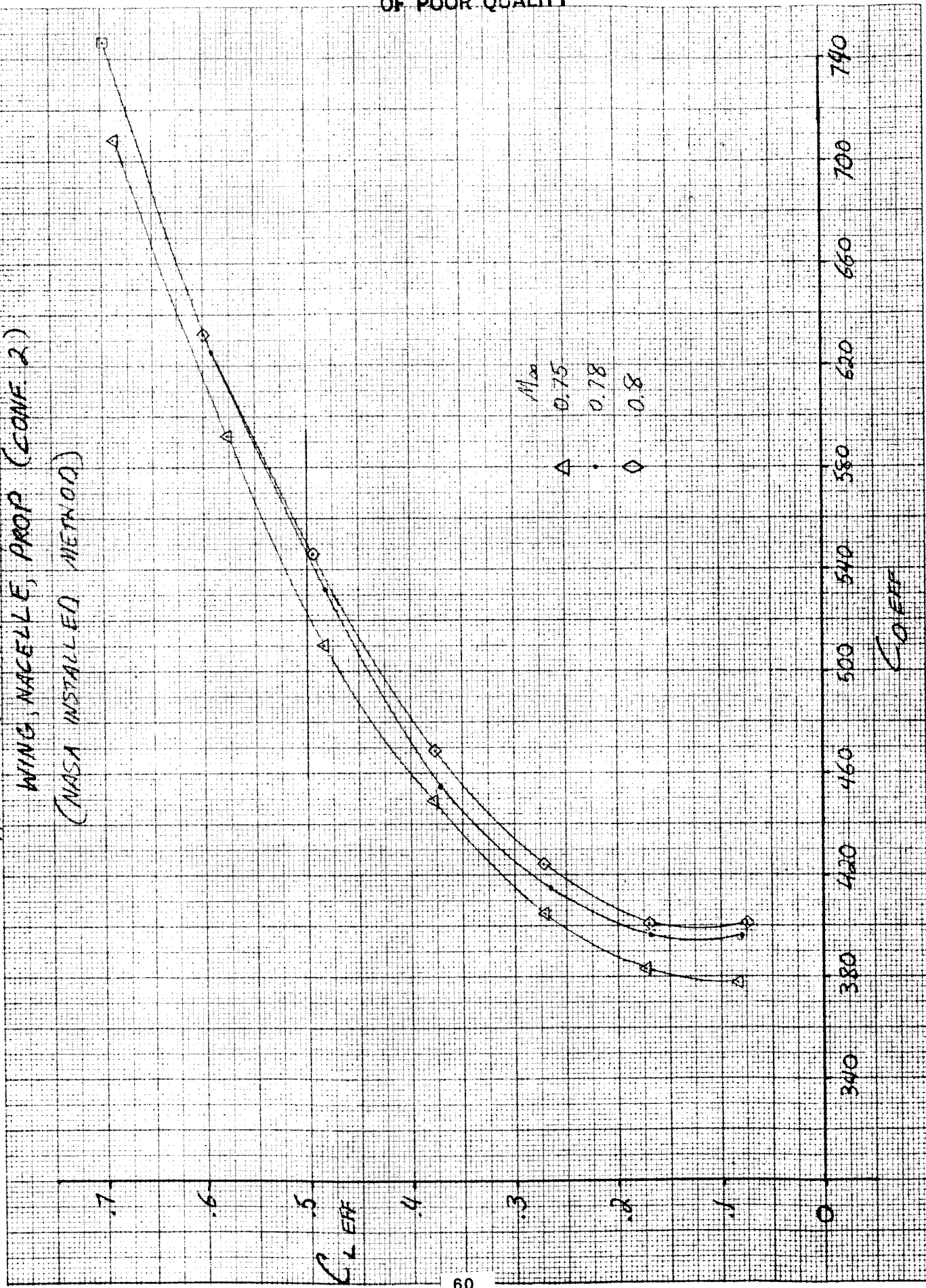
PRECEDING PAGE BLANK NOT FILMED

DRAG POLARS
CLEAN WING (CONF 4)

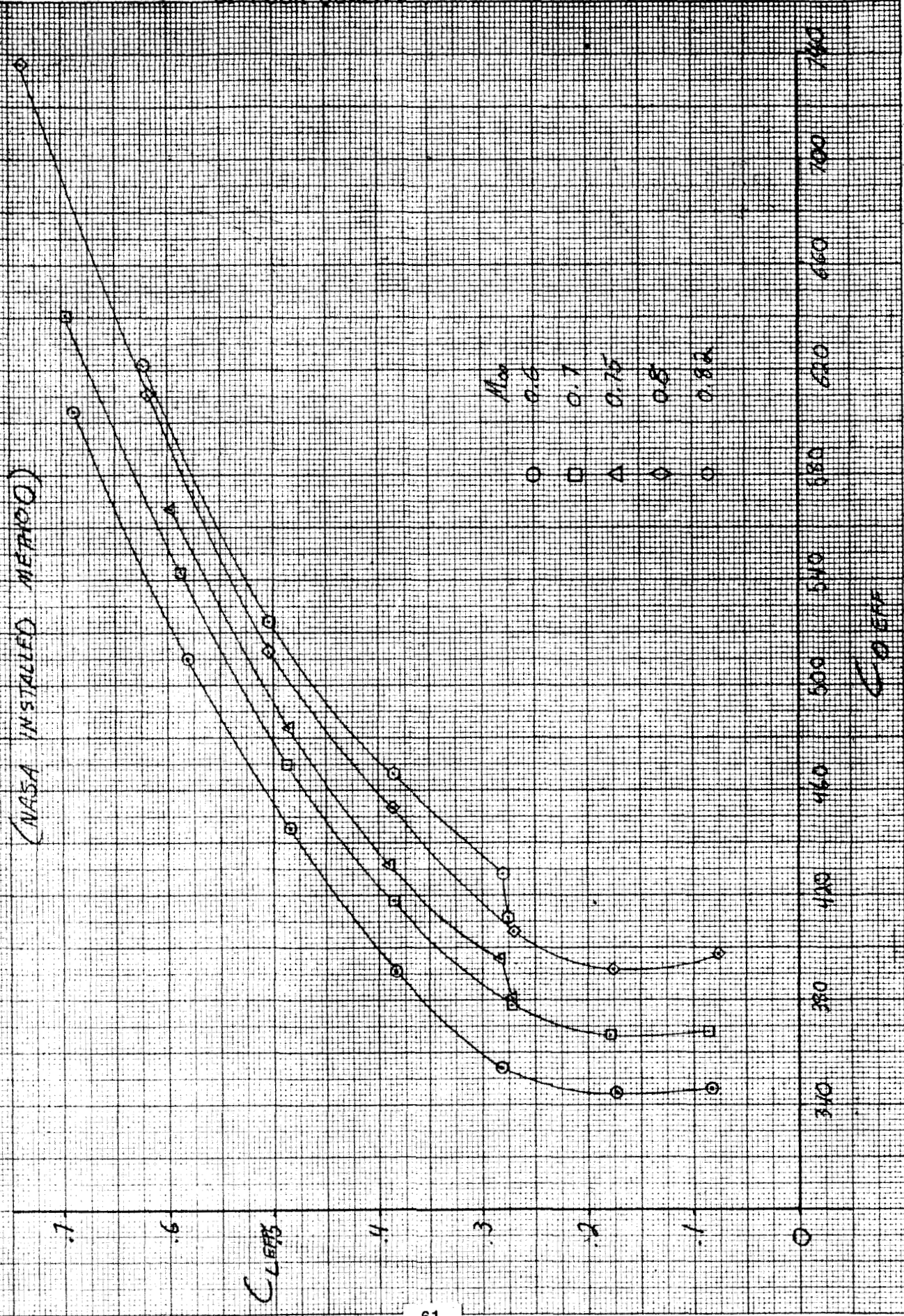


C_D

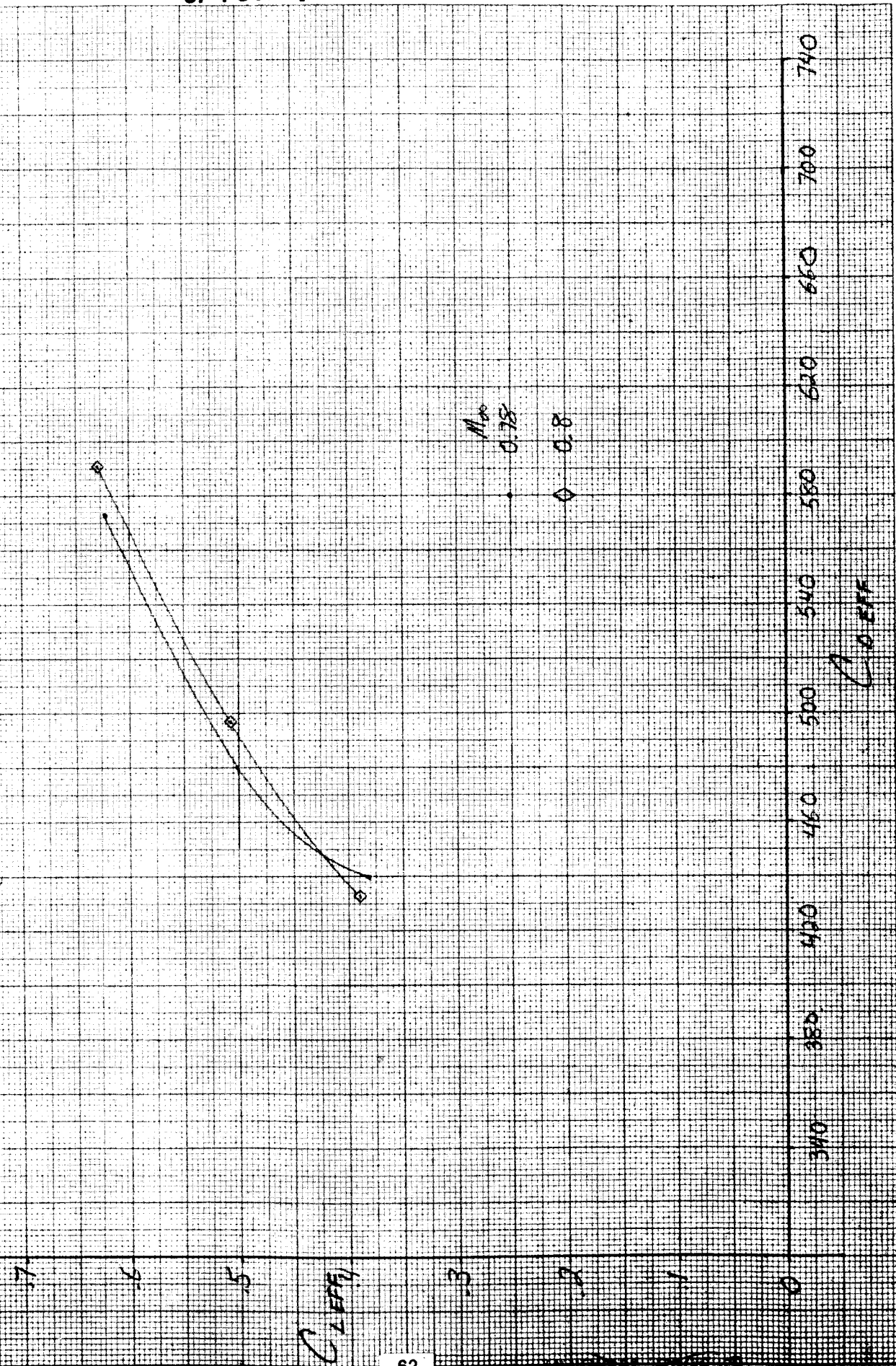
THRUST REMOVED DRAG POLARS
WING, NACELLE, PROP (CONF. 2)
(NASA INSTALLED METHOD)



THRUST REMOVED DRAG POLARS
 (WING, NACELLE, LEX, PROP (CONF.))
 (NASA INSTALLED METHOD)



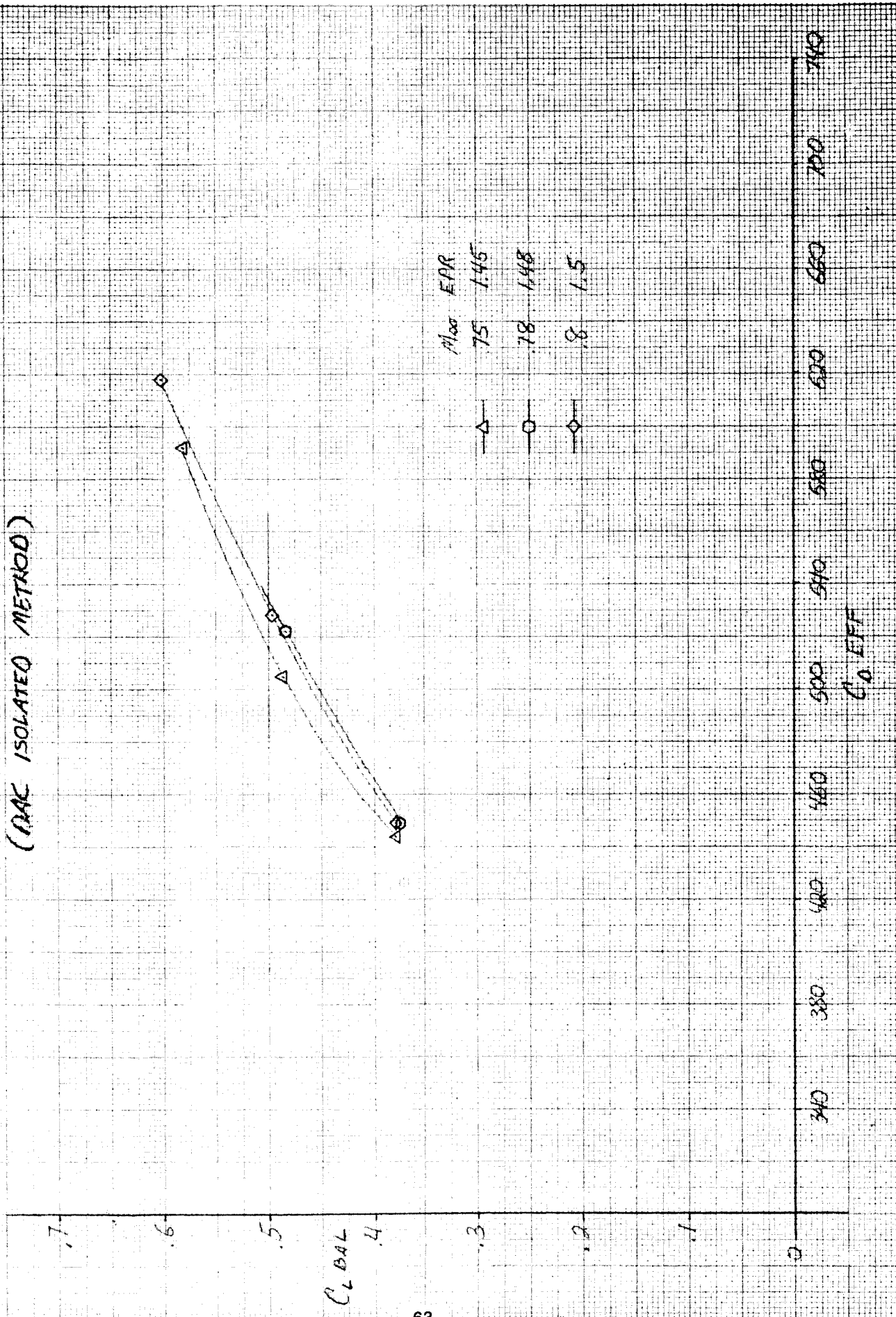
THRUST REMOVED DRAG POLARS
WING, MACELLE, LEX, STRAKE, PROP (CONF II)
(NASA INSTALLED METHOD)



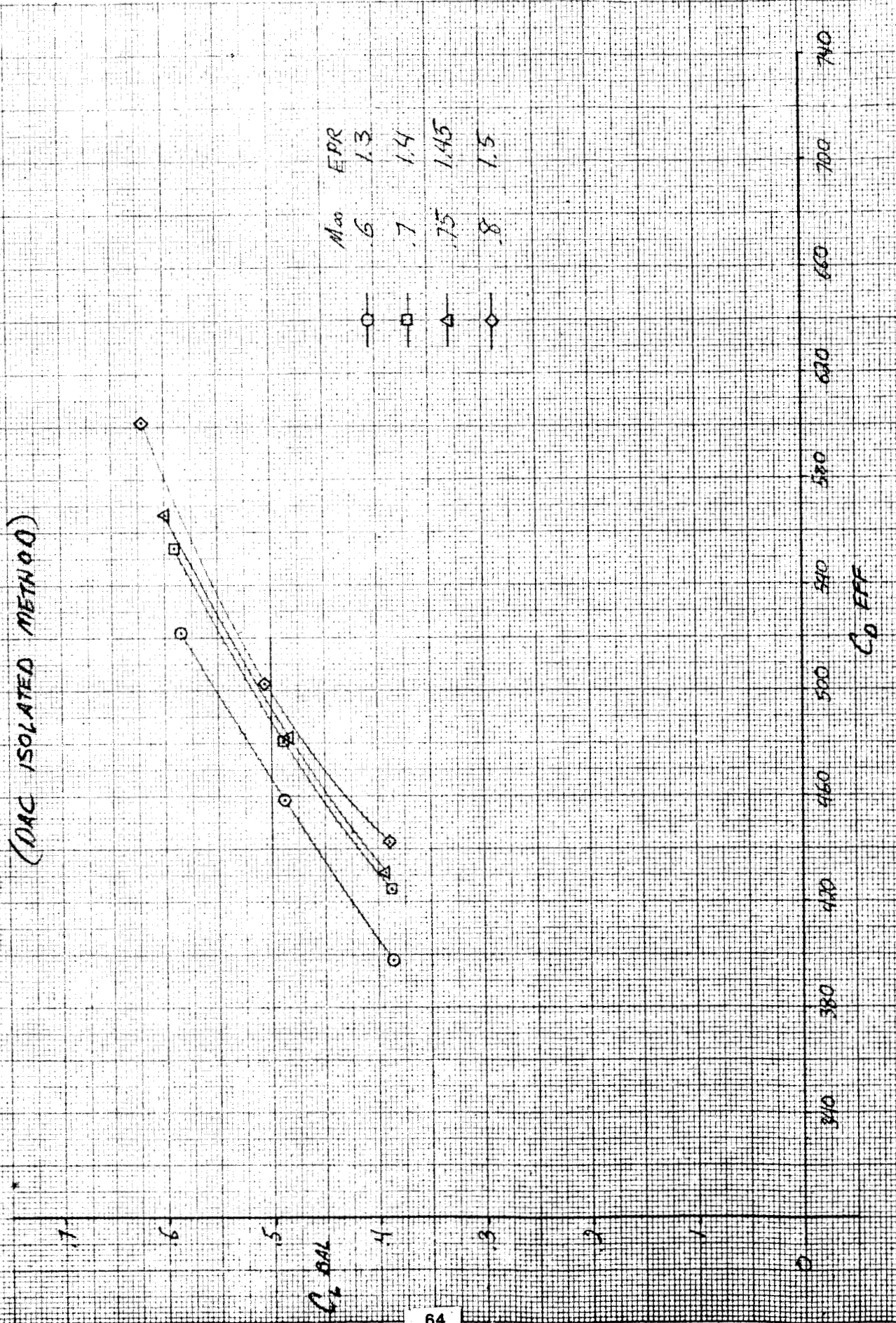
M_{∞}
0.78

0.8

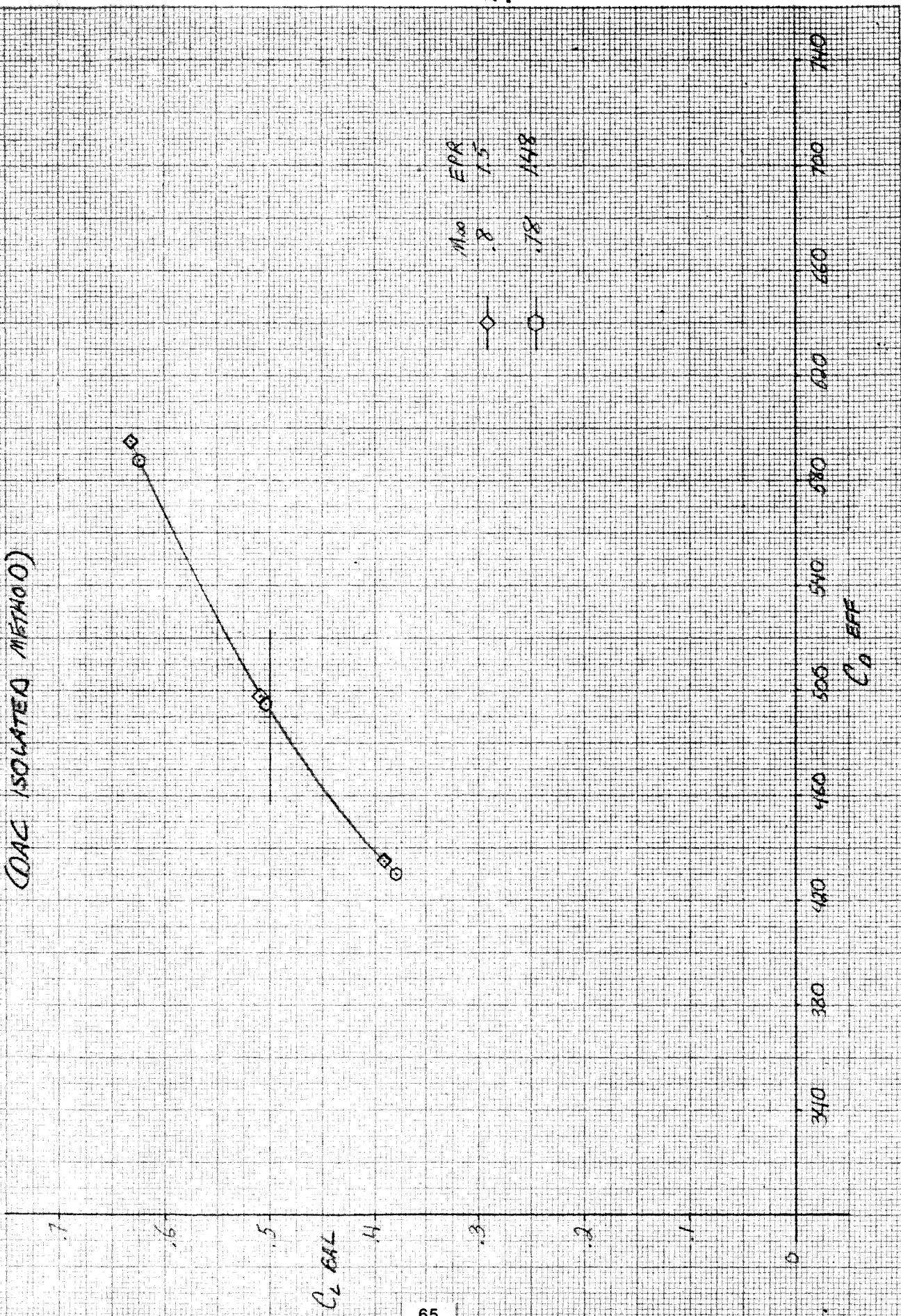
THRUST REMOVED DRAG POLARS
WING, NACELLE, PROP (CONF 2)
(OAK ISOLATED METHOD)



THRUST REMOVED DRAG POLARS
WING, NACELLE, LEX, PROP (CONF 6)
(DAG ISOLATED METHOD)



THRUST REMOVED DRAG POLARS
WING, MACELLE, LEX, FILLET, PROP (CONFII)
(OAC ISOLATED METHOD)



9.0 REFERENCES

- (1) (A) H. R. Welge, and J. P. Crowder, "Simulated Propeller Slipstream Effects on a Supercritical Wing." (Douglas Aircraft Company; NASA Contract NAS2-9472.) NASA CR-152138, June 1978.
- (2) H. R. Welge, D. H. Neuhart and J. A. Dahlin, "Analysis of Mach Number 0.8 Turboprop Slipstreams Wing/Nacelle Interactions." NASA CR 166214, August 1981.
- (3) Turboprop Model Calibration and Proof Tests (TD 1234M), TR80-111.
- (4) Smith, R. C. and Levin, A. D.: "Propfan Installation Aerodynamics of a Supercritical Swept Wing Transport Configuration," AIAA Report 81-1563, July 1981.
- (5) J. DeYoung, C. W. Harper, "Theoretical Symmetric Span Loading at Subsonic Speeds for Wings Having Arbitrary Plan Form" NACA TR 921, May 1950.
- (6) D. P. Mack and S. M. Schimke, "User's Manual For a Fully Automatic Three-Dimensional Potential Flow Calculation Methods." Report MDC J7644/01, August 1977.
- (7) P. A. Henne and R. M. Hicks, "Wing Analysis Using a Transonic Potential Flow Computation Method." NASA TM78464, July 1978.
- (8) H. R. Welge, "Prop-Fan Integration at Cruise Speeds." AGARD PAPER 33, Douglas Paper 6970, May 1981.

PRECEDING PAGE BLANK NOT FILMED

10.0 FIGURES

PRECEDING PAGE BLANK NOT FILMED

PAGE 66 INTENTIONALLY BLANK



FIGURE 1. STRAIGHT UNDERWING NACELLE MODEL IN AMES TUNNEL

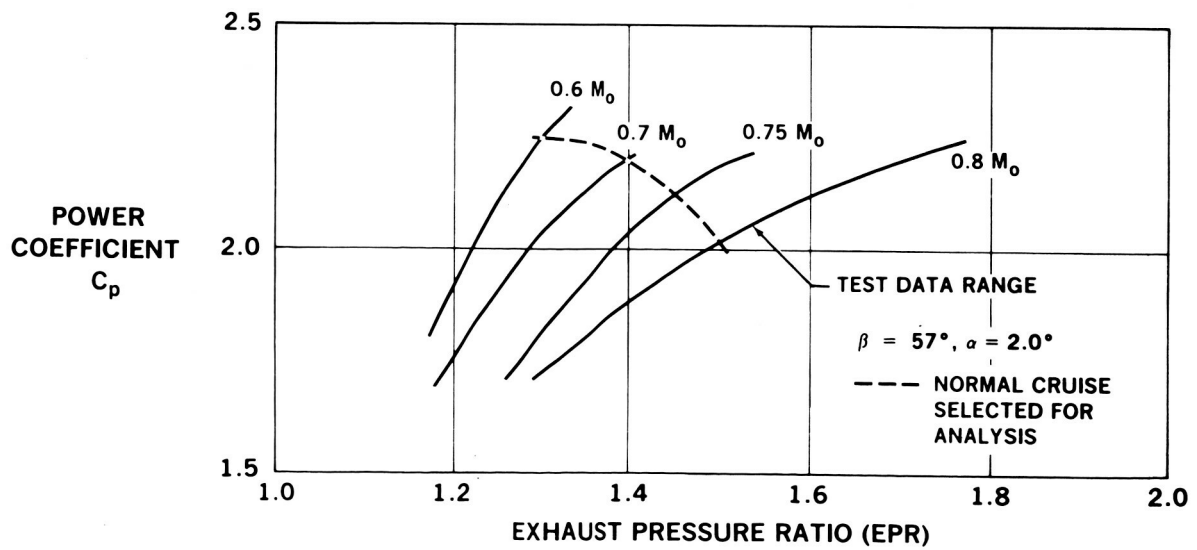


FIGURE 2. TEST CONDITIONS SELECTED FOR ANALYSIS

ORIGINAL PAGE IS
OF POOR QUALITY

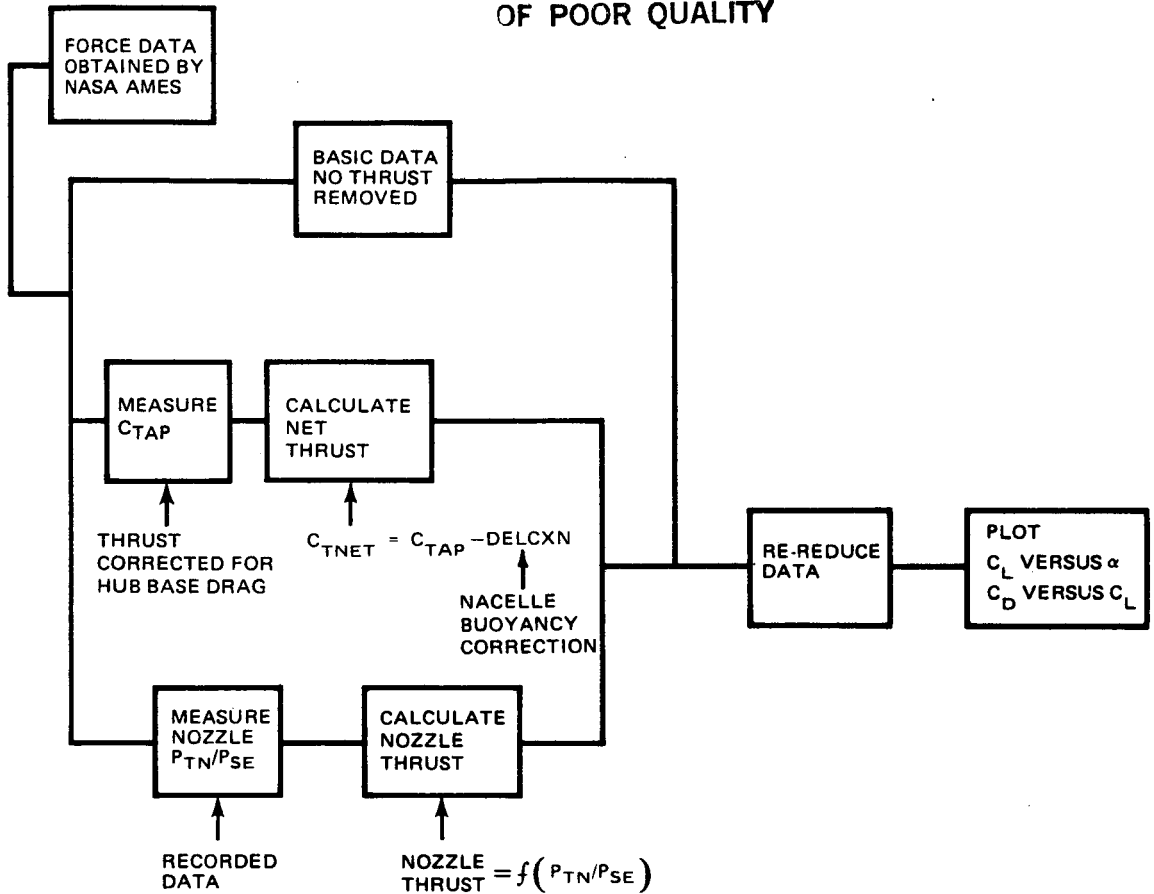


FIGURE 3. INSTALLED PERFORMANCE METHOD

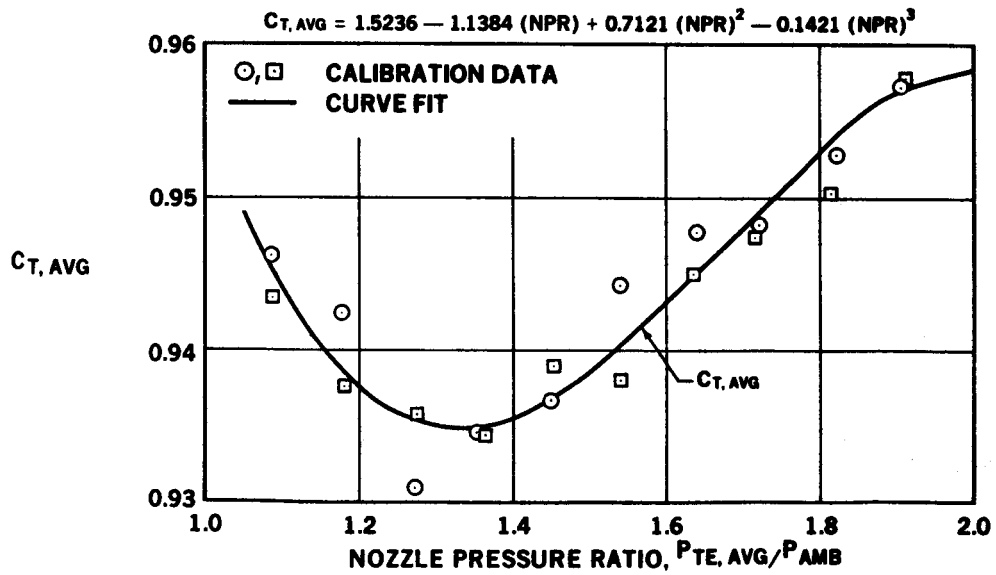


FIGURE 4. EXHAUST DUCT THRUST COEFFICIENT CALIBRATION

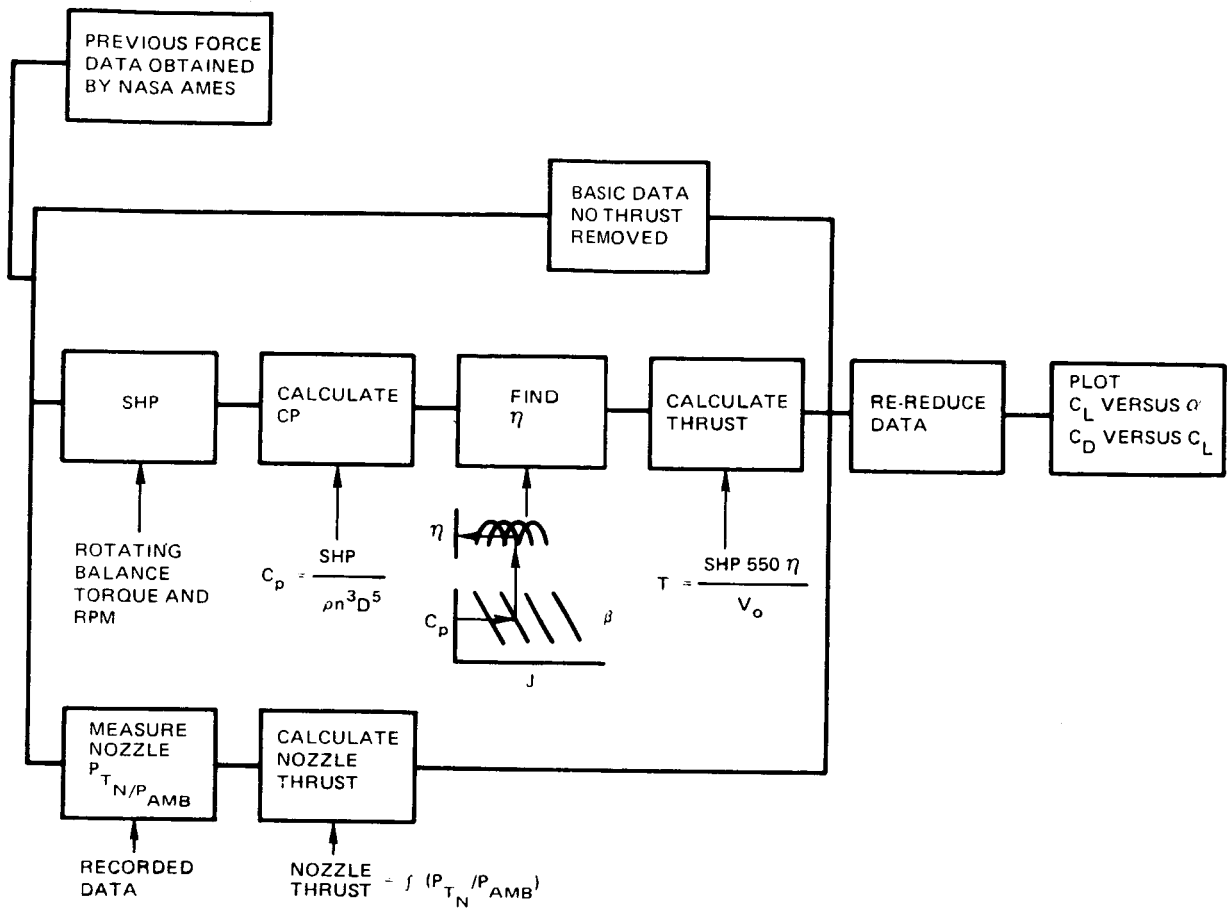


FIGURE 5. DAC ISOLATED PERFORMANCE METHOD

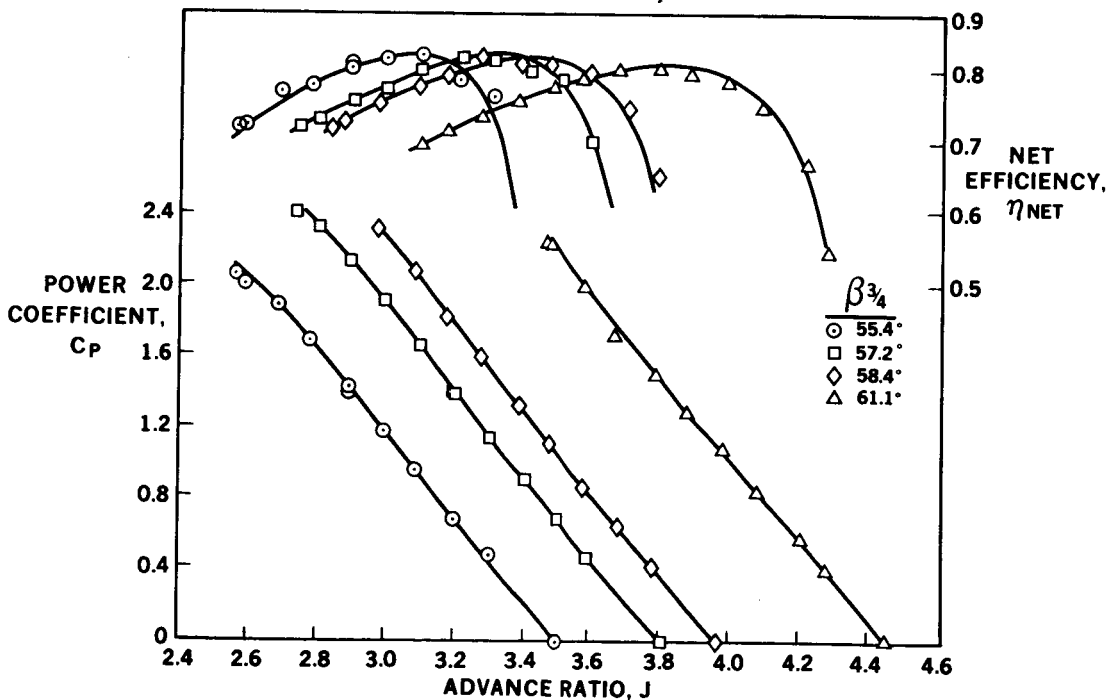


FIGURE 6. SR-2C PROPELLER PERFORMANCE $M_0 = 0.7$

ORIGINAL PAGE IS
OF POOR QUALITY

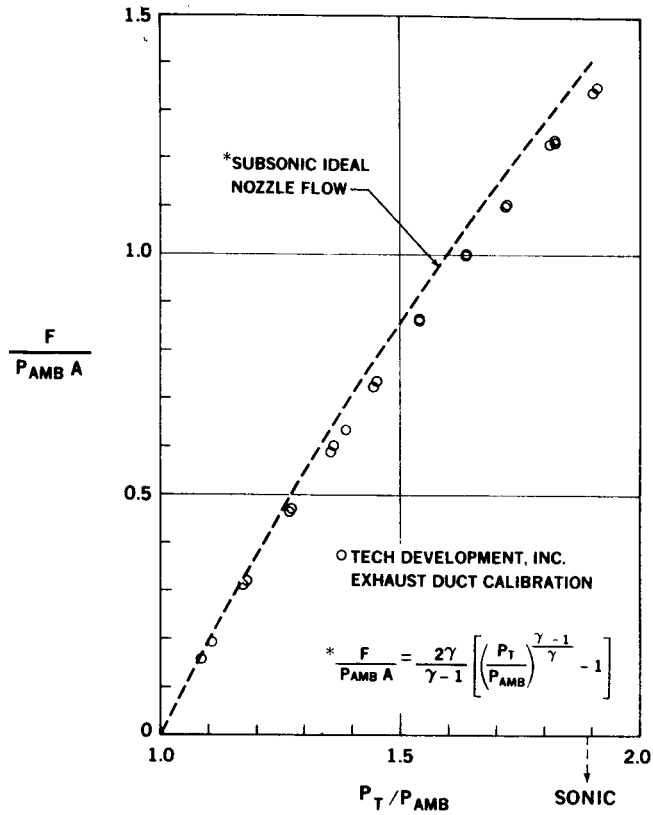


FIGURE 7. ISOLATED EXHAUST NOZZLE CALIBRATION (SUBSONIC IDEAL NOZZLE FLOW)

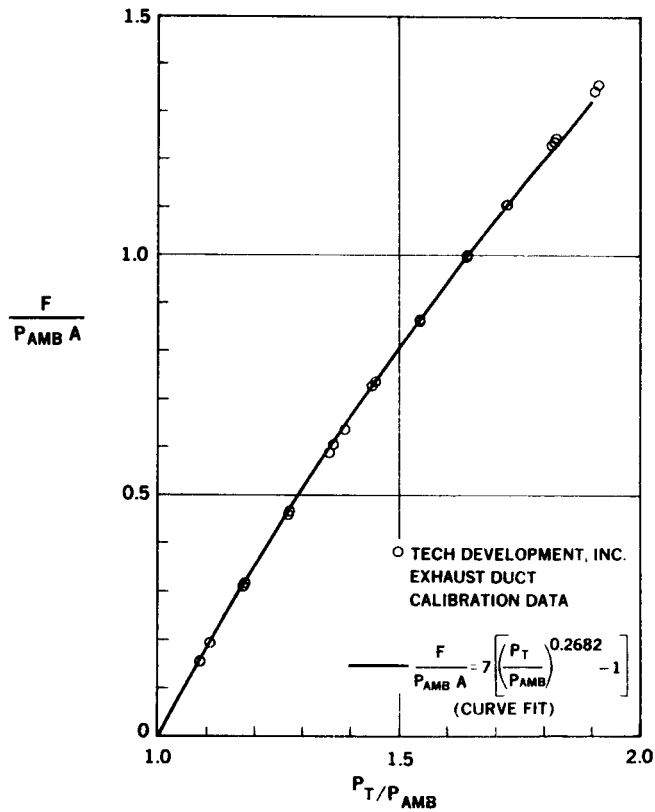


FIGURE 8. ISOLATED EXHAUST NOZZLE CALIBRATION (EXPERIMENTAL DATA CURVE FIT)

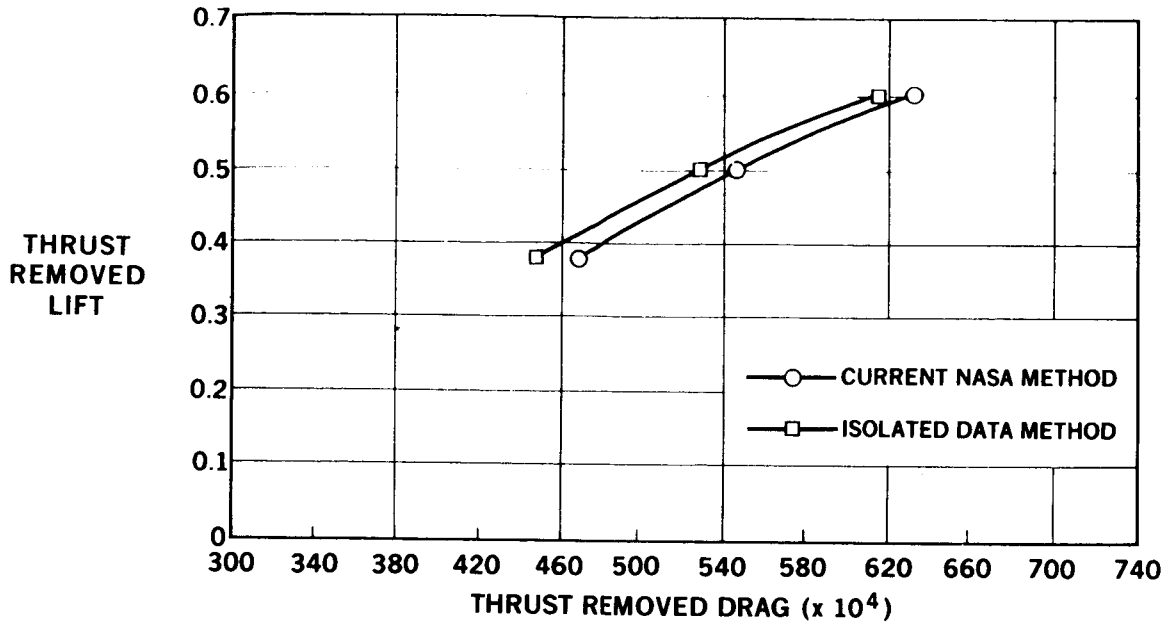


FIGURE 9. THRUST REMOVED DRAG POLAR COMPARISON FOR WING, NACELLE WITH POWER, $M_0 = 0.8$

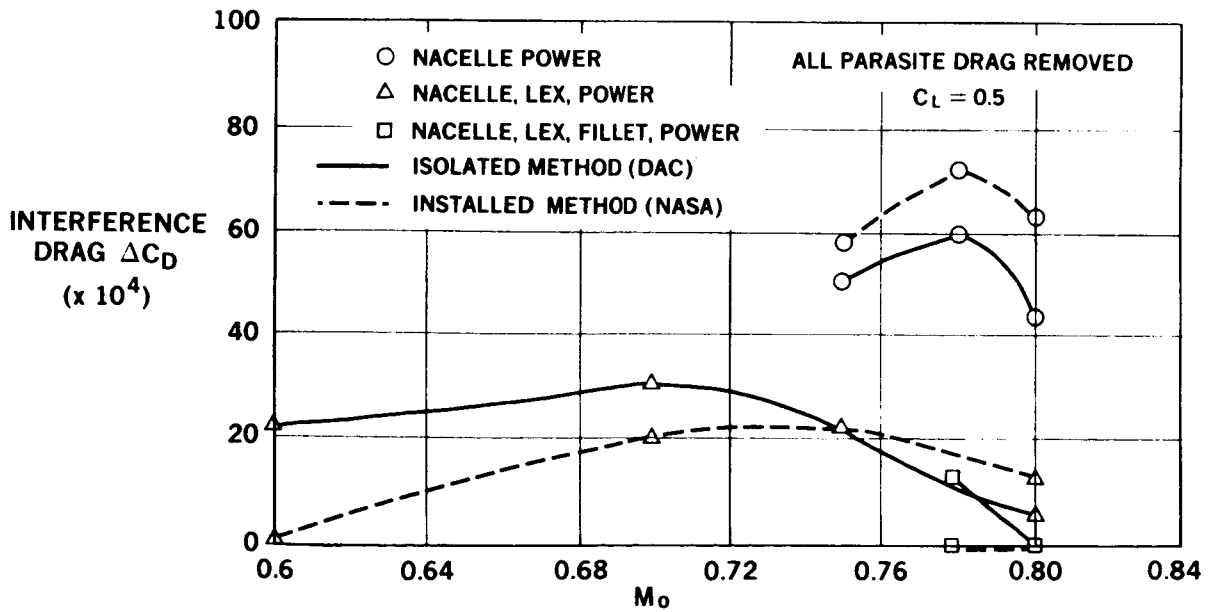


FIGURE 10. THRUST/DRAG BOOKKEEPING COMPARISON, INTERFERENCE DRAG LEVELS

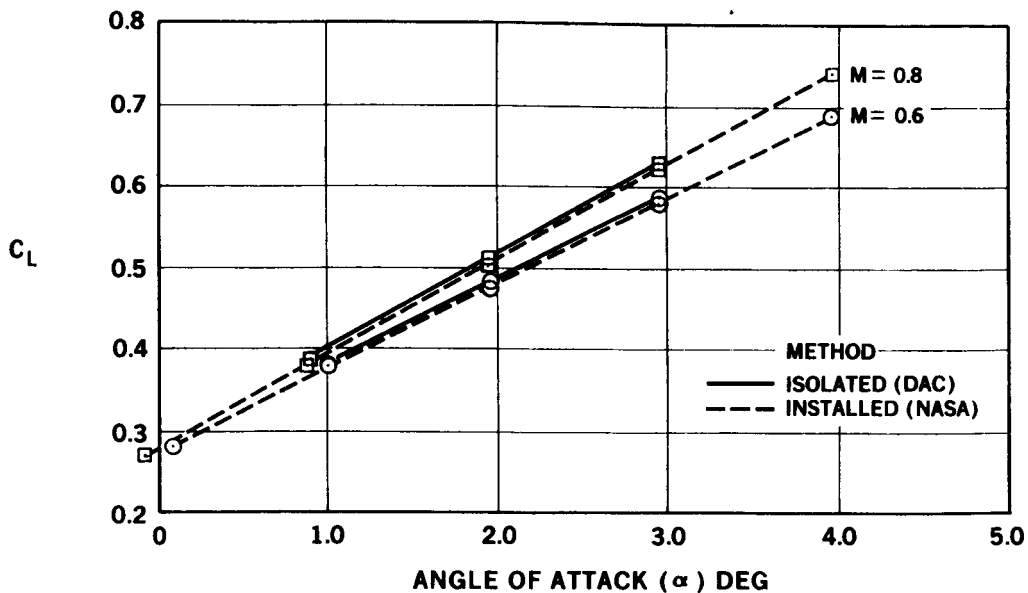


FIGURE 11. THRUST REMOVED LIFT CURVE COMPARISON FOR WING, NACELLE, LEX, PROP

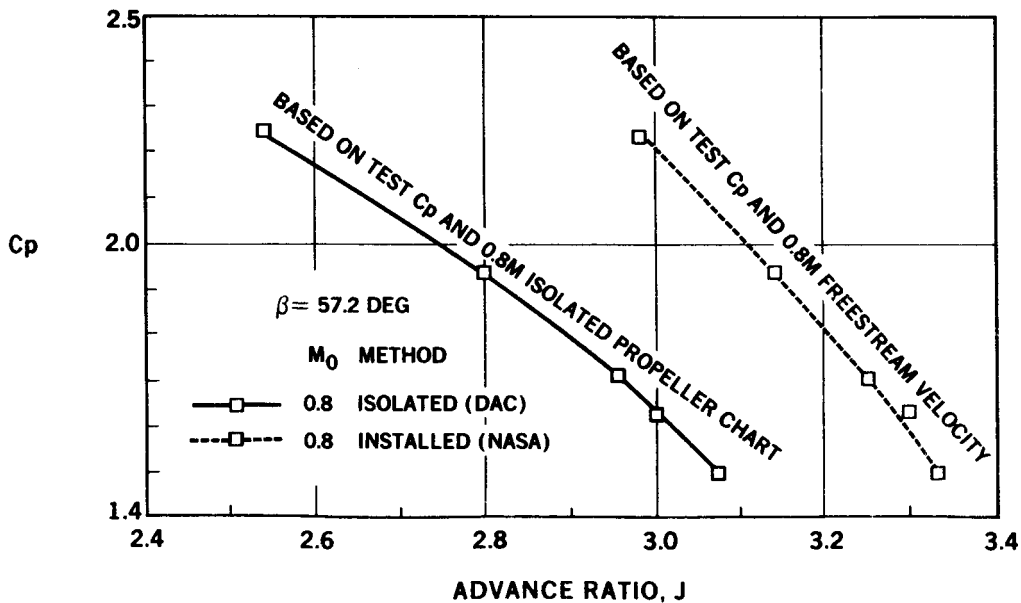


FIGURE 12. POWER COEFFICIENT VERSUS ADVANCED RATIO

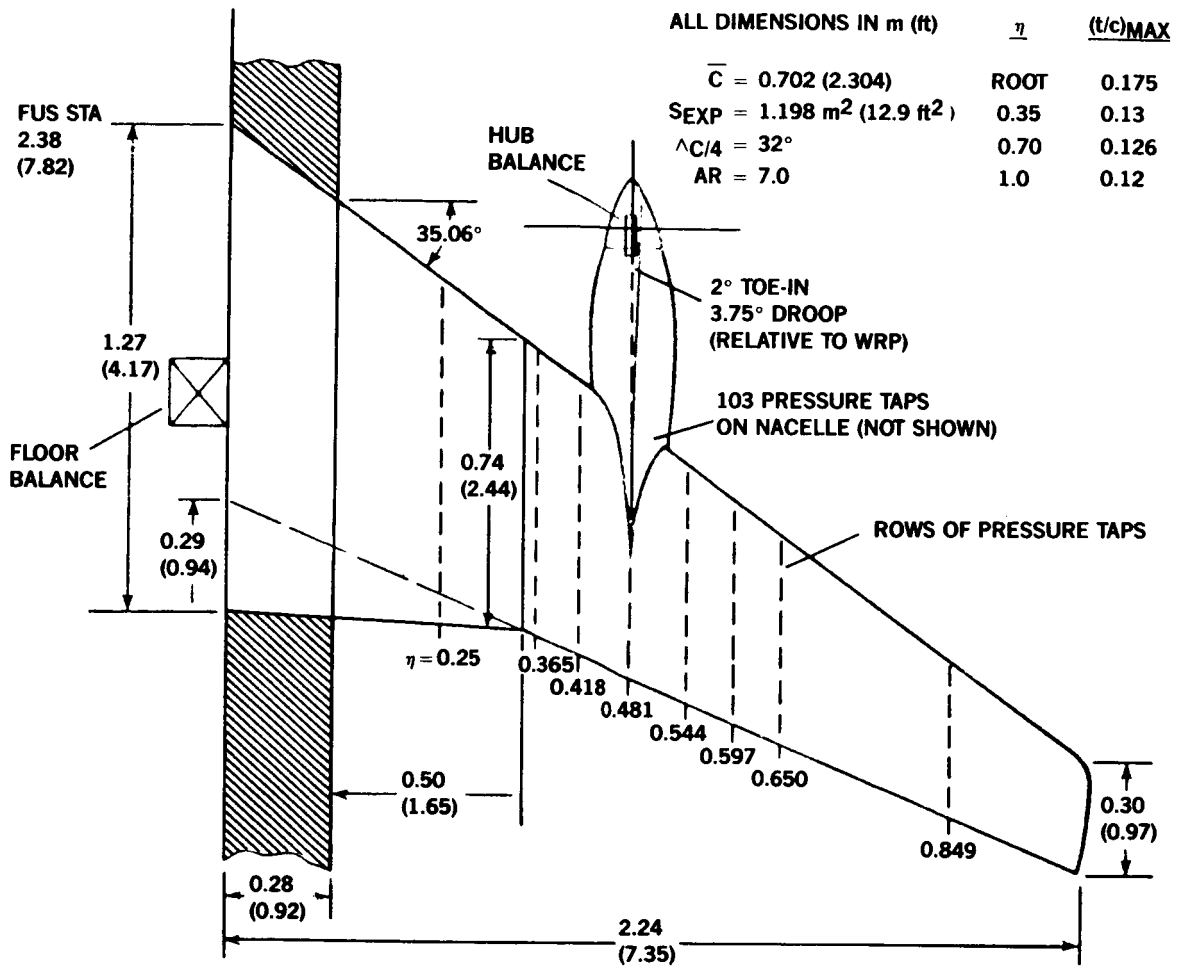


FIGURE 13. WING GEOMETRY AND INSTRUMENTATION (TOP VIEW)

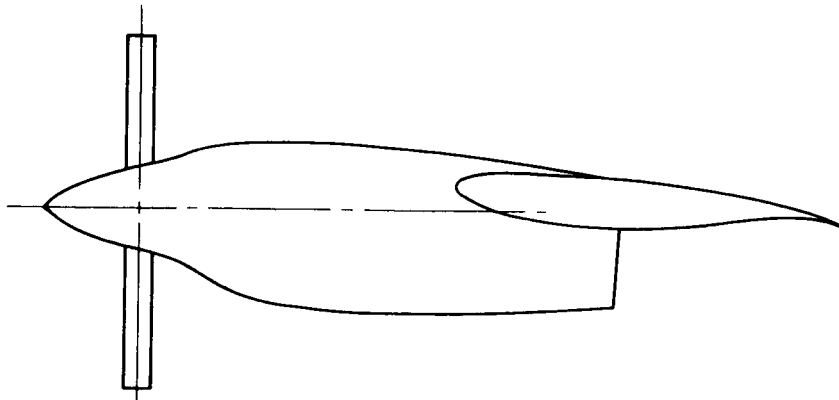


FIGURE 14. SIDE VIEW OF UNDERWING NACELLE

ORIGINAL PAGE IS
OF POOR QUALITY

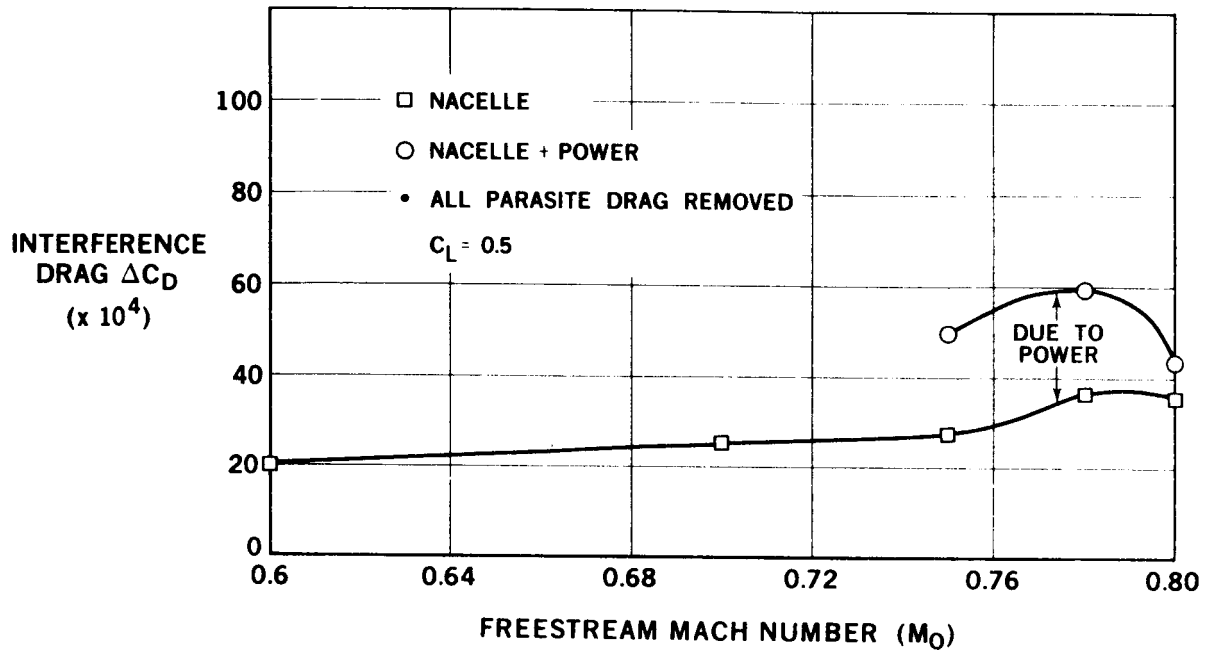


FIGURE 15. INTERFERENCE DRAG LEVELS FOR STRAIGHT UNDERWING NACELLE

ORIGINAL PAGE IS
OF POOR QUALITY

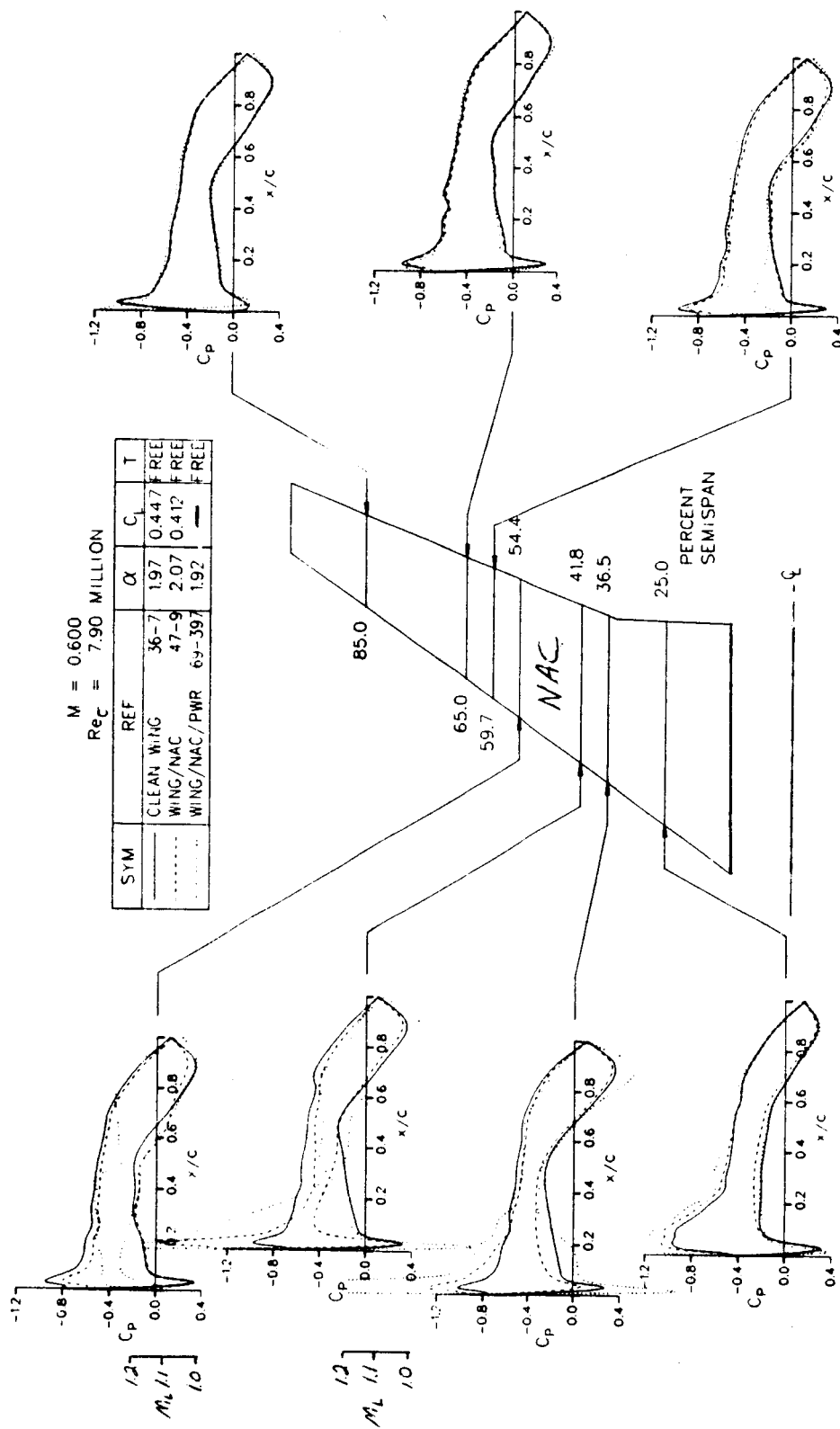


FIGURE 16. EXPERIMENTAL CHORDWISE PRESSURE DISTRIBUTIONS FOR STRAIGHT UNDERWING NACELLE, $0.6M_\infty$, $\alpha = 2$ DEGREES

ORIGINAL PAGE IS
OF POOR QUALITY

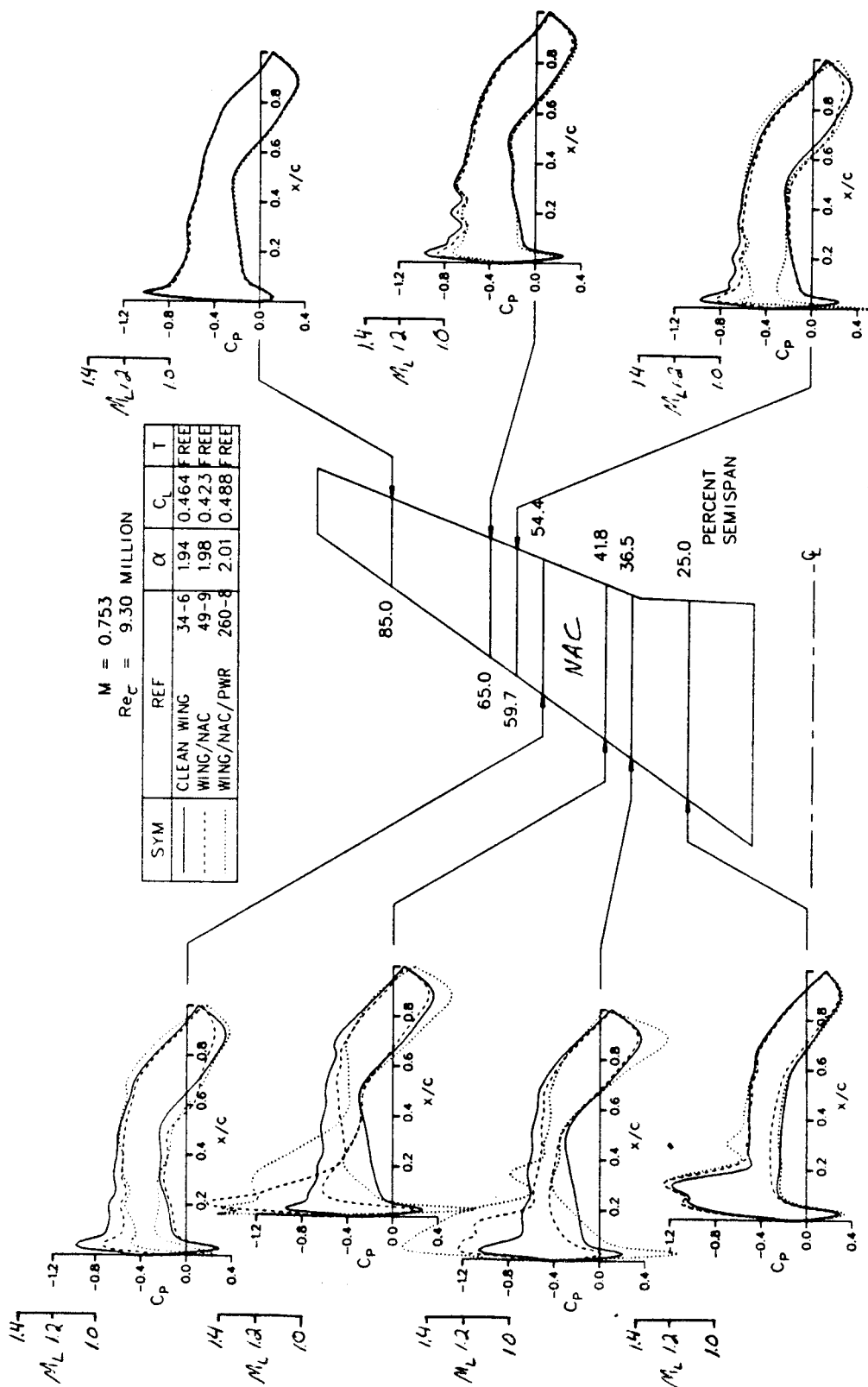


FIGURE 17. EXPERIMENTAL CHORDWISE PRESSURE DISTRIBUTIONS FOR STRAIGHT UNDERWING NACELLE, $0.75M$, $\alpha = 2$ DEGREES

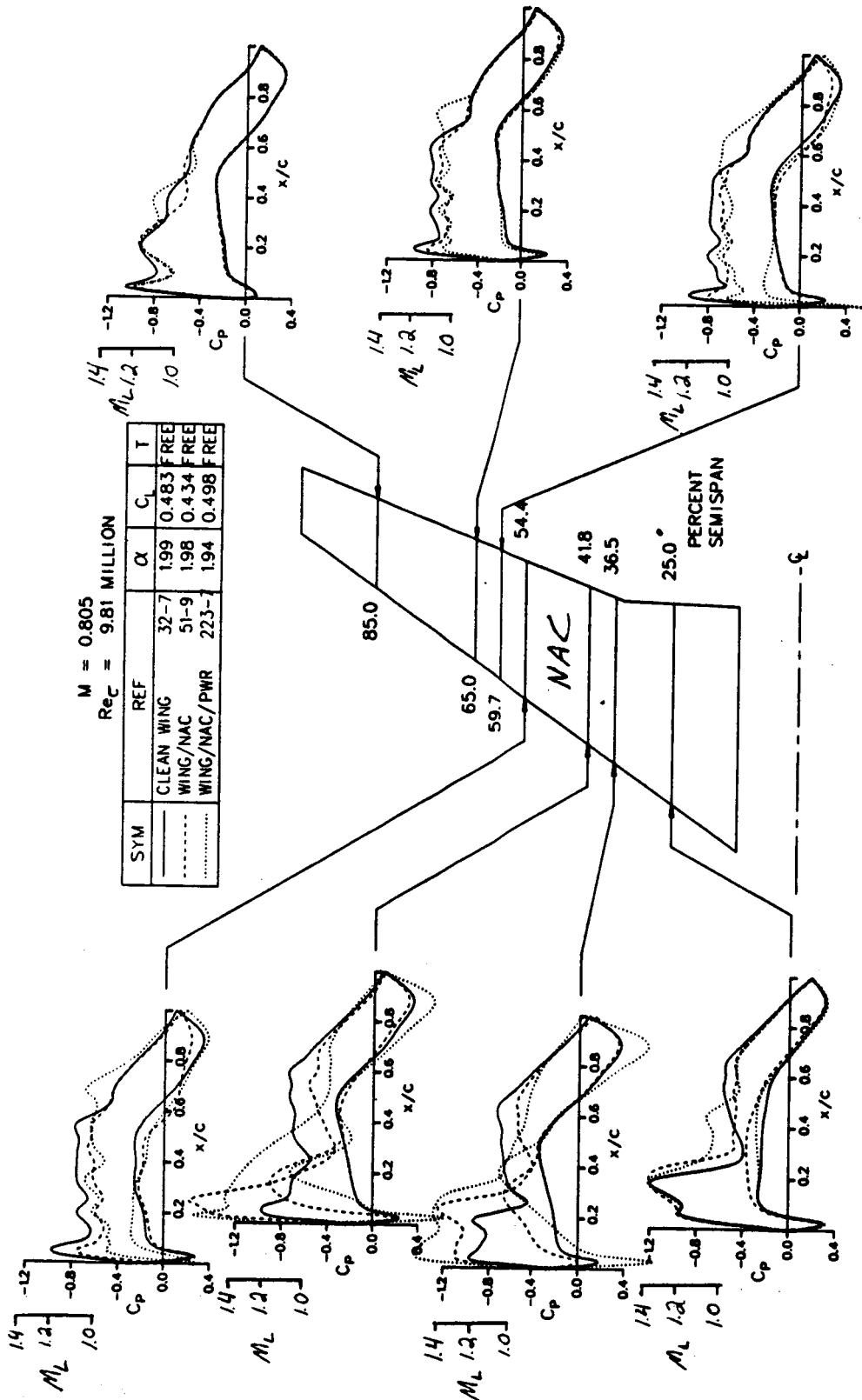
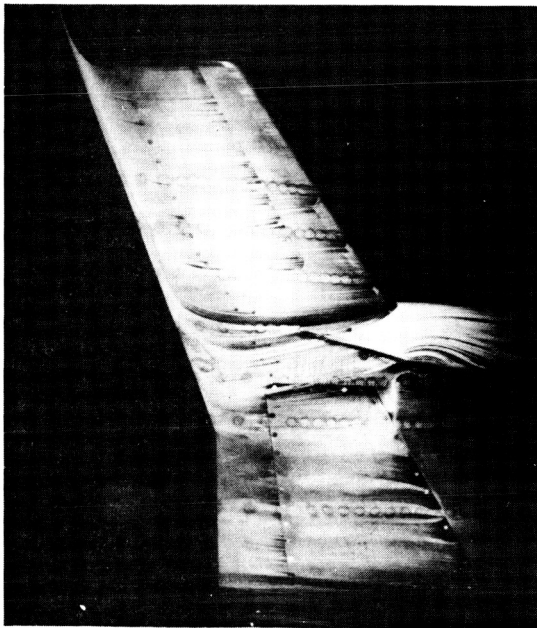


FIGURE 18. EXPERIMENTAL CHORDWISE PRESSURE DISTRIBUTIONS FOR STRAIGHT UNDERWING NACELLE, $0.8M_\infty$, $\alpha = 2$ DEGREES



$M_o = 0.75$
 $\alpha = 2 \text{ DEG}$
WINDMILL
UPPER SURFACE

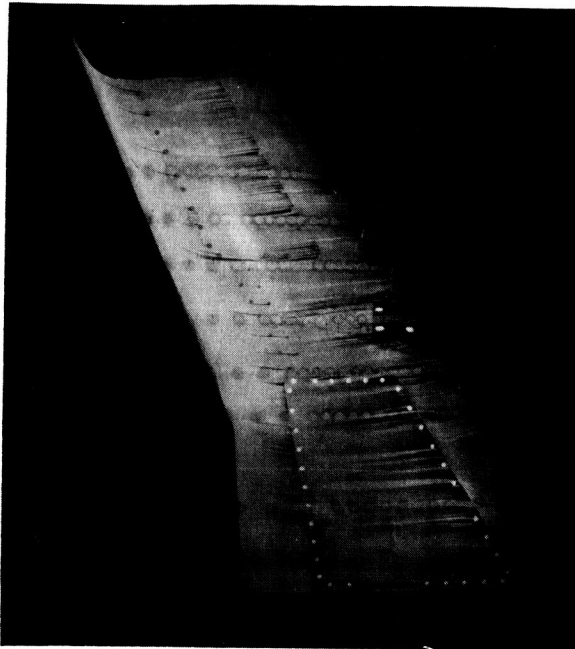
FIGURE 19. OIL FLOW PHOTOGRAPH FOR STRAIGHT UNDERWING NACELLE AT $M_o = 0.75$ – WINDMILL CONDITIONS



$M_o = 0.8$
 $\alpha = 2 \text{ DEG}$
WINDMILL
UPPER SURFACE

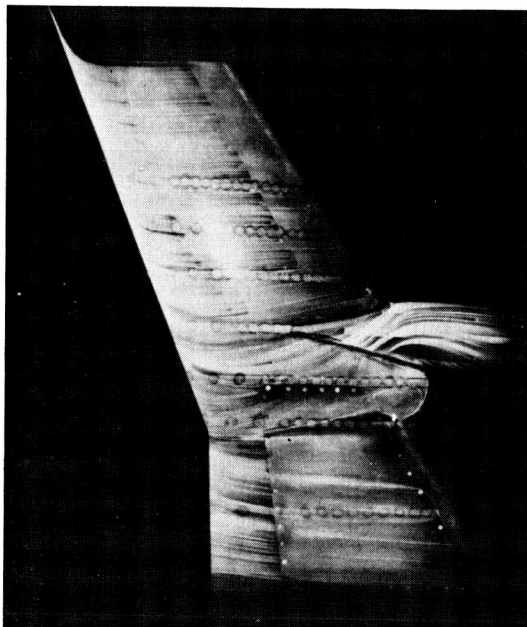
FIGURE 20. OIL FLOW PHOTOGRAPH FOR STRAIGHT UNDERWING NACELLE AT $M_o = 0.8$ – WINDMILL CONDITIONS

ORIGINAL PAGE IS
OF POOR QUALITY



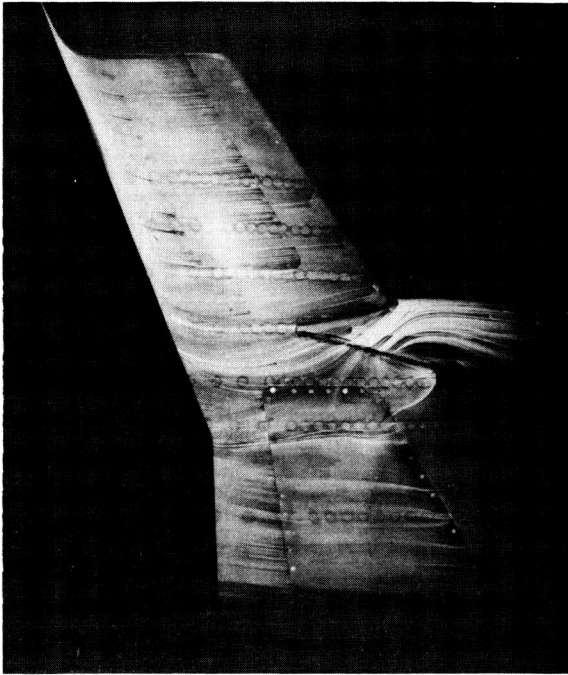
$M_o = 0.8$
 $\alpha = 2 \text{ DEG}$

FIGURE 21. OIL FLOW PHOTOGRAPH FOR CLEAN WING W4 AT $M_o = 0.8$



$M_o = 0.75$
 $\alpha = 2 \text{ DEG}$
8,100 RPM
UPPER SURFACE

FIGURE 22. OIL FLOW PHOTOGRAPH FOR STRAIGHT UNDERWING NACELLE AT $M_o = 0.75$ —
WITH POWER



$M_o = 0.8$
 $\alpha = 2 \text{ DEG}$
8500 RPM
UPPER SURFACE

FIGURE 23. OIL FLOW PHOTOGRAPH AT $M_o = 0.8$ - MAXIMUM POWER

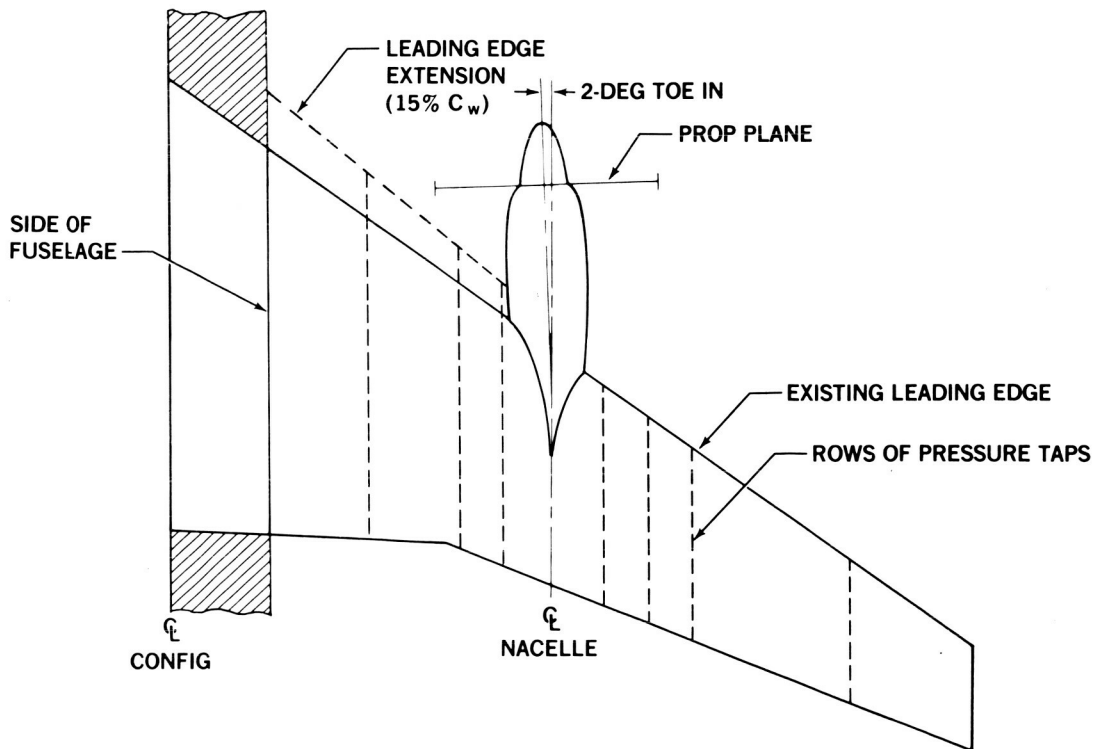


FIGURE 24. PLAN VIEW OF STRAIGHT UNDERWING NACELLE WITH LEX

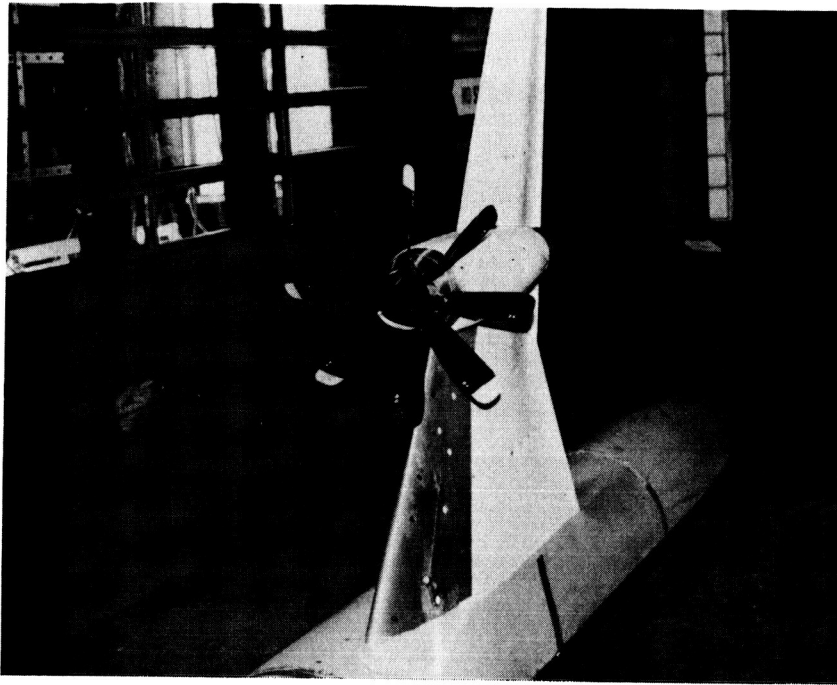


FIGURE 25. STRAIGHT UNDERWING NACELLE WITH LEX MODEL INSTALLED IN AMES 11-FOOT TUNNEL

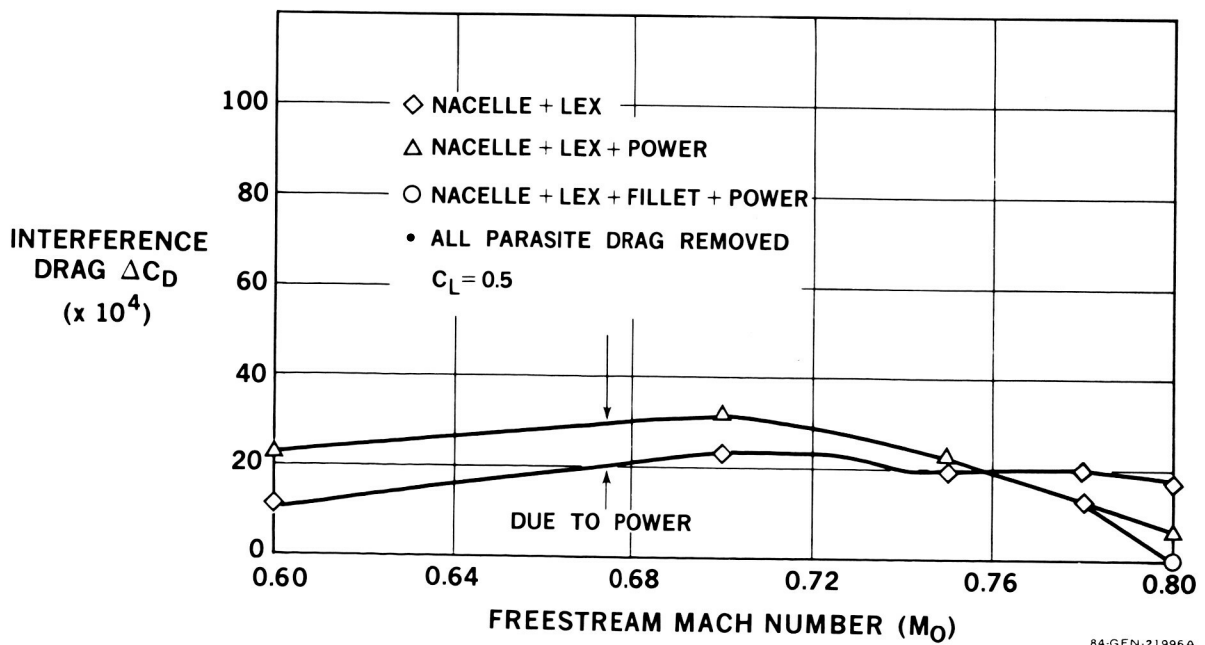


FIGURE 26. INTERFERENCE DRAG LEVELS FOR STRAIGHT UNDERWING NACELLE WITH LEX

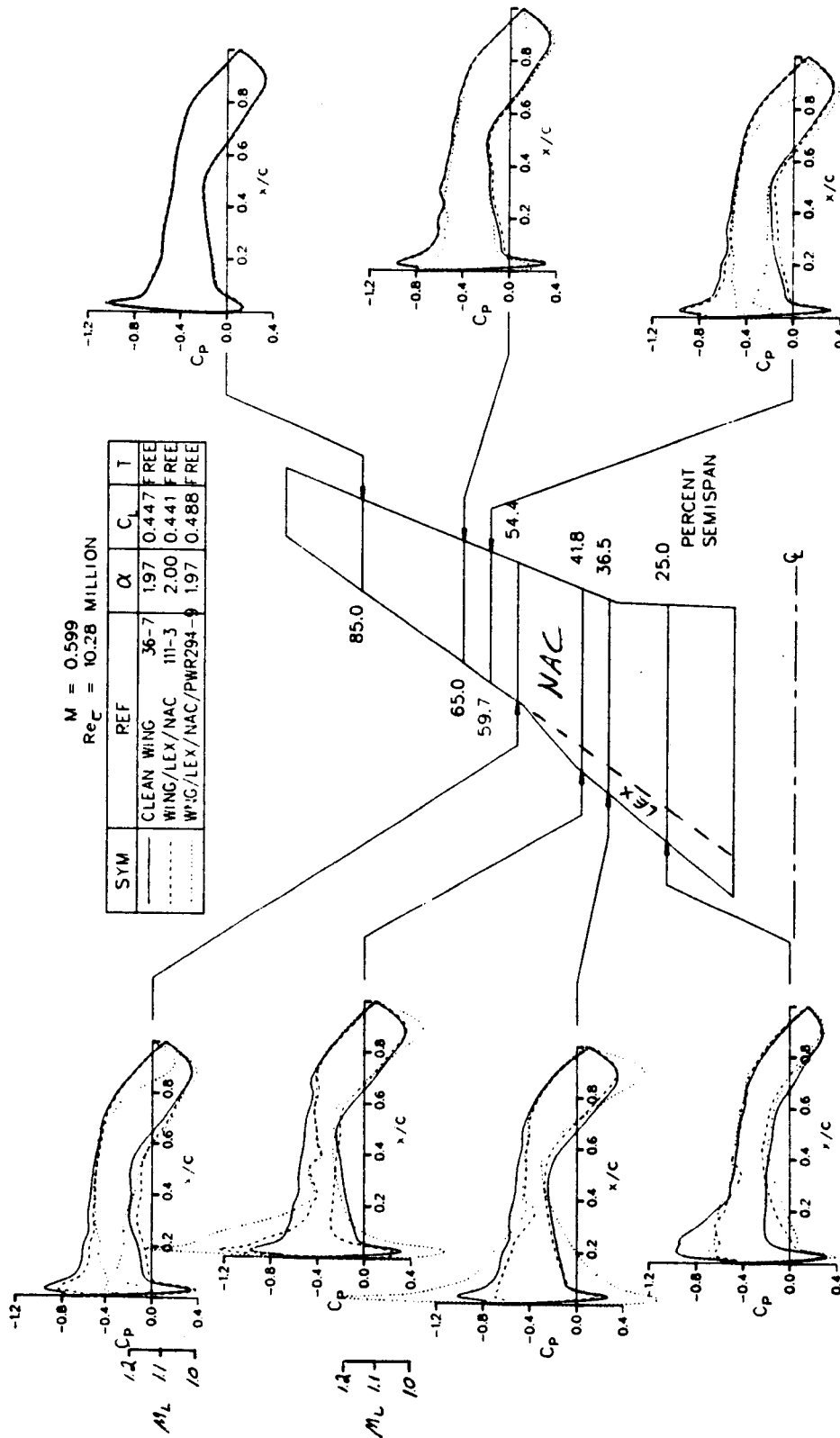


FIGURE 27. EXPERIMENTAL CHORDWISE PRESSURE DISTRIBUTIONS FOR STRAIGHT UNDERWING NACELLE WITH LEX, $0.6M_\infty$, $\alpha = 2$ DEGREES

ORIGINAL PAGE IS
OF POOR QUALITY

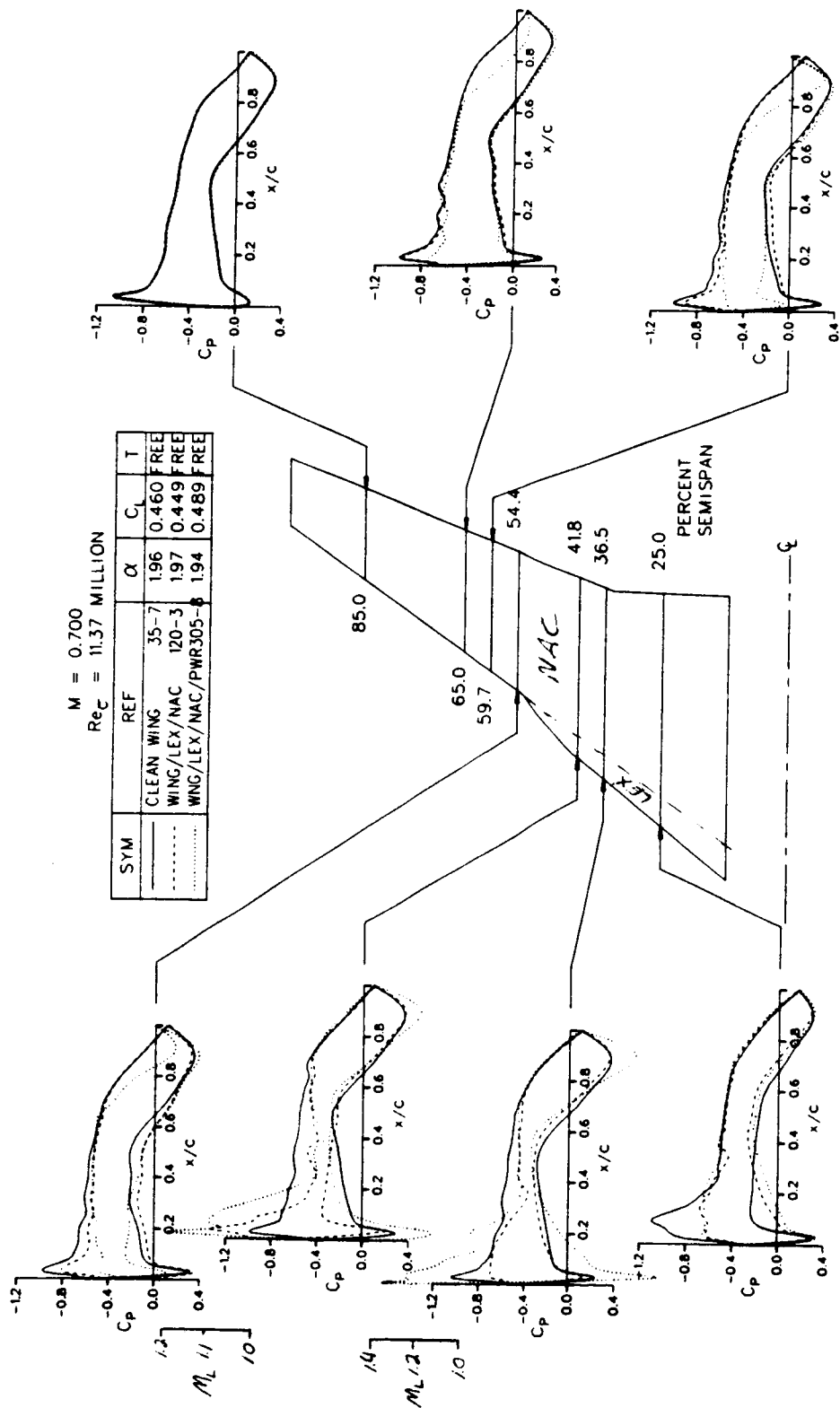


FIGURE 28. EXPERIMENTAL CHORDWISE PRESSURE DISTRIBUTIONS FOR STRAIGHT UNDERWING NACELLE WITH LEX, $0.7M_0$, $\alpha = 2$ DEGREES

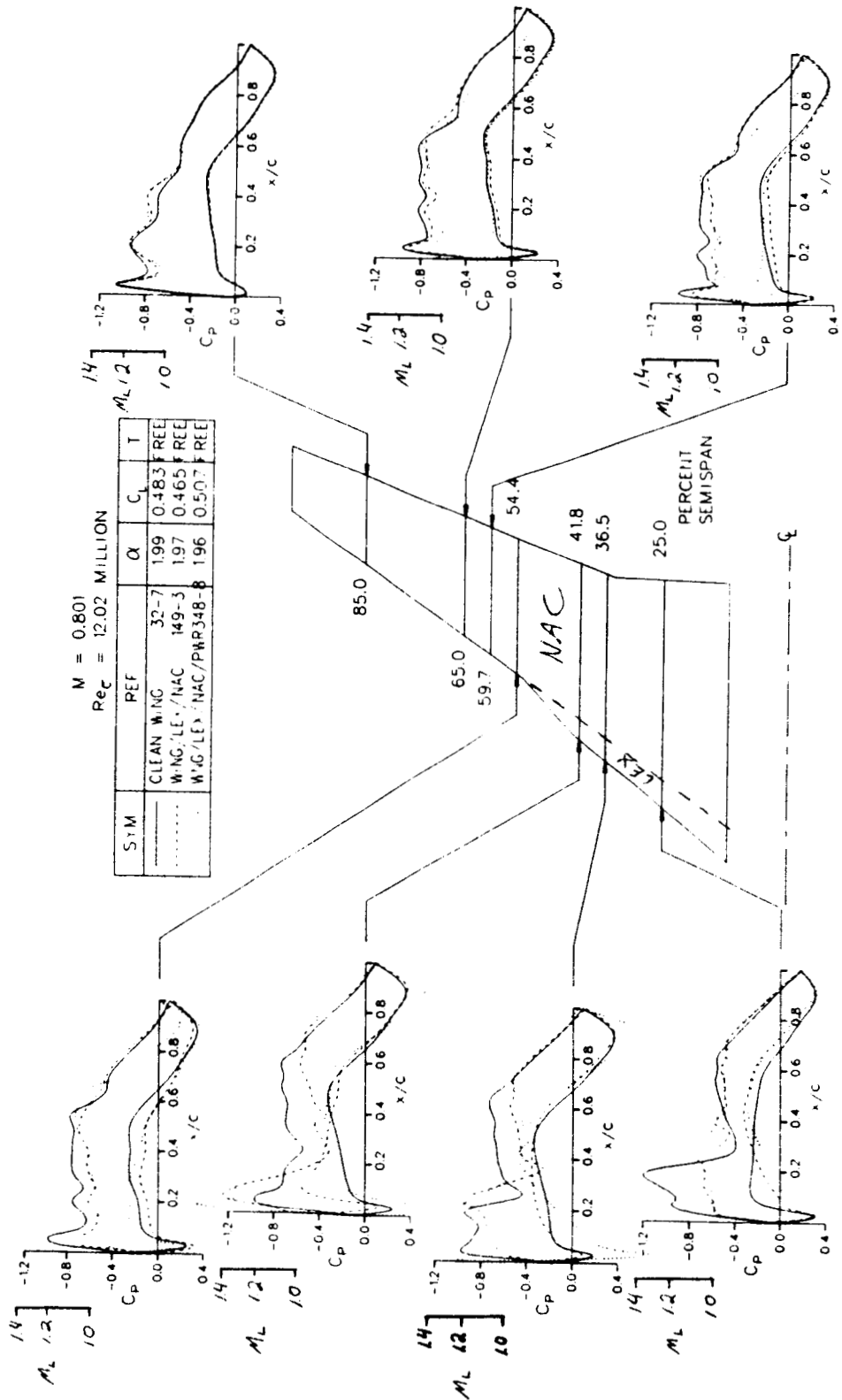


FIGURE 29. EXPERIMENTAL CHORDWISE PRESSURE DISTRIBUTIONS FOR STRAIGHT UNDERWING NACELLE WITH LEX, $0.8M_\infty$, $\alpha = 2$ DEGREES

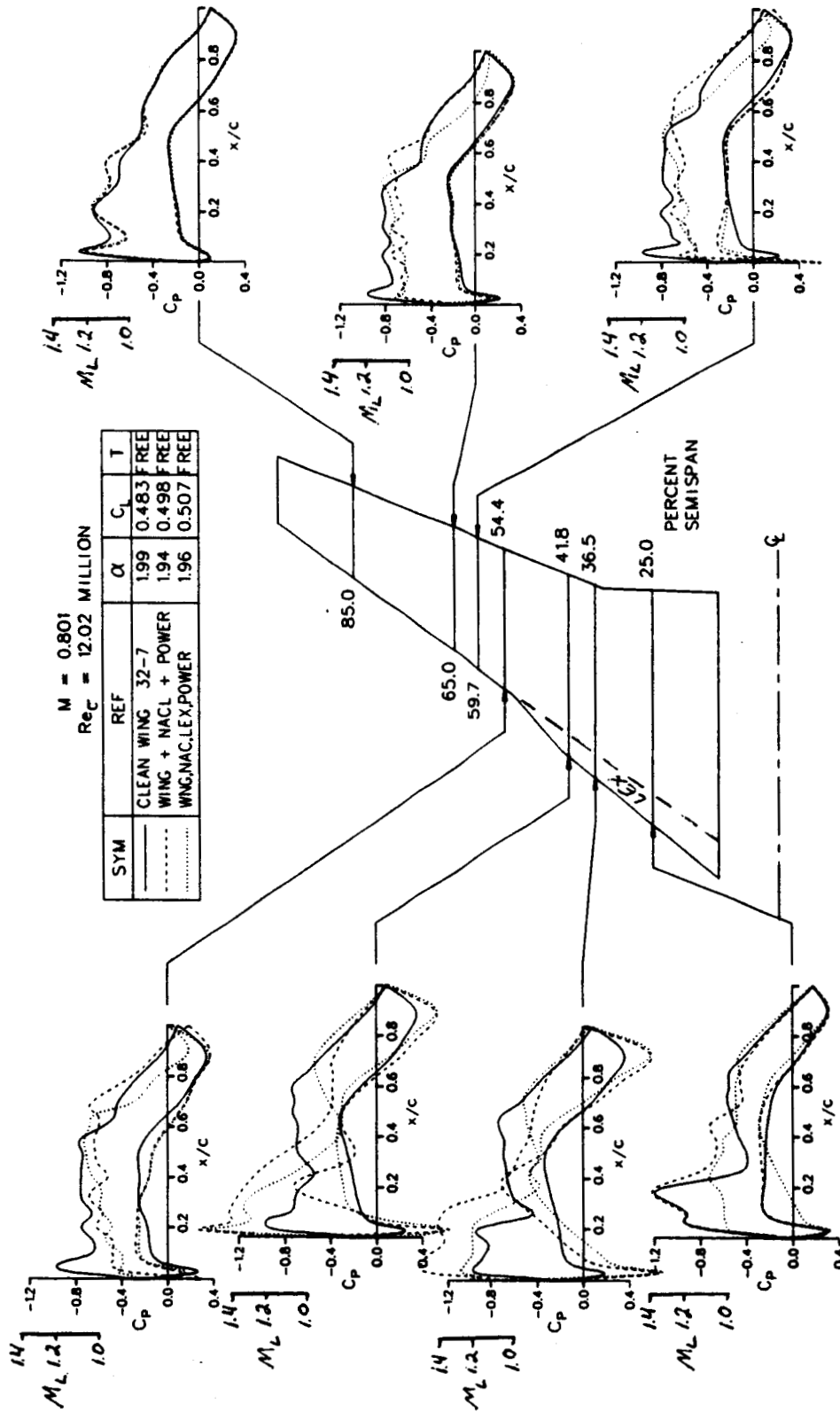
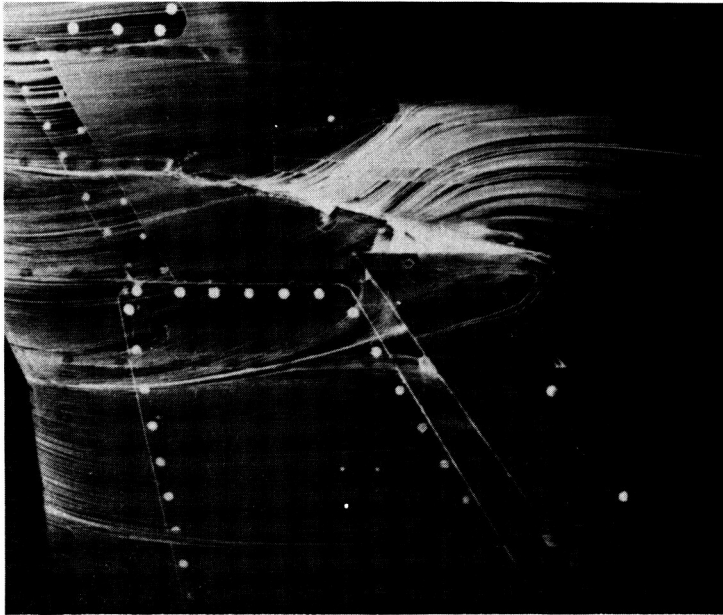


FIGURE 30. EXPERIMENTAL CHORDWISE PRESSURE DISTRIBUTIONS FOR STRAIGHT UNDERWING NACELLE WITH AND WITHOUT LEX AT $M_0 = 0.8$ - WITH POWER



$M_o = 0.8$
 $\alpha = 2 \text{ DEG}$
8,400 RPM
UPPER SURFACE

FIGURE 31. OIL FLOW PHOTOGRAPH FOR STRAIGHT UNDERWING NACELLE WITH LEX
AT $M_o = 0.8$ - WITH POWER

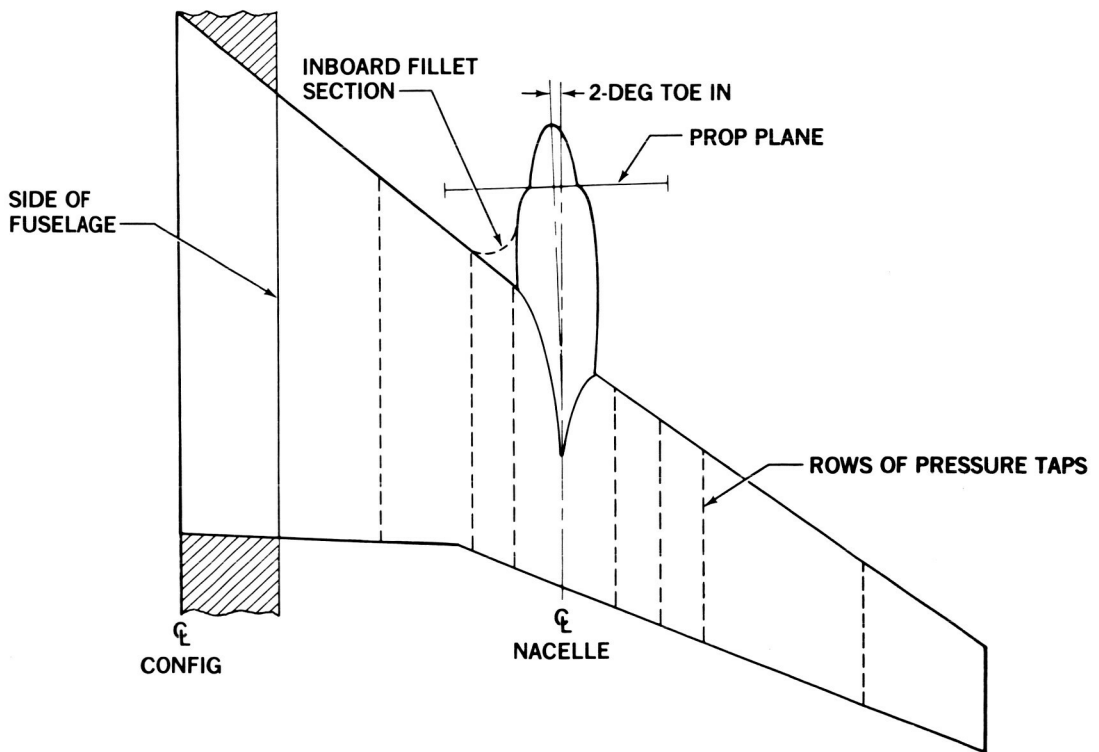


FIGURE 32. PLAN VIEW OF STRAIGHT UNDERWING NACELLE WITH LEX AND FILLET

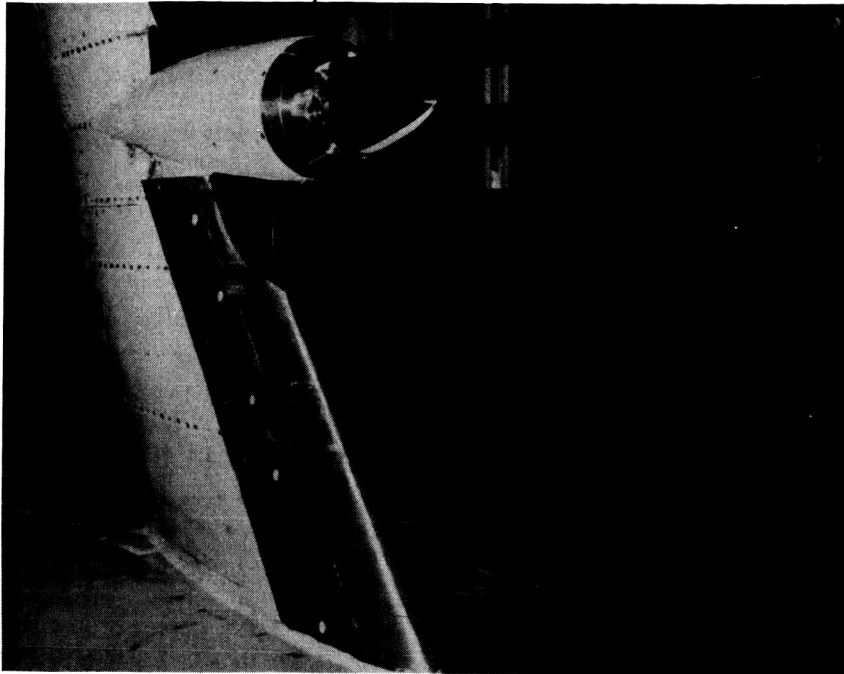


FIGURE 33. STRAIGHT UNDERWING NACELLE WITH LEX AND FILLET

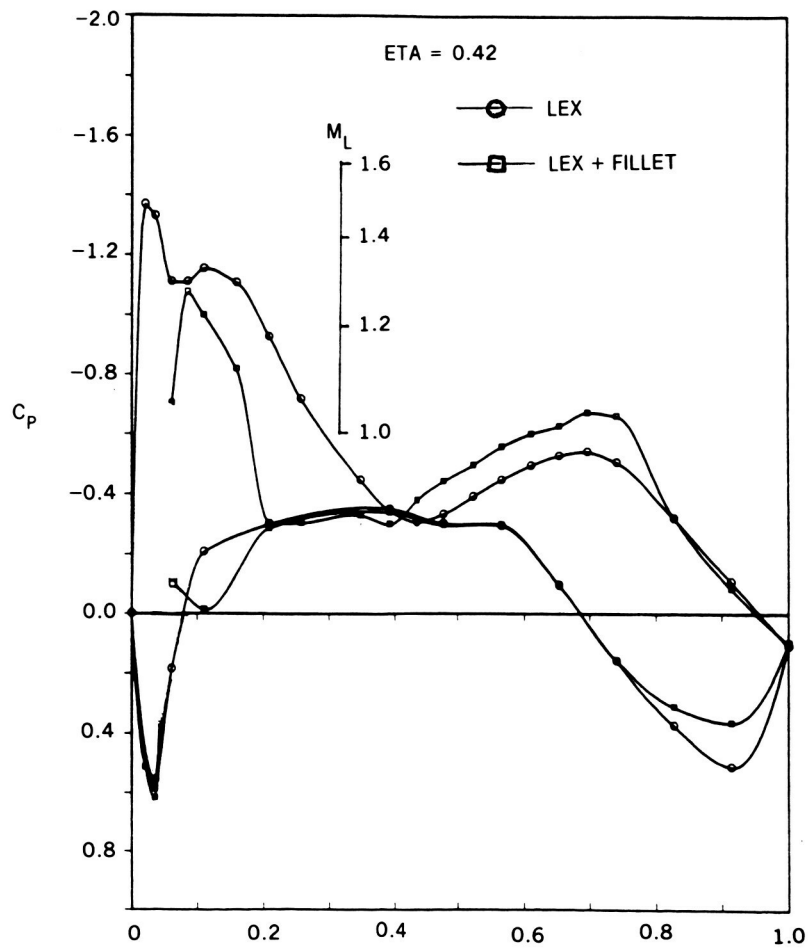


FIGURE 34. EXPERIMENTAL CHORDWISE PRESSURE DISTRIBUTION FOR STRAIGHT UNDERWING NACELLE WITH LEX AND FILLET - WITH POWER, 8250 RPM, $0.8M_0$, $\alpha = 2$ DEGREES

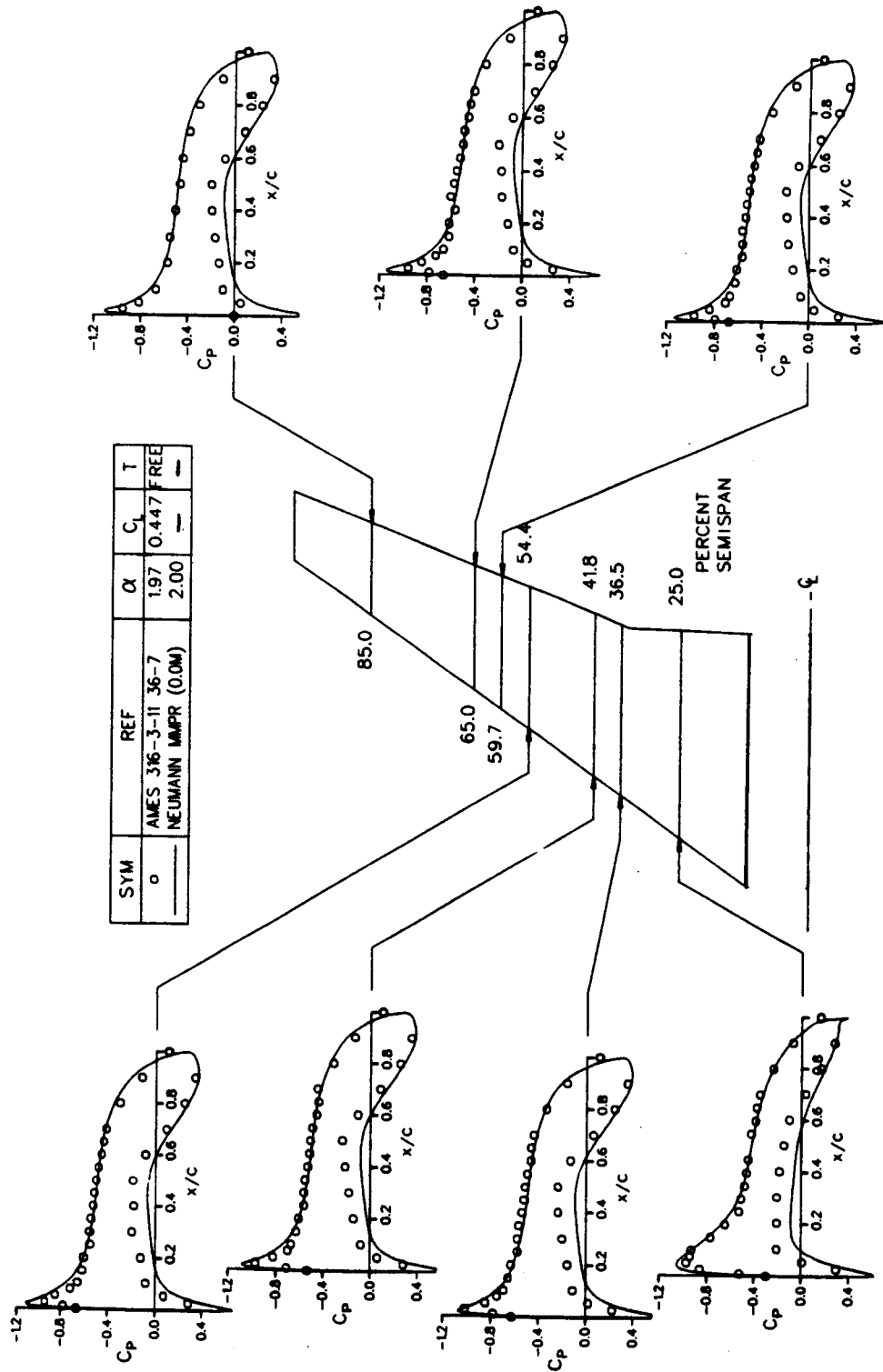


FIGURE 35. COMPARISON OF DAC-NEUMANN AND 0.6M₀ DATA FOR CLEAN WING W4, $\alpha = 2$ DEGREES

ORIGINAL PAGE IS
OF POOR QUALITY

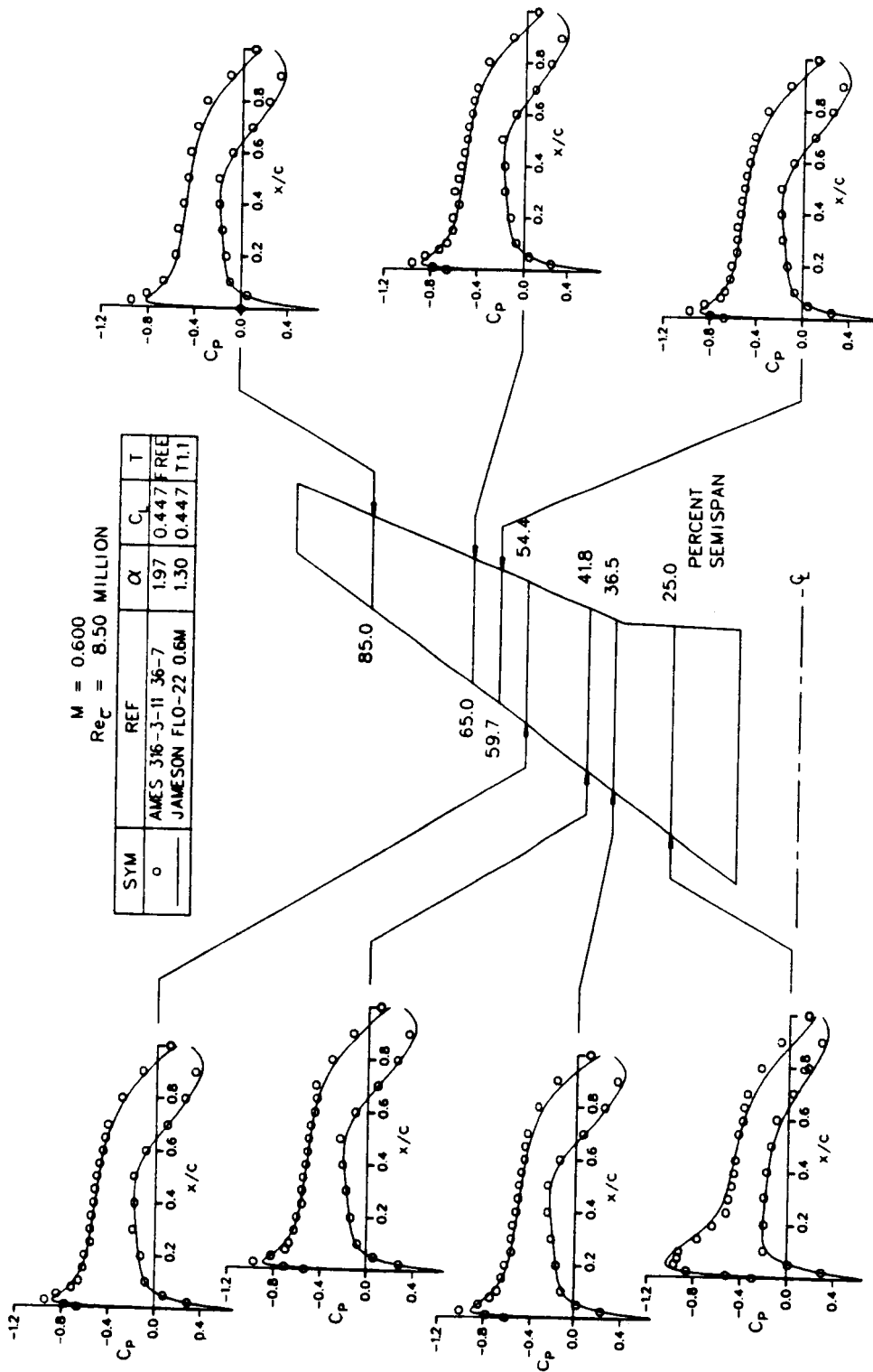


FIGURE 36. COMPARISON OF DAC-JAMESON AND DATA FOR CLEAN WING W4, $0.6M_0$, $C_L = 0.45$

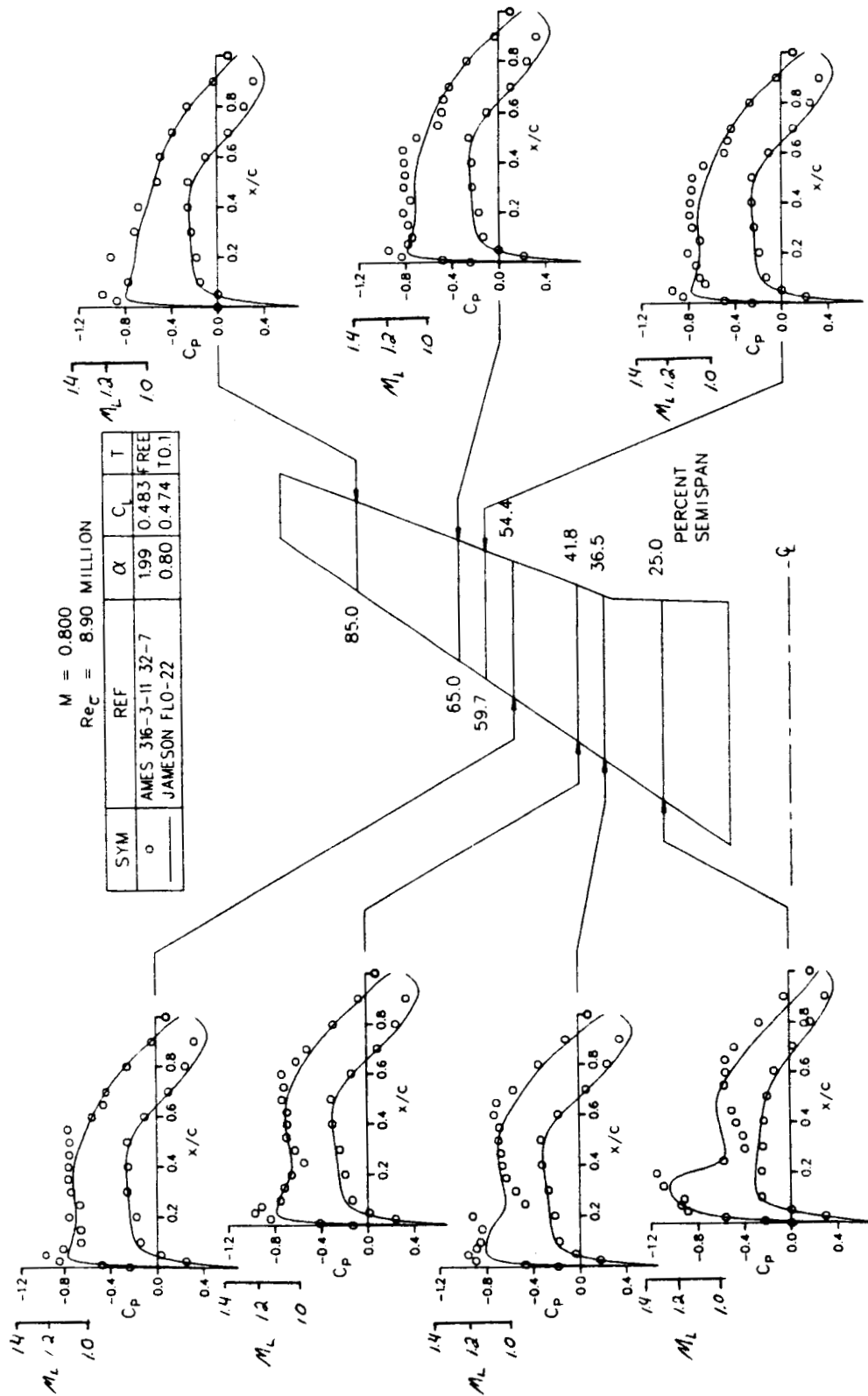


FIGURE 37. COMPARISON OF DAC-JAMESON AND DATA FOR CLEAN WING W4, $0.8M_0$, $C_L = 0.48$

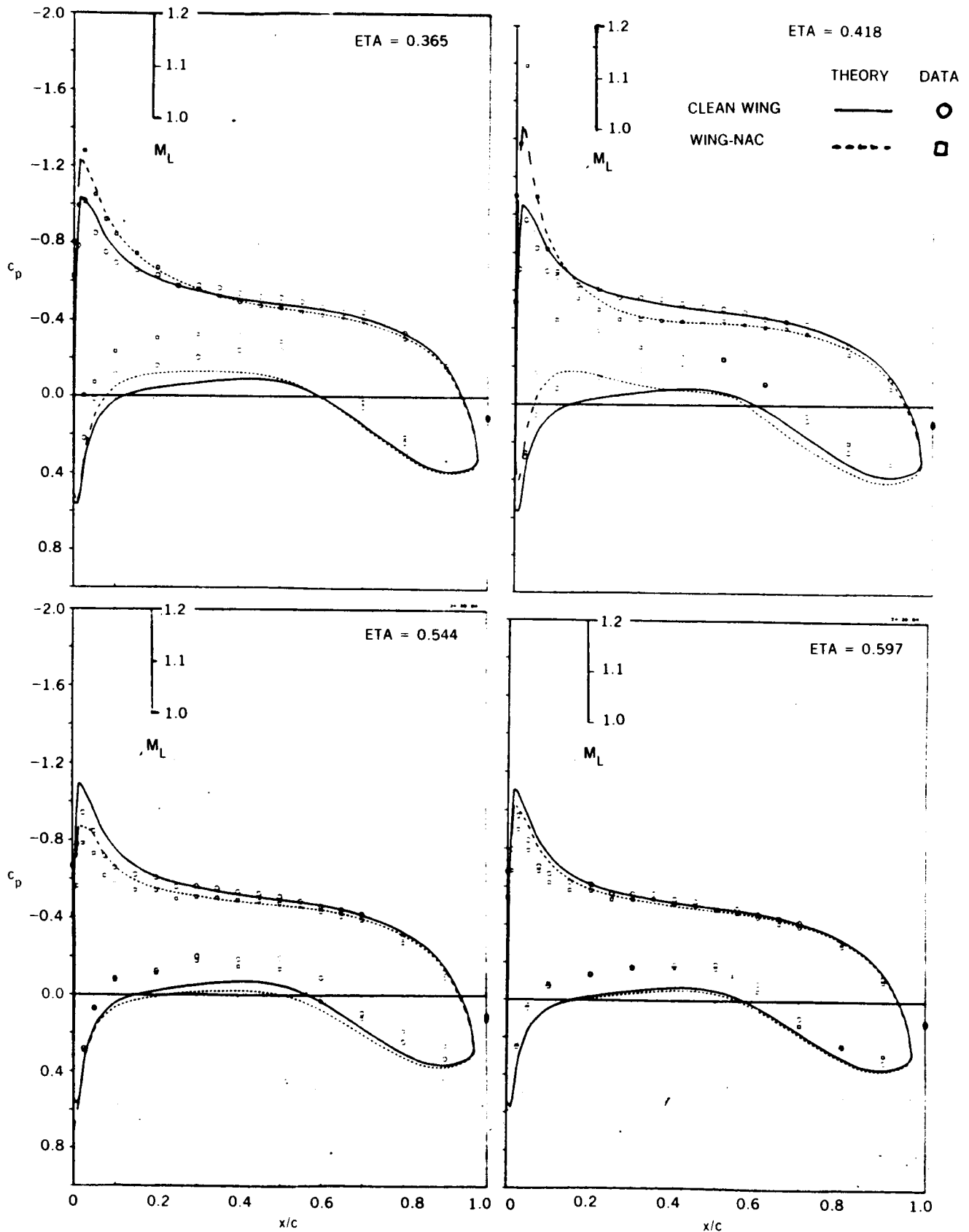


FIGURE 38. COMPARISON OF DAC-NEUMANN AND $0.6M_0$ DATA FOR STRAIGHT UNDERWING NACELLE
— NO POWER, $\alpha = 2$ DEGREES

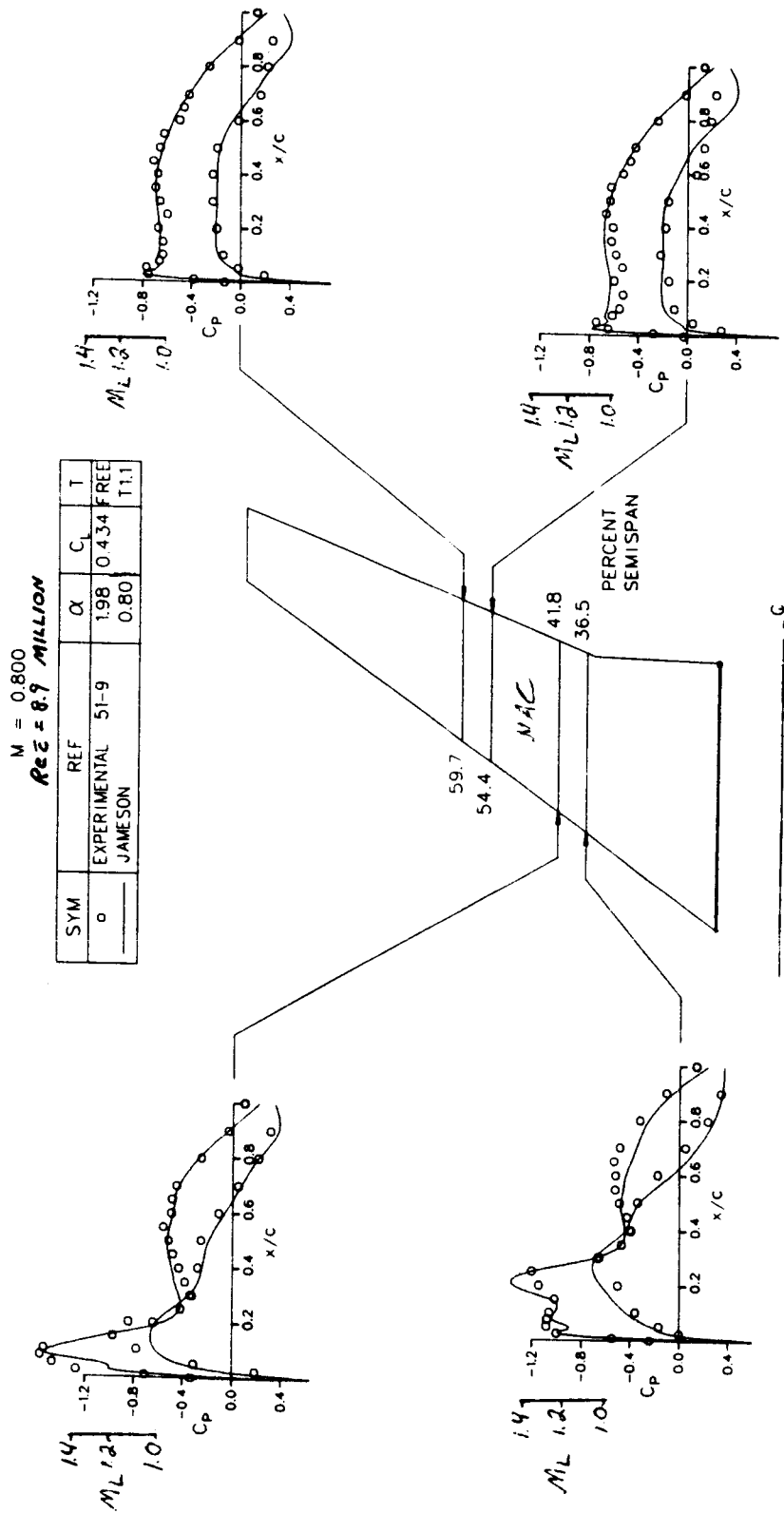


FIGURE 39. COMPARISON OF DAC-JAMESON AND DATA FOR STRAIGHT UNDERWING NACELLE -
NO POWER, 0.8M₀

ORIGINAL PAGE IS
OF POOR QUALITY

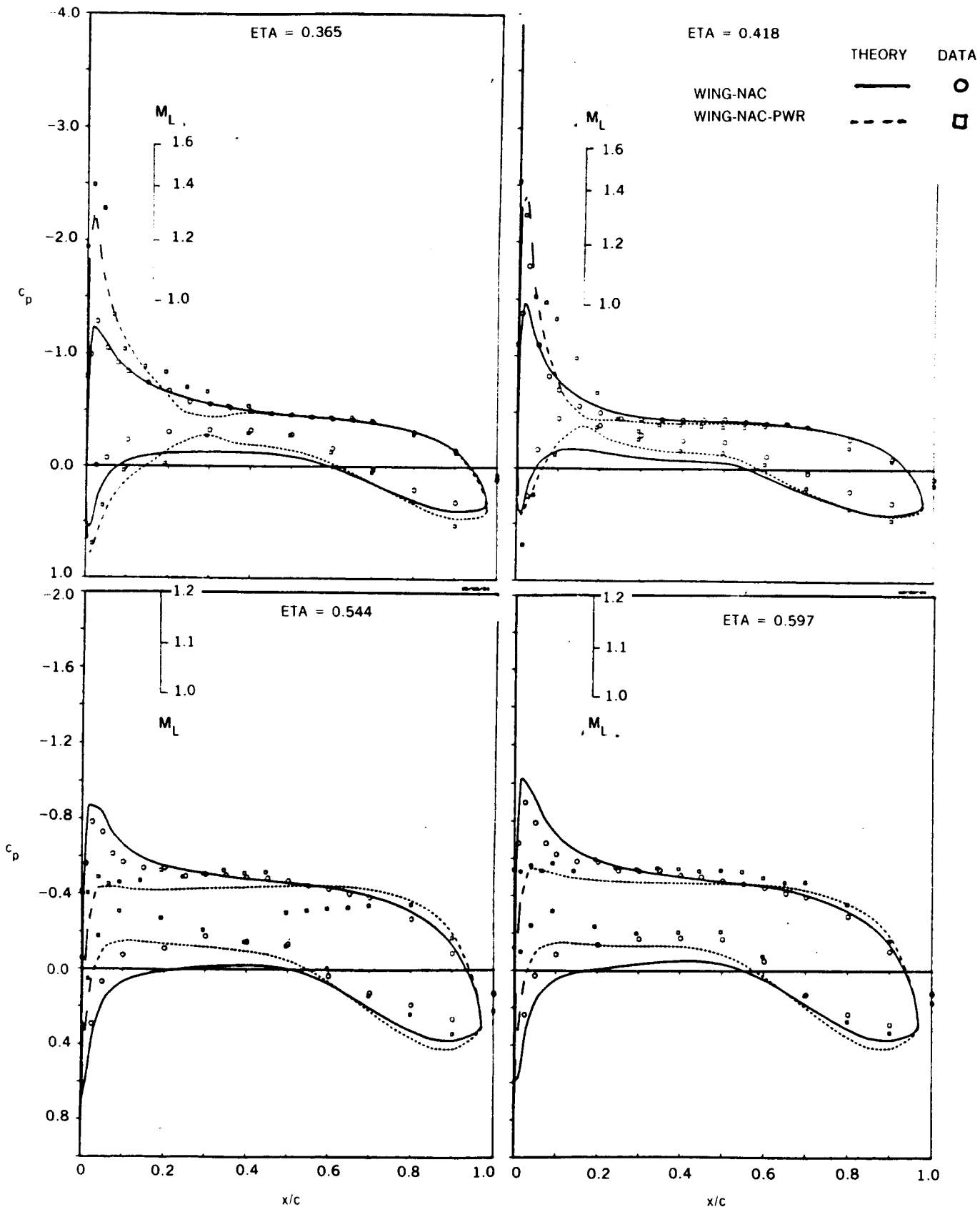


FIGURE 40. COMPARISON OF DAC-NEUMANN AND 0.6M₀ DATA FOR STRAIGHT UNDERWING NACELLE
- WITH POWER, $\alpha = 2$ DEGREES

ORIGINAL PAGE IS
OF POOR QUALITY

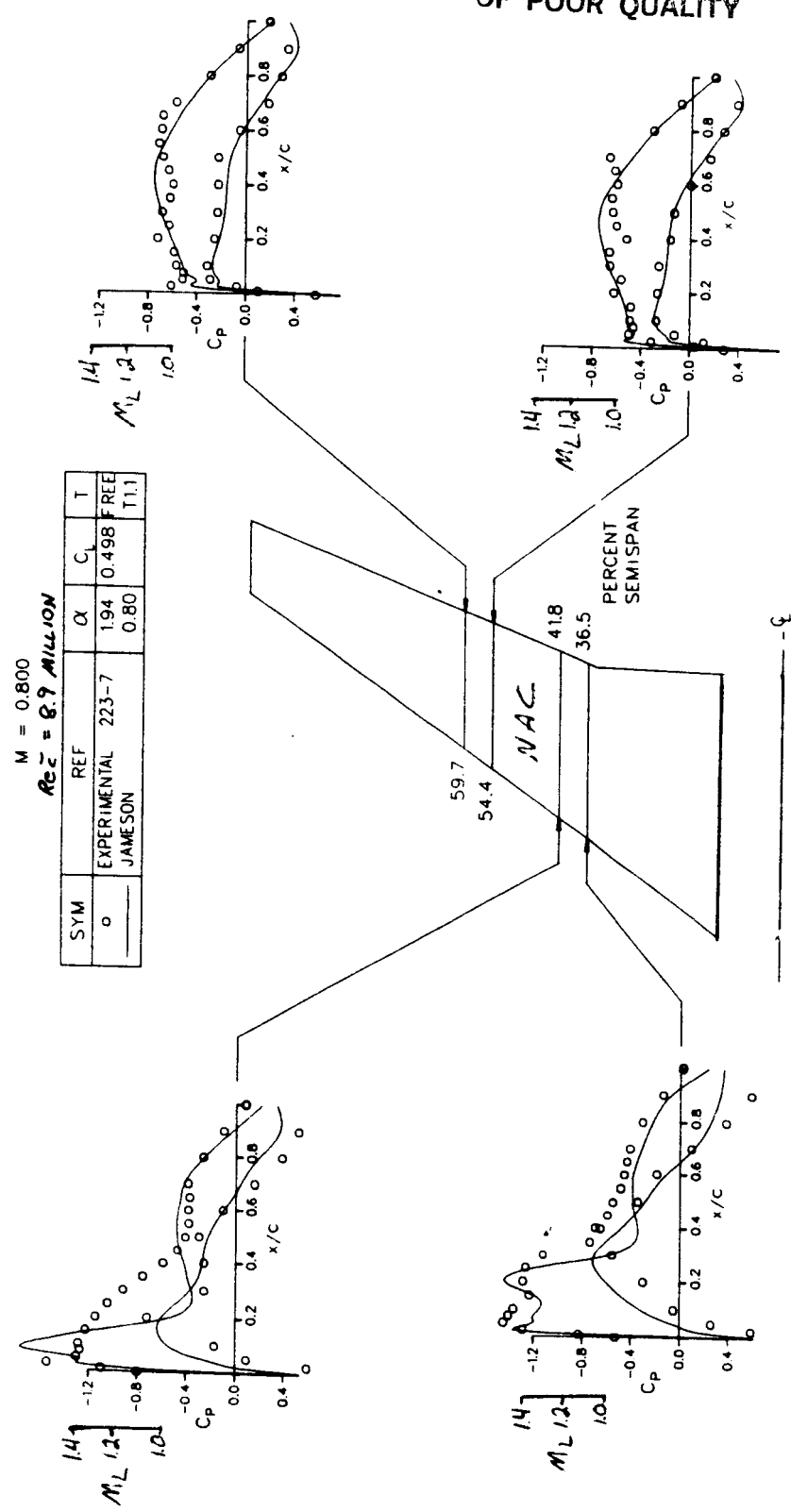


FIGURE 41. COMPARISON OF DAC-JAMESON AND DATA FOR STRAIGHT UNDERWING NACELLE - WITH POWER, 0.8M₀

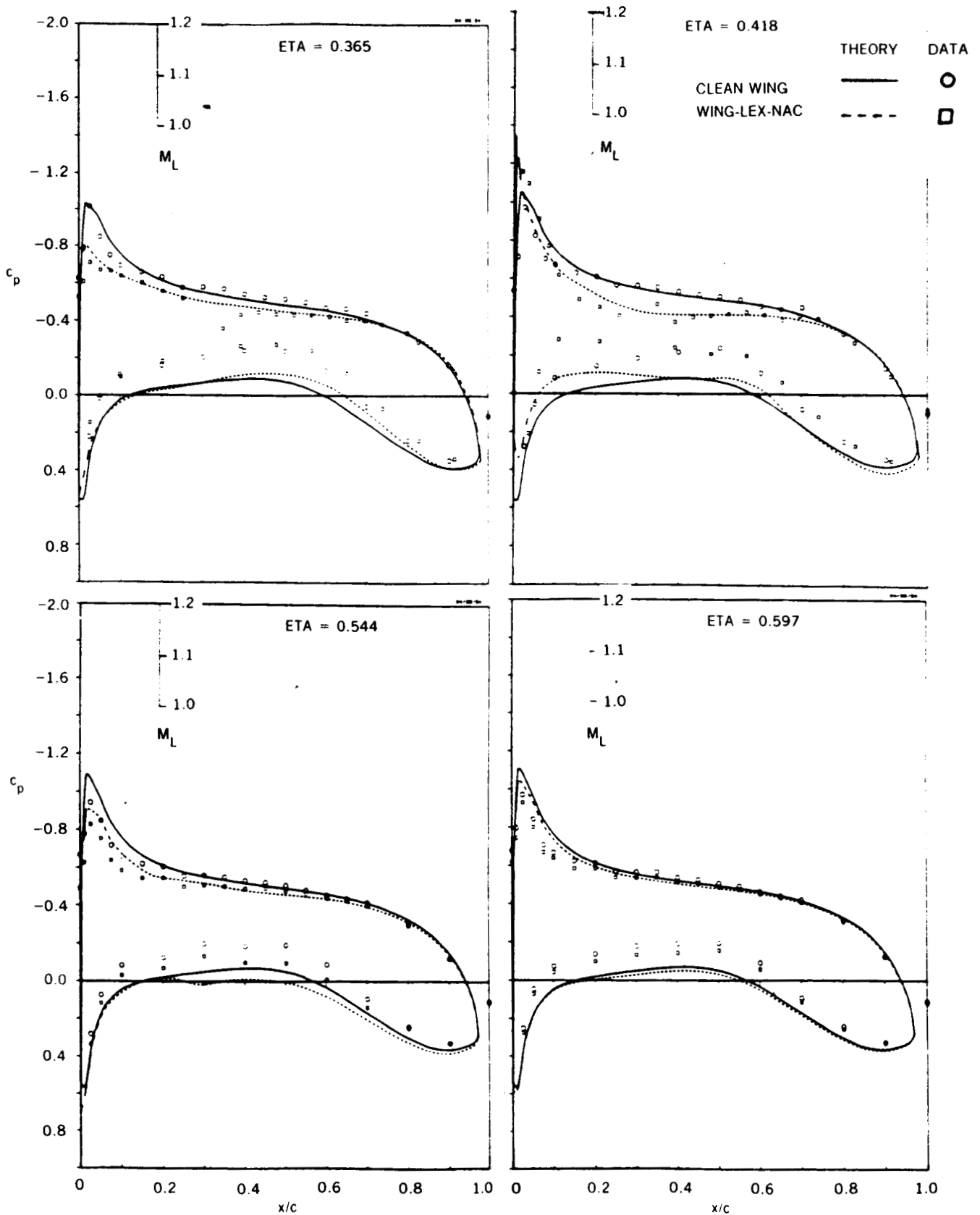


FIGURE 42. COMPARISON OF DAC-NEUMANN AND $0.6M_0$ DATA FOR STRAIGHT UNDERWING NACELLE WITH LEX - NO POWER, $\alpha = 2$ DEGREES

ORIGINAL PAGE IS
OF POOR QUALITY

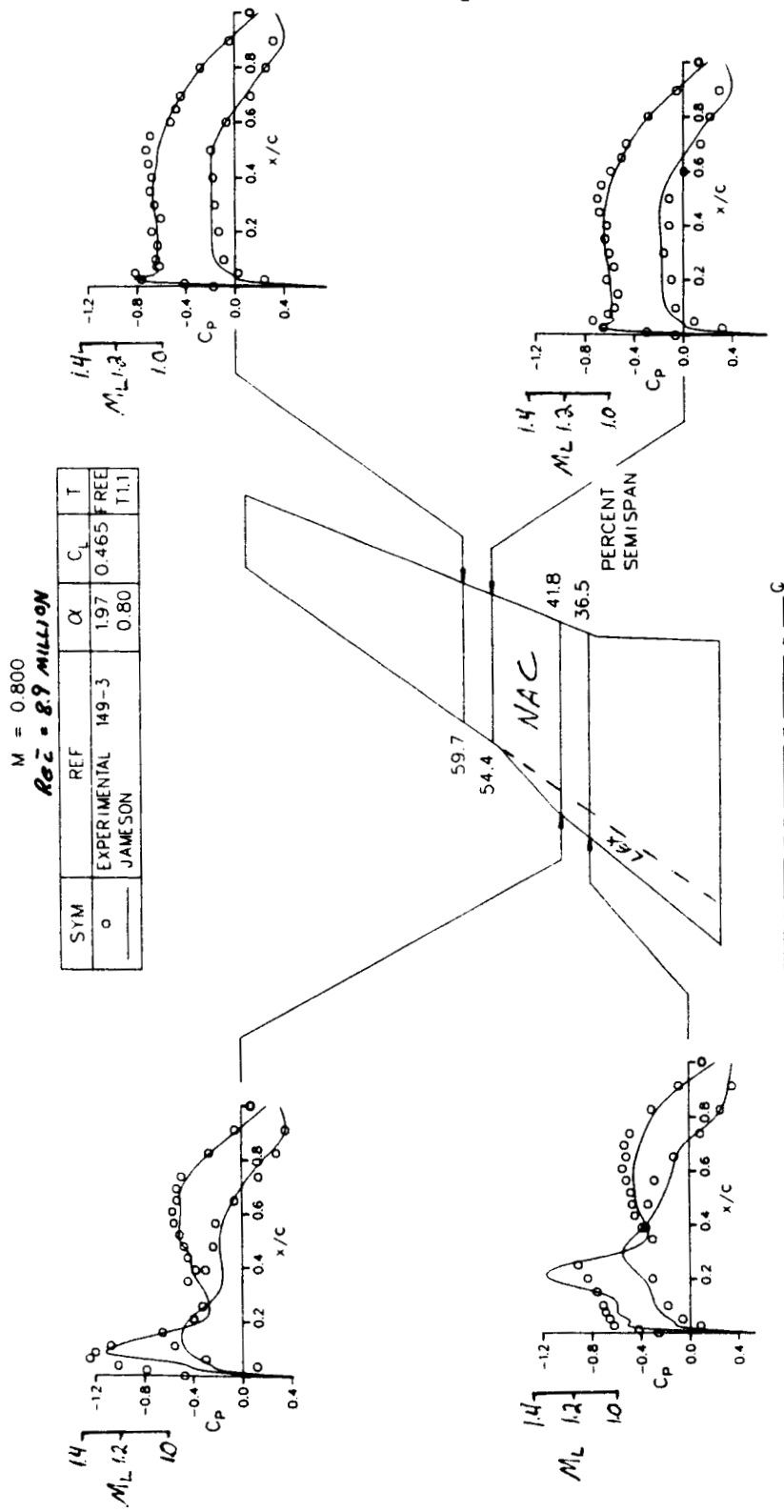


FIGURE 43. COMPARISON OF DAC-JAMESON AND DATA FOR STRAIGHT UNDERLYING NACELLE WITH LEX - NO POWER, 0.8M₀

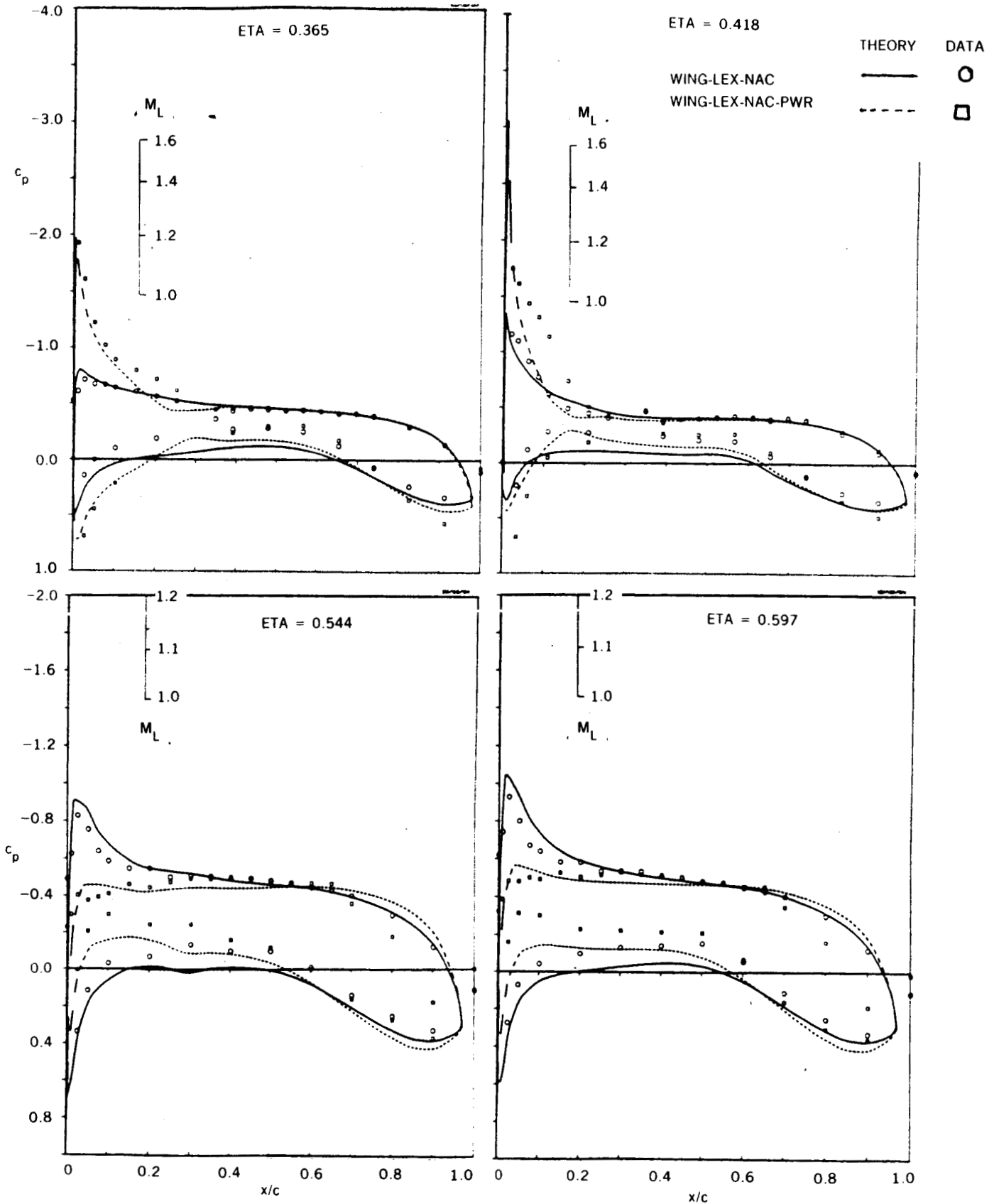


FIGURE 44. COMPARISON OF DAC-NEUMANN AND $0.6M_0$ DATA FOR STRAIGHT UNDERWING NACELLE WITH LEX - WITH POWER, $\alpha = 2$ DEGREES

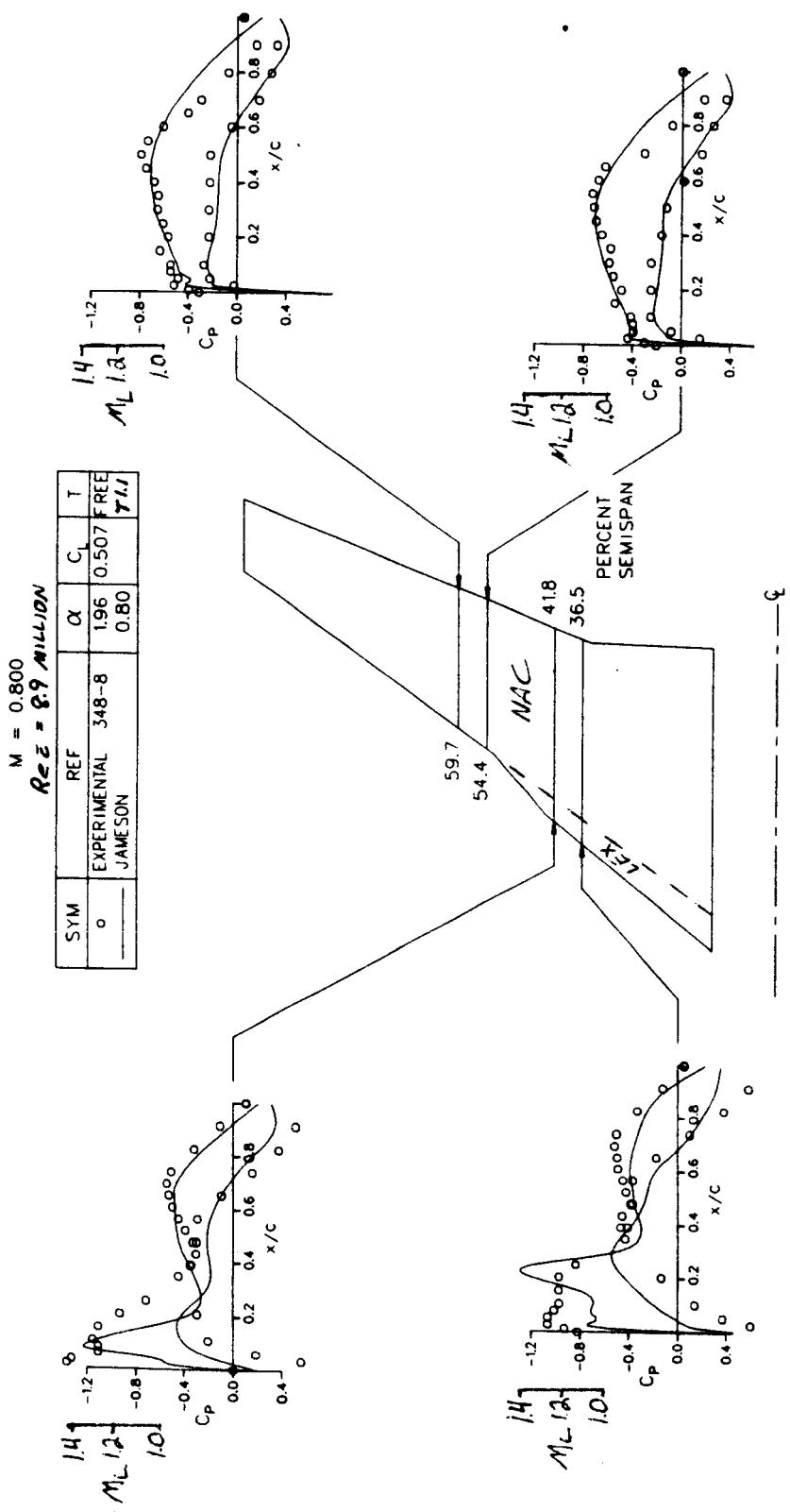


FIGURE 45. COMPARISON OF DAC-JAMESON AND DATA FOR STRAIGHT UNDERWING NACELLE WITH LEX - WITH POWER, $0.8M_0$

ORIGINAL PAGE IS
OF POOR QUALITY

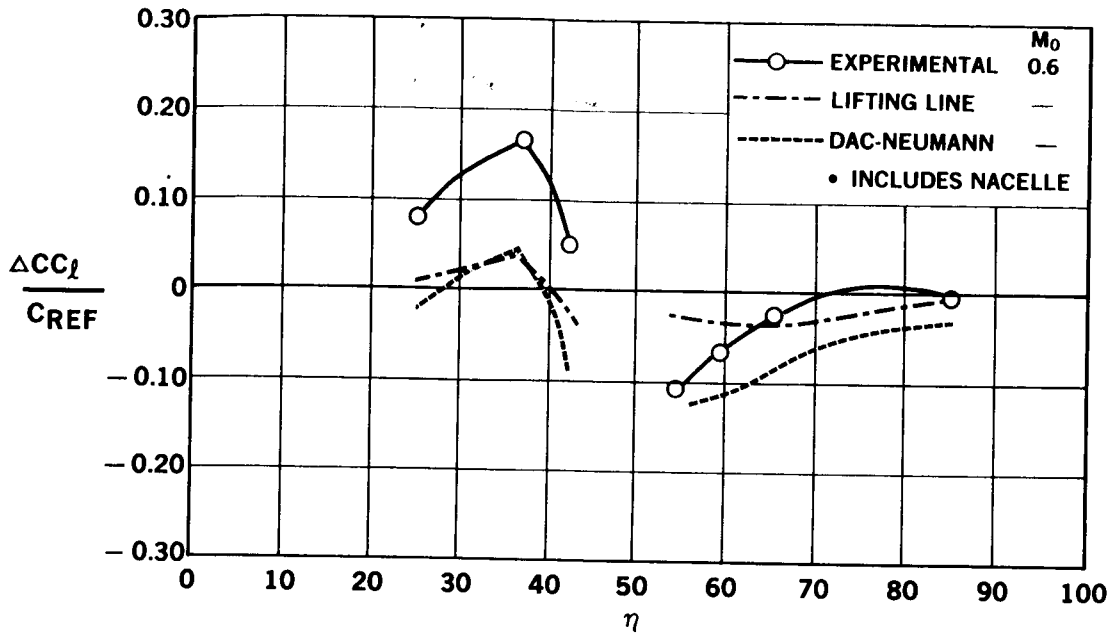


FIGURE 46. DATA-THEORY COMPARISON OF SPAN LOADING INCREMENTS DUE TO POWER FOR STRAIGHT UNDERWING NACELLE

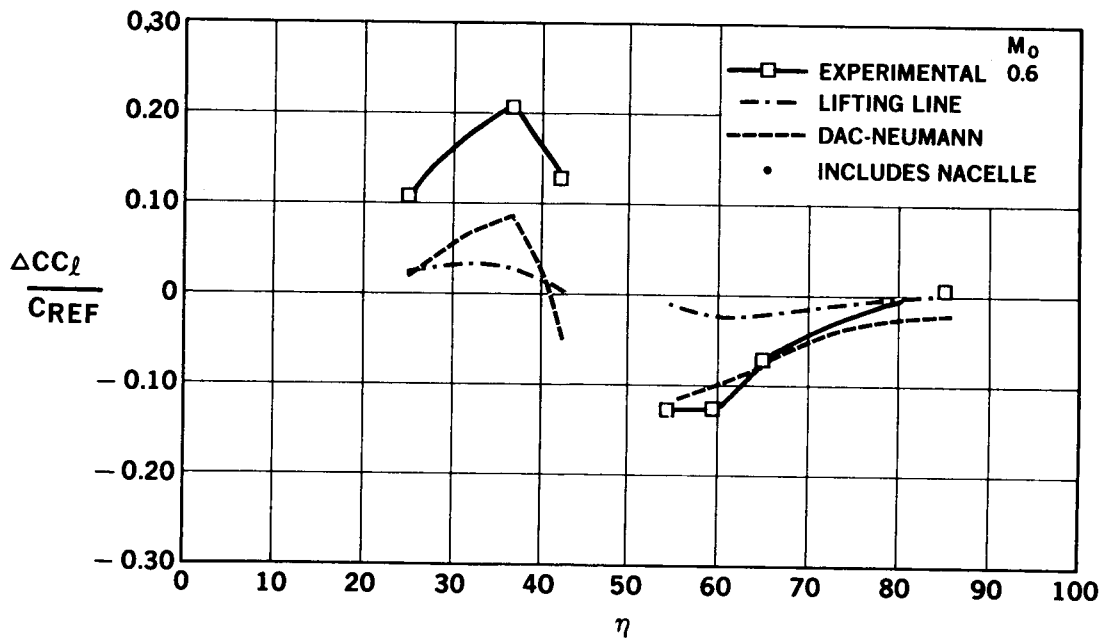


FIGURE 47. DATA-THEORY COMPARISON OF SPAN LOADING INCREMENTS DUE TO POWER FOR STRAIGHT UNDERWING NACELLE WITH LEX

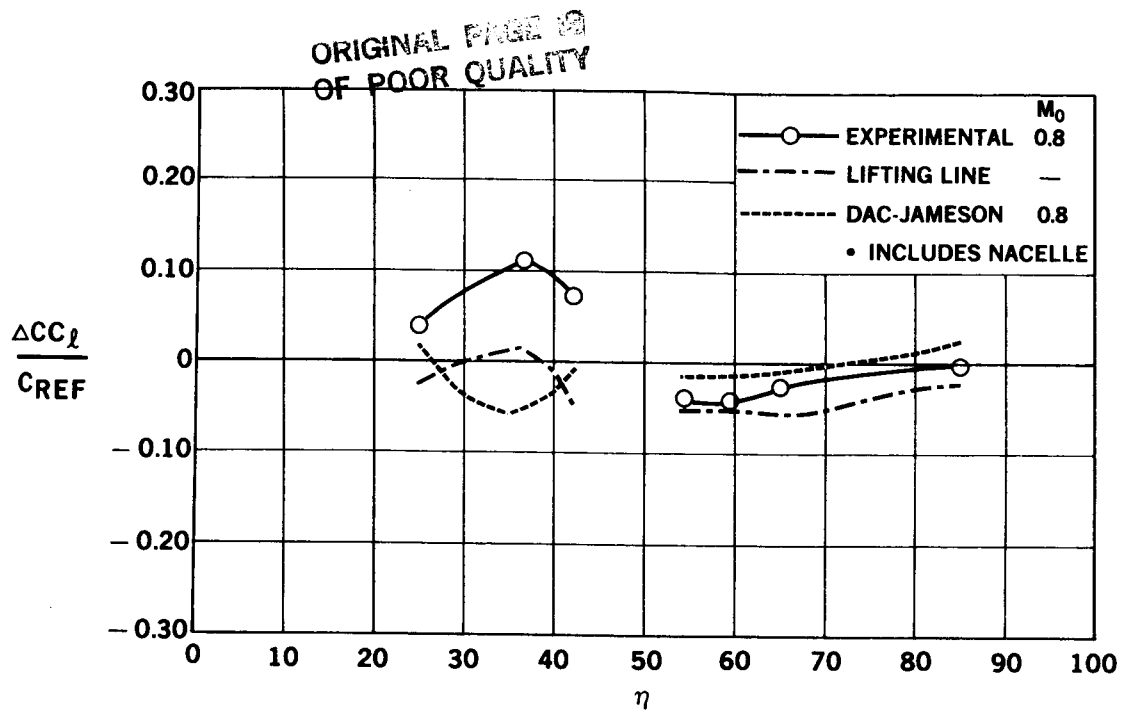


FIGURE 48. DATA-THEORY COMPARISON OF SPAN LOADING INCREMENTS DUE TO POWER FOR STRAIGHT UNDERWING NACELLE

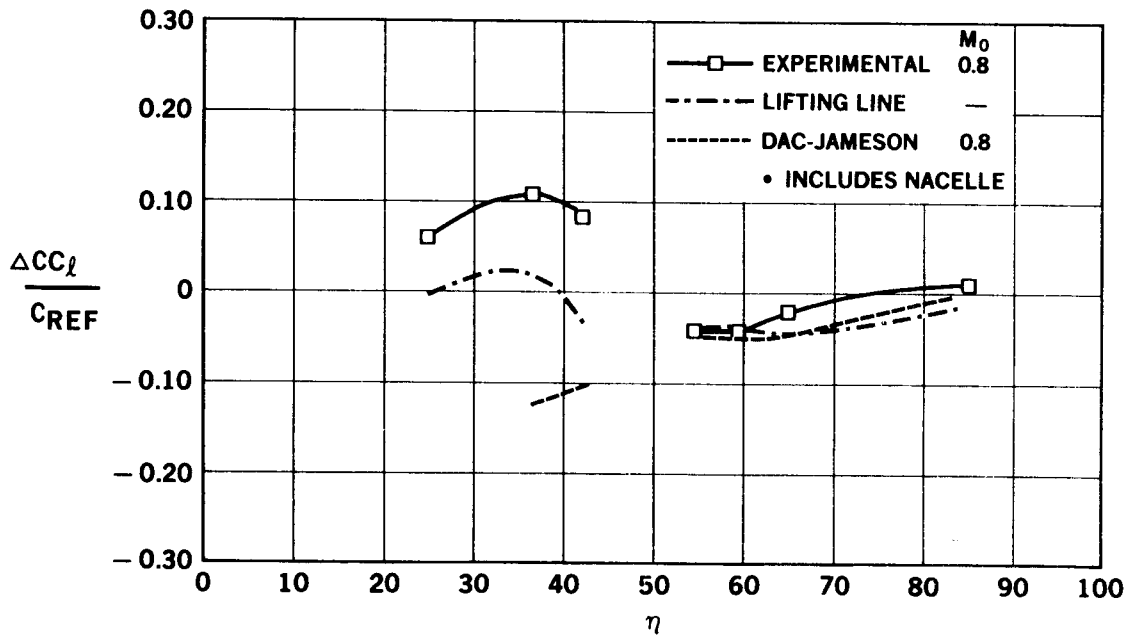


FIGURE 49. DATA-THEORY COMPARISON OF SPAN LOADING INCREMENTS DUE TO POWER FOR STRAIGHT UNDERWING NACELLE WITH LEX

ORIGINAL PAGE IS
OF POOR QUALITY

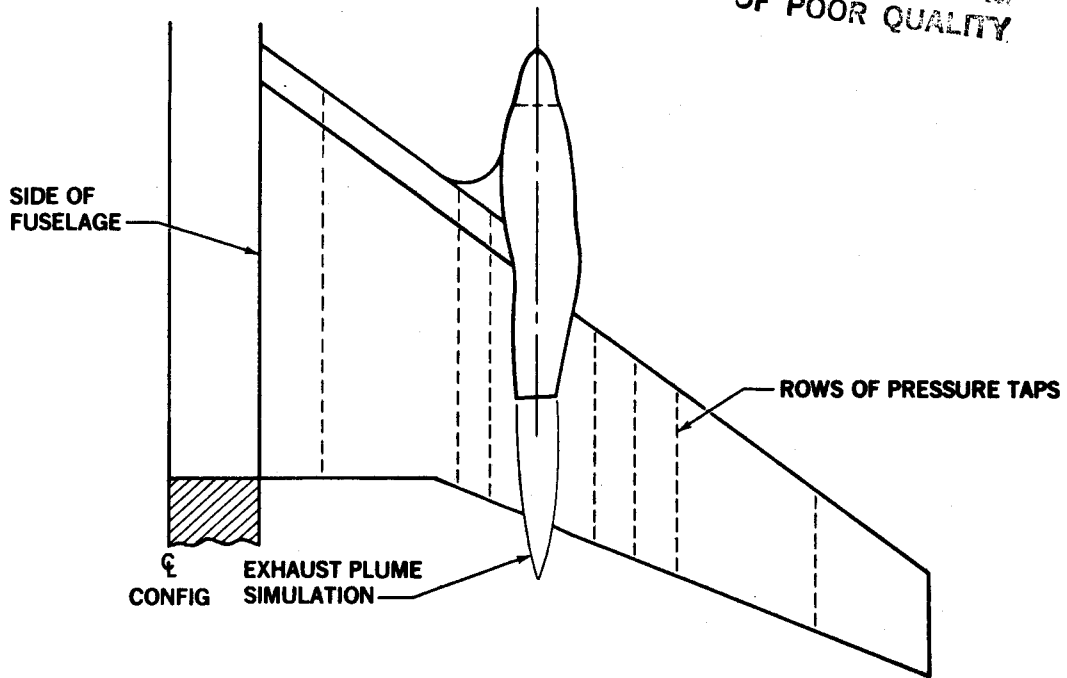


FIGURE 50. PLAN VIEW OF OVERWING CONTOURED NACELLE

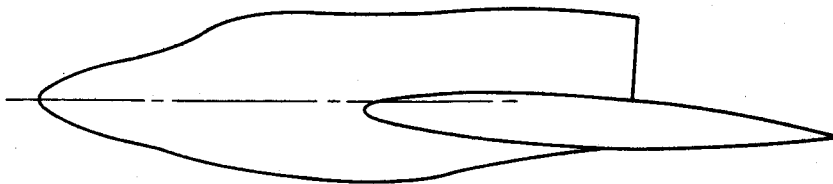


FIGURE 51. SIDE VIEW OF OVERWING CONTOURED NACELLE



ORIGINAL PAGE IS
OF POOR QUALITY

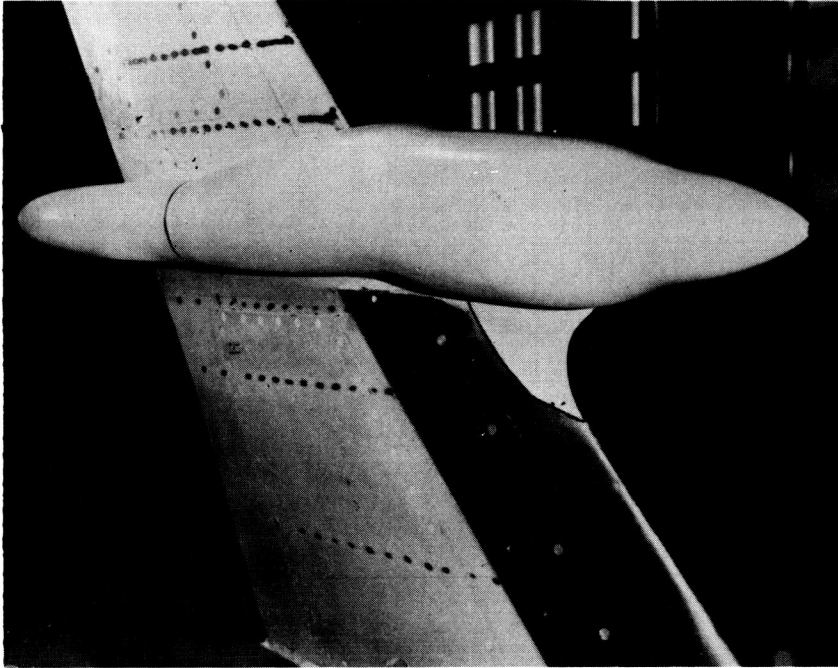


FIGURE 52. CONTOURED OVERWING NACELLE WITH LEX AND FILLET INSTALLED IN AMES 11-FOOT TUNNEL

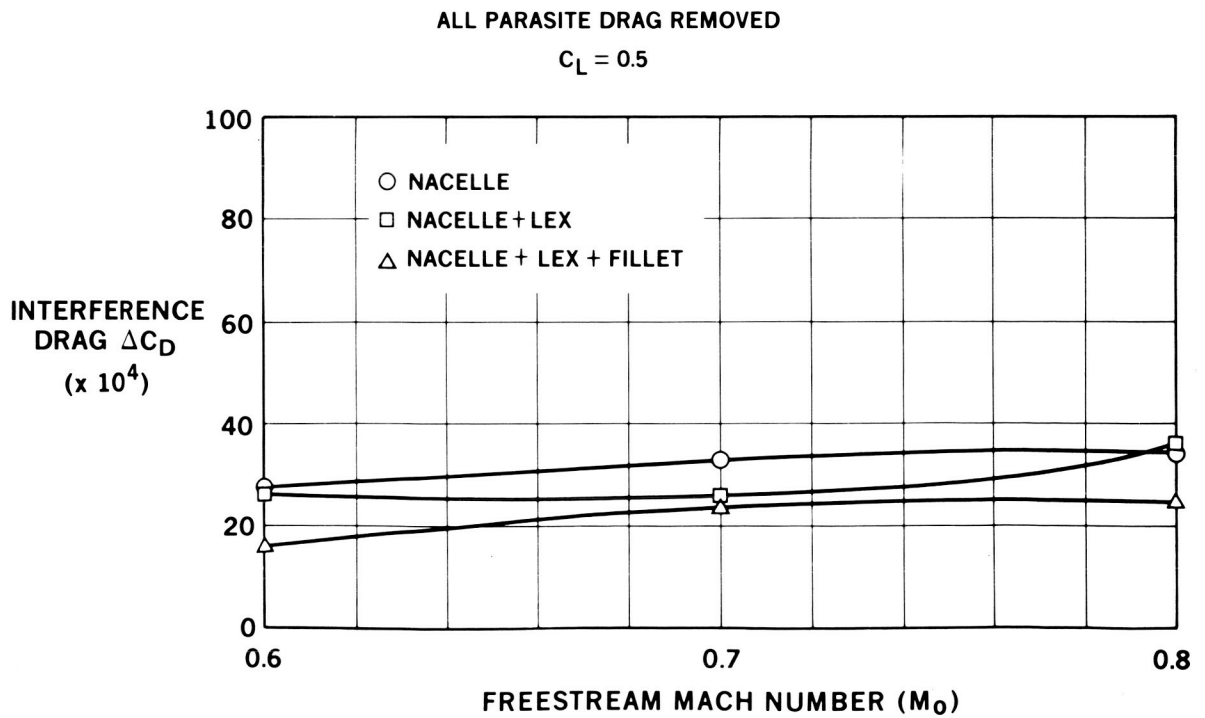


FIGURE 53. INTERFERENCE DRAG LEVELS FOR CONTOURED OVERWING NACELLE

107

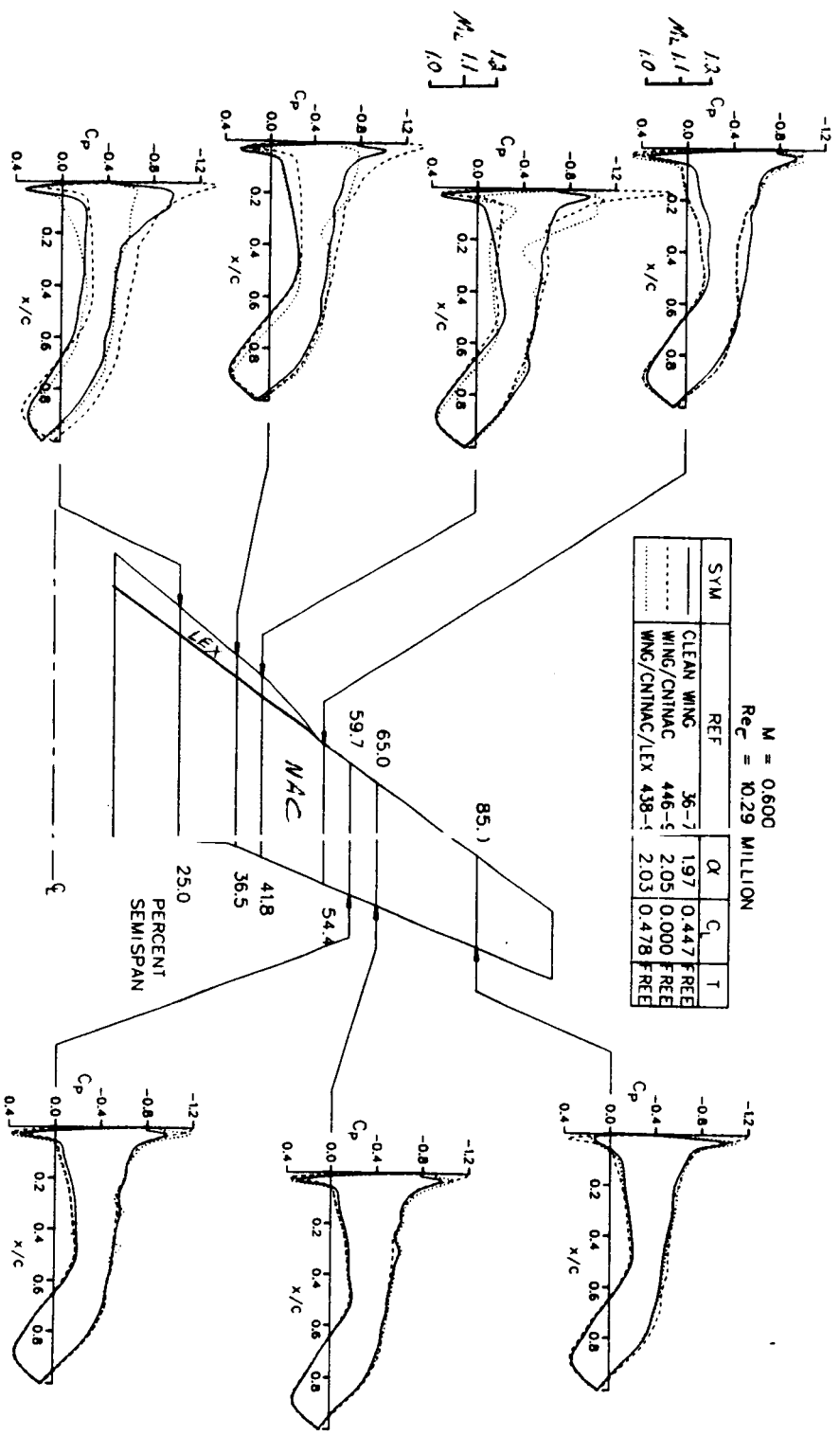


FIGURE 54. EXPERIMENTAL CHORDWISE PRESSURE DISTRIBUTIONS FOR CONTOURED OVERWING
 NACELLE, $0.6 M_0$, $\alpha = 2$ DEGREES

ORIGINAL PAGE IS OF POOR QUALITY

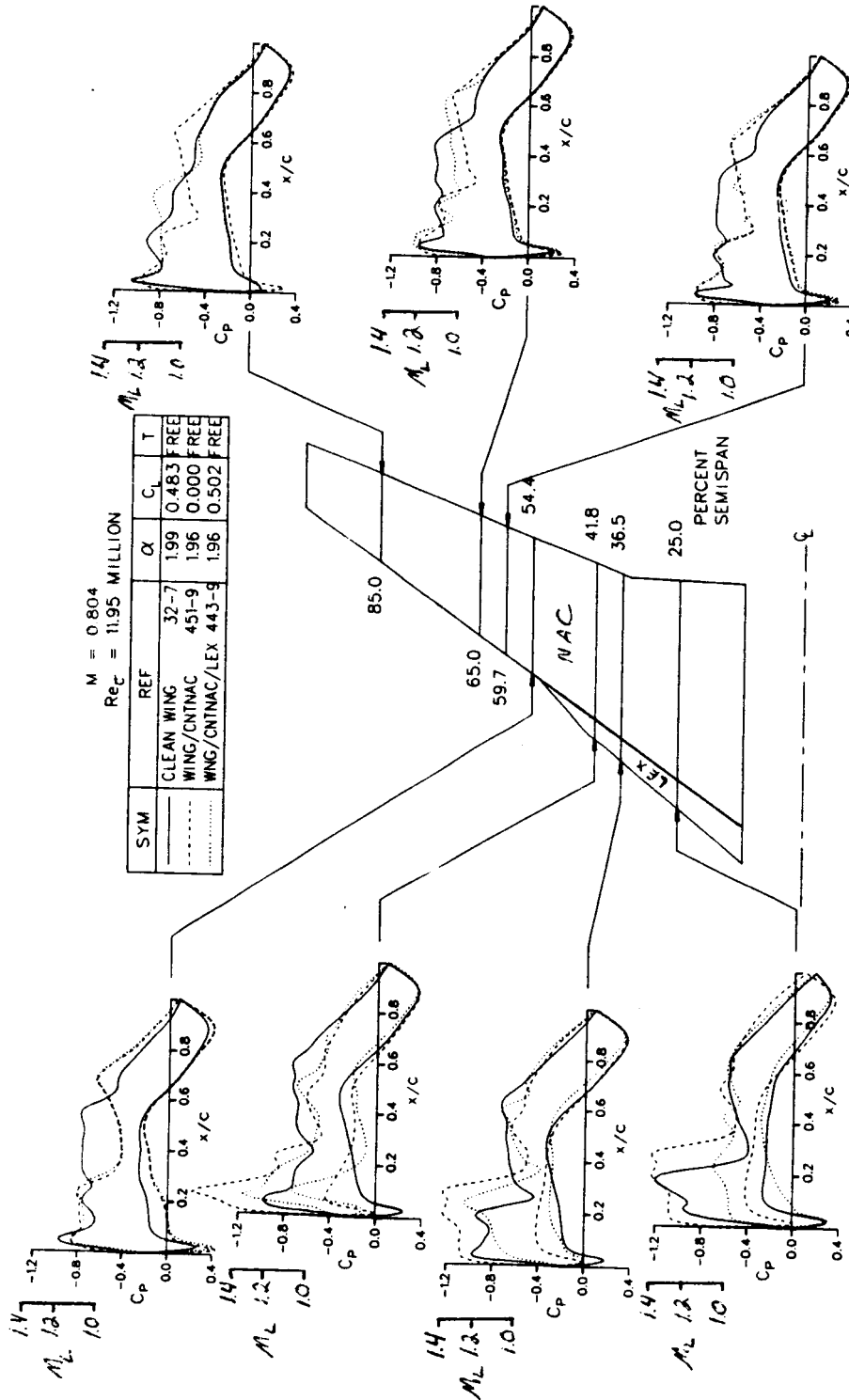
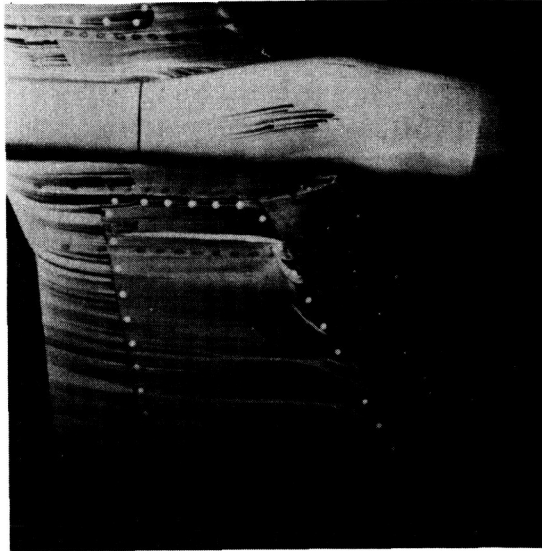


FIGURE 55. EXPERIMENTAL CHORDWISE PRESSURE DISTRIBUTIONS FOR CONTOURED OVERWING
NACELLE, $0.8 M_0$, $\alpha = 2$ DEGREES

ORIGINAL PAGE IS
OF POOR QUALITY



$$M_o = 0.8$$

$$\alpha = 2 \text{ DEG}$$

FIGURE 56. OIL FLOW-PHOTOGRAPH FOR CONTOURED OVERWING NACELLE, NO POWER

ORIGINAL PAGE IS
OF POOR QUALITY

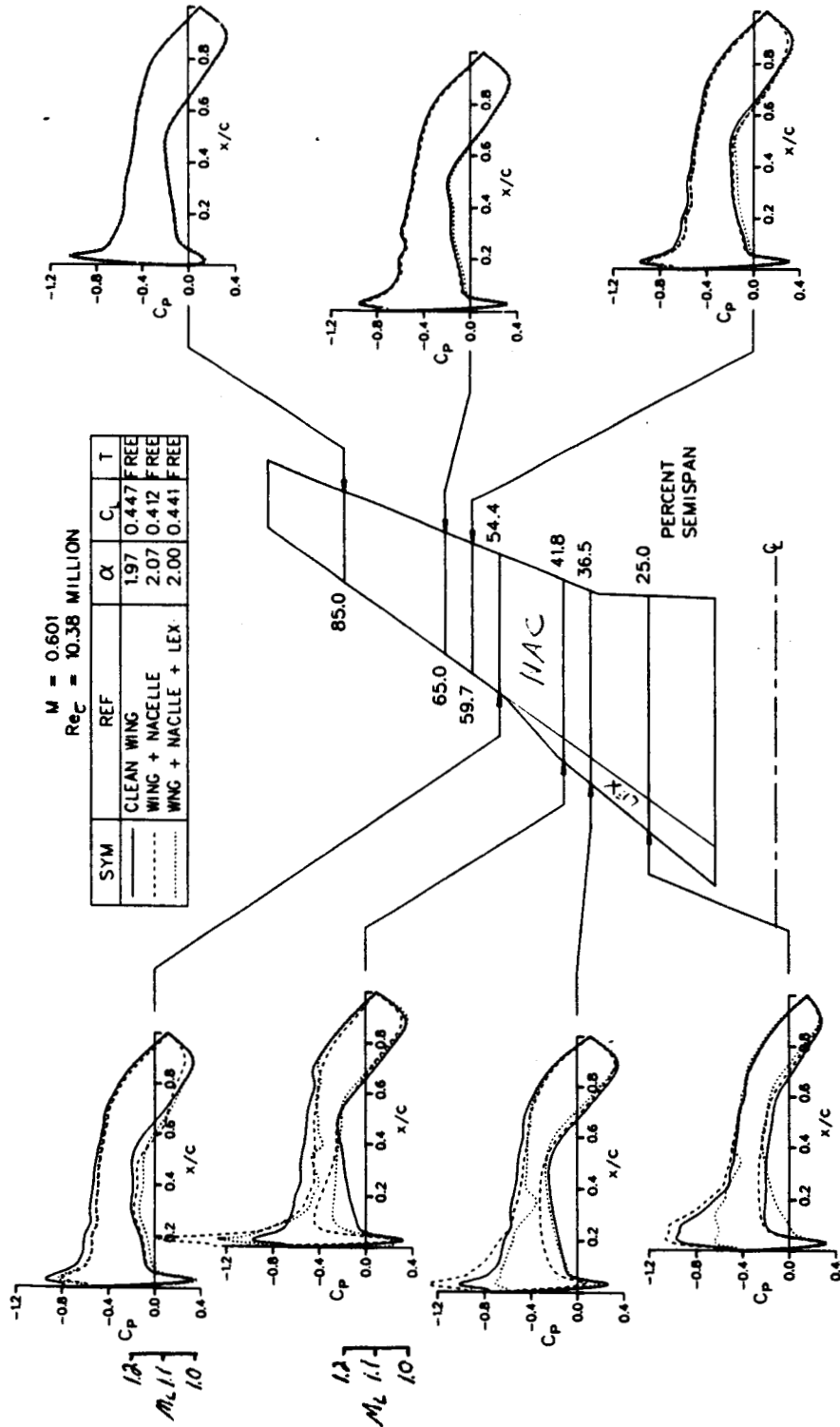


FIGURE 57. EXPERIMENTAL CHORDWISE PRESSURE DISTRIBUTIONS FOR STRAIGHT UNDERWING NACELLE WITH AND WITHOUT LEX, $M_0 = 0.6$, $\alpha = 2$ DEGREES

ORIGINAL PAGE IS
OF POOR QUALITY

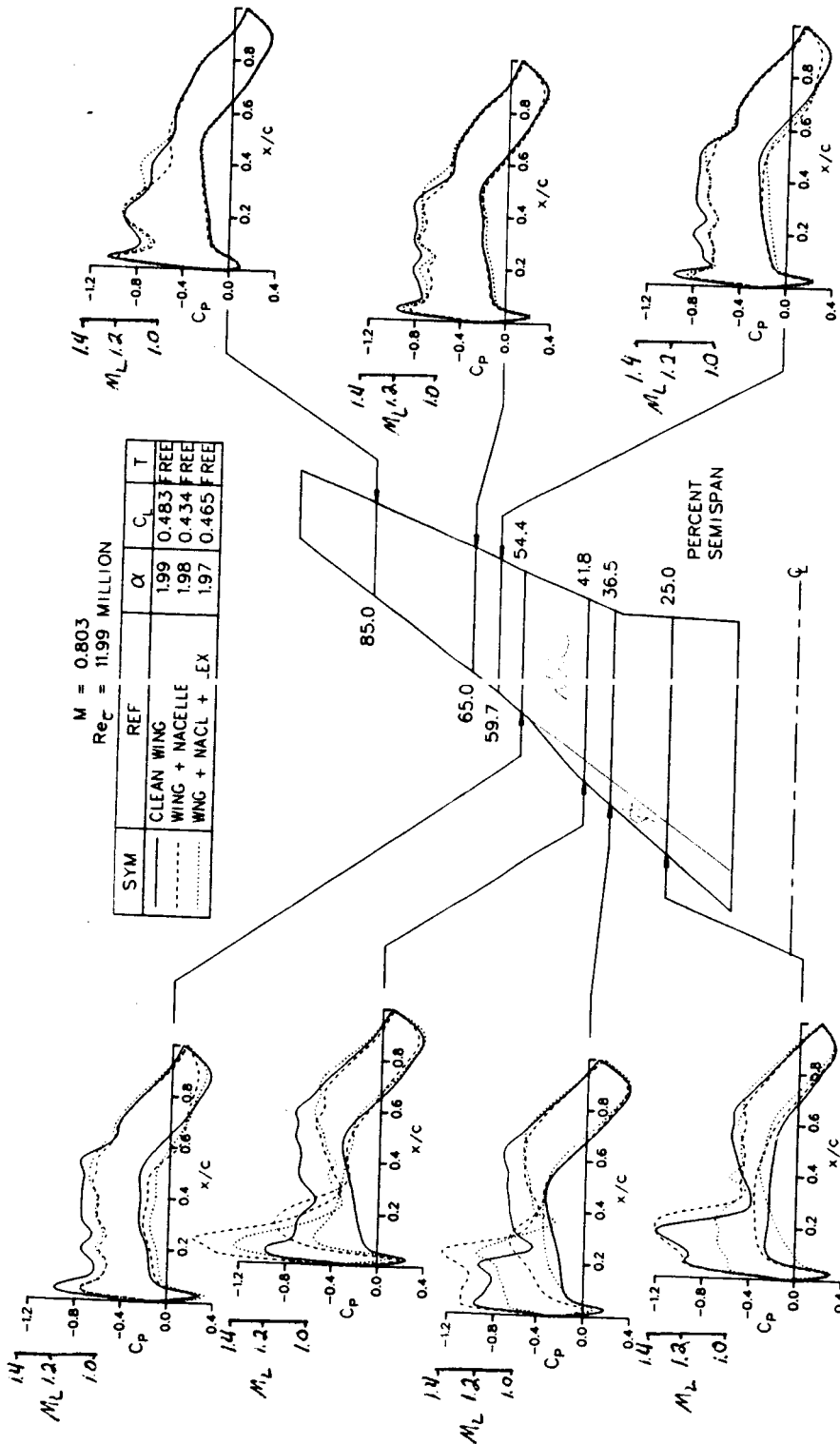


FIGURE 58. EXPERIMENTAL CHORDWISE PRESSURE DISTRIBUTIONS FOR STRAIGHT UNDERWING NACELLE WITH AND WITHOUT LEX, $M_\infty = 0.8$, $\alpha = 2$ DEGREES

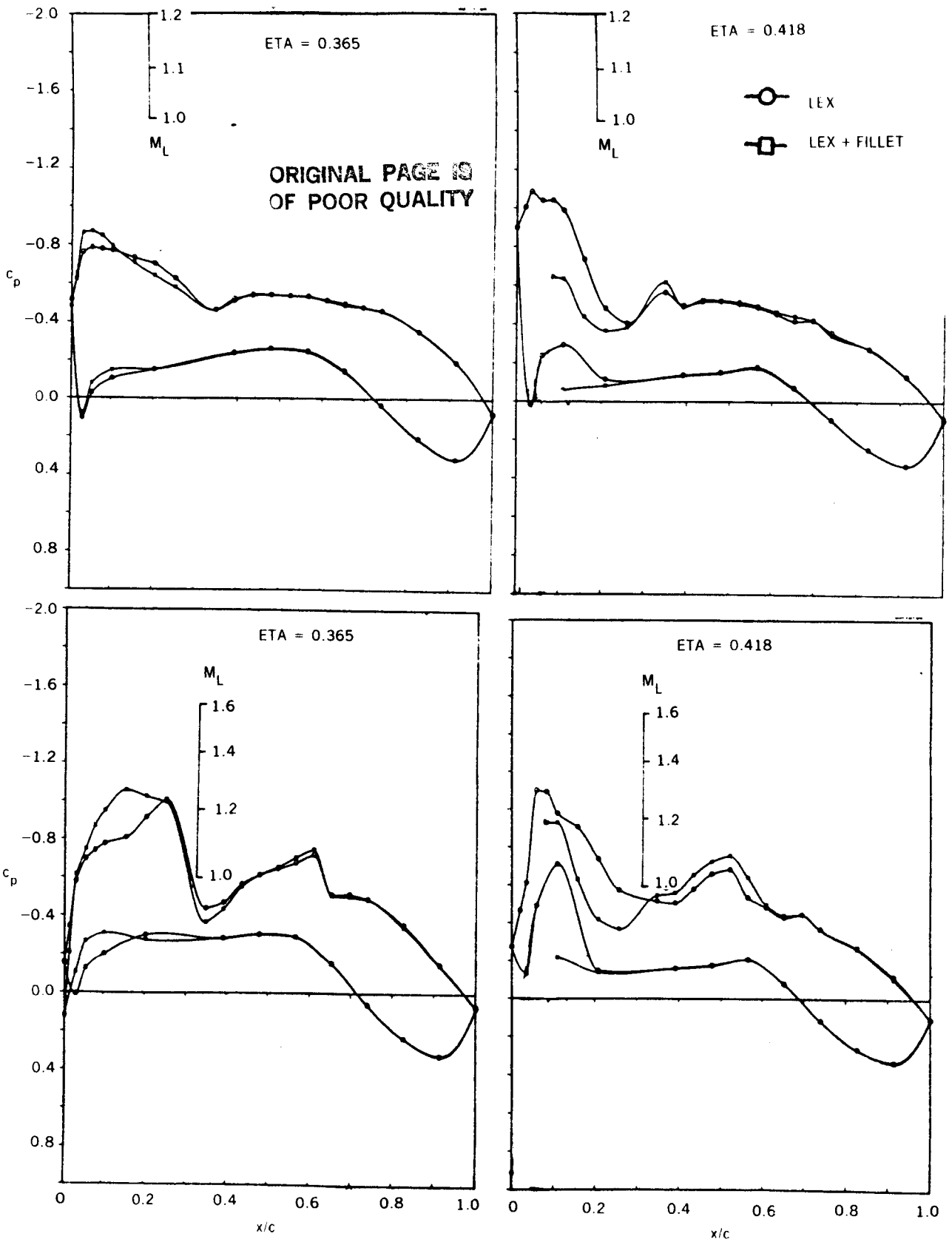


FIGURE 59. EXPERIMENTAL CHORDWISE PRESSURE DISTRIBUTIONS FOR CONTOURED OVERWING NACELLE WITH LEX AND FILLET, $M_o = 0.6$ AND 0.8 , $\alpha = 2$ DEGREES

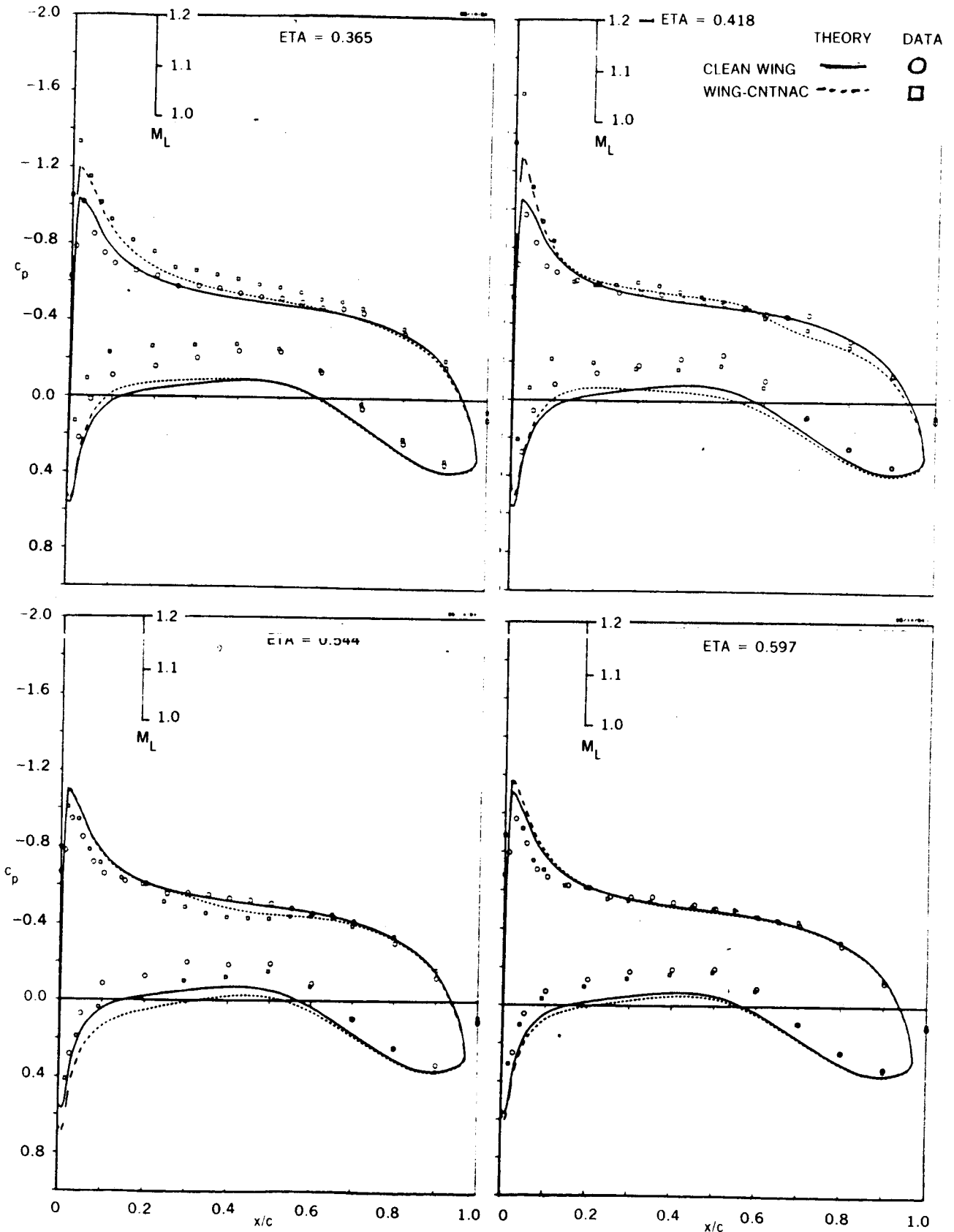
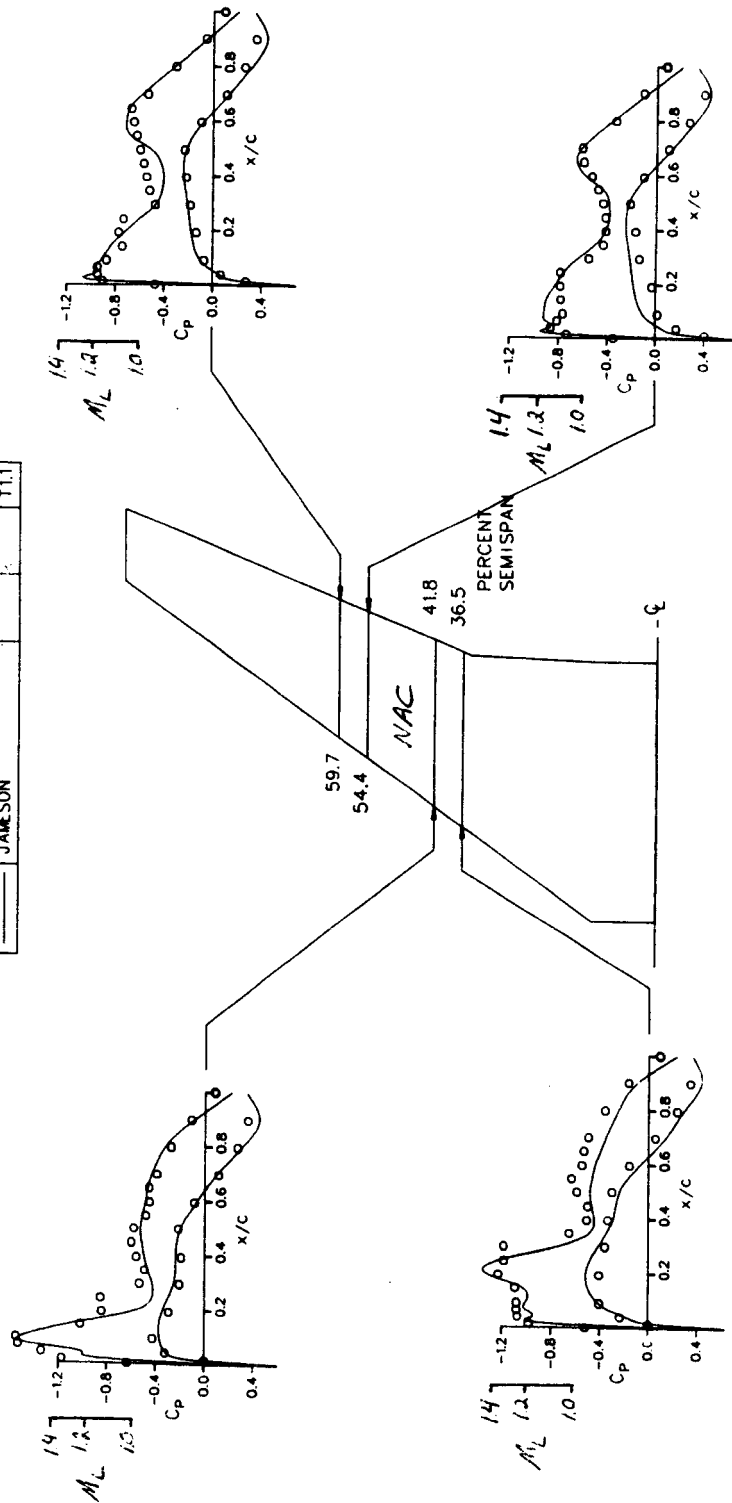


FIGURE 60. COMPARISON OF DAC-NEUMANN AND DATA FOR CONTOURED OVERWING NACELLE - NO POWER

ORIGINAL PAGE
OF POOR QUALITY

$M = 0.8$

| SYM | REF | α | C_L | T |
|-----|--------------------|----------|-------|--------------|
| o | RUN 451 JAMESON | 1.96 | | FREE T1.1 |



06/04/84

FIGURE 61. COMPARISON OF DAC-JAMESON AND DATA FOR CONTOURED OVERWING NACELLE - NO POWER

ORIGINAL PAGE IS
OF POOR QUALITY

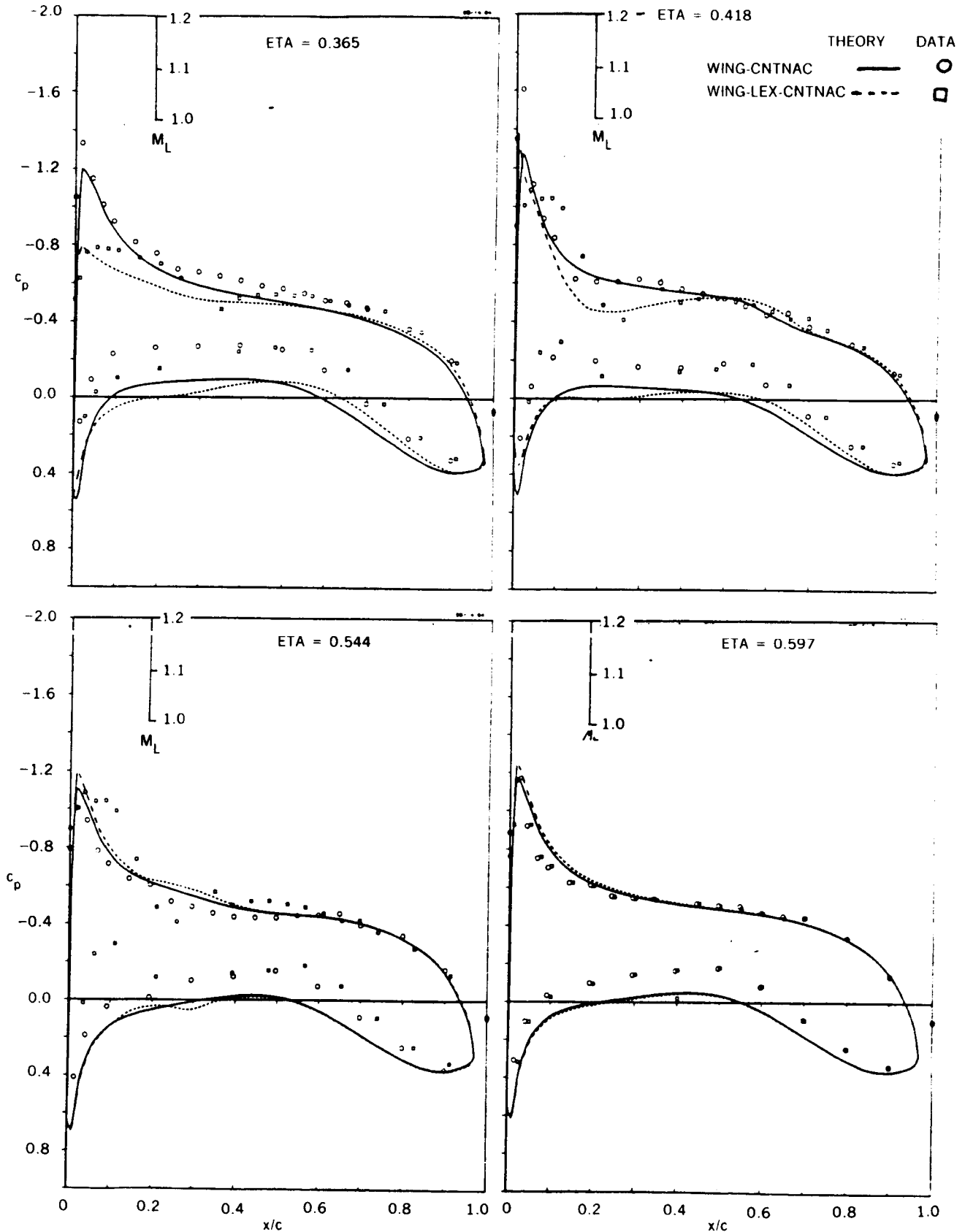


FIGURE 62. COMPARISON OF DAC-NEUMANN AND DATA FOR CONTOURED OVERWING NACELLE WITH LEX - NO POWER

ORIGINAL PAGE IS
OF POOR QUALITY

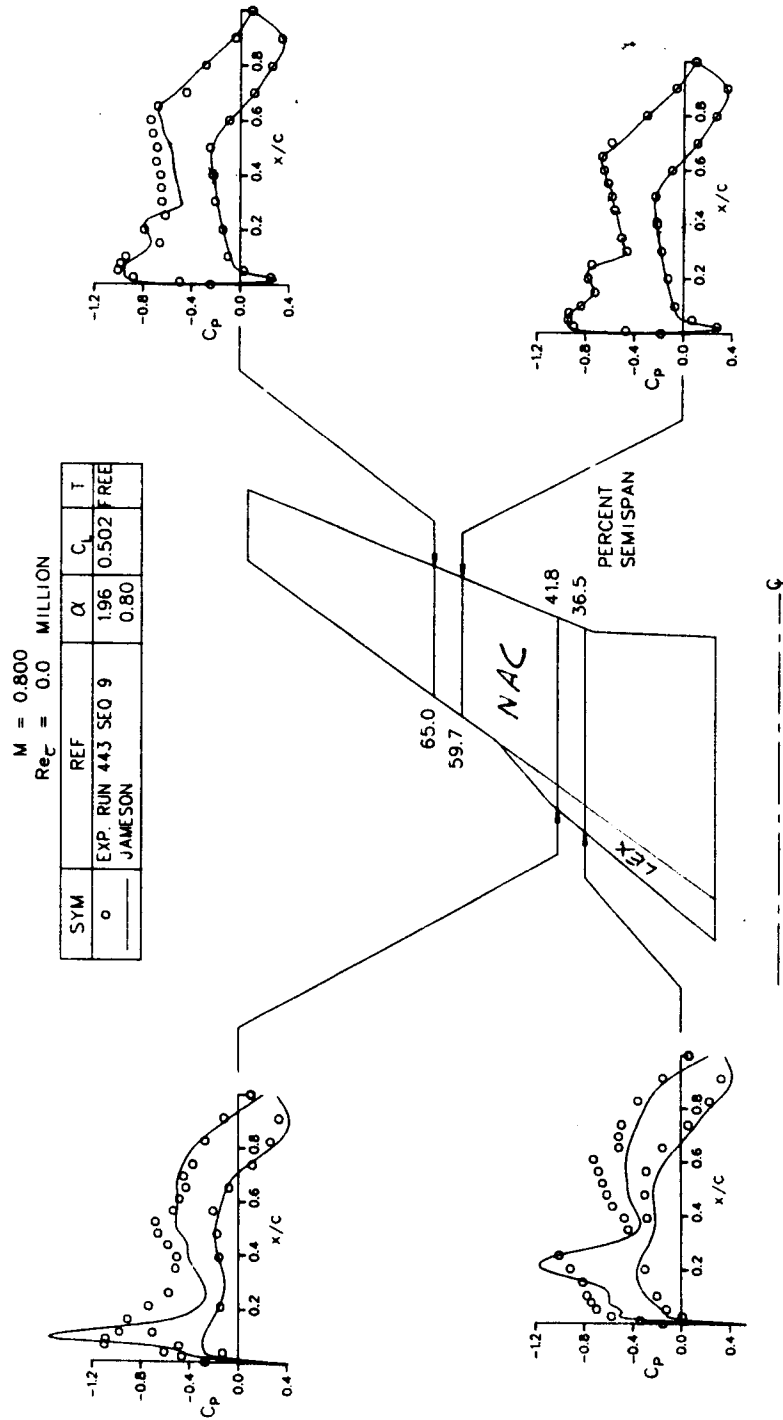


FIGURE 63. COMPARISON OF DAC-JAMESON AND DATA FOR CONTOURED OVERWING NACELLE WITH
LEX — NO POWER

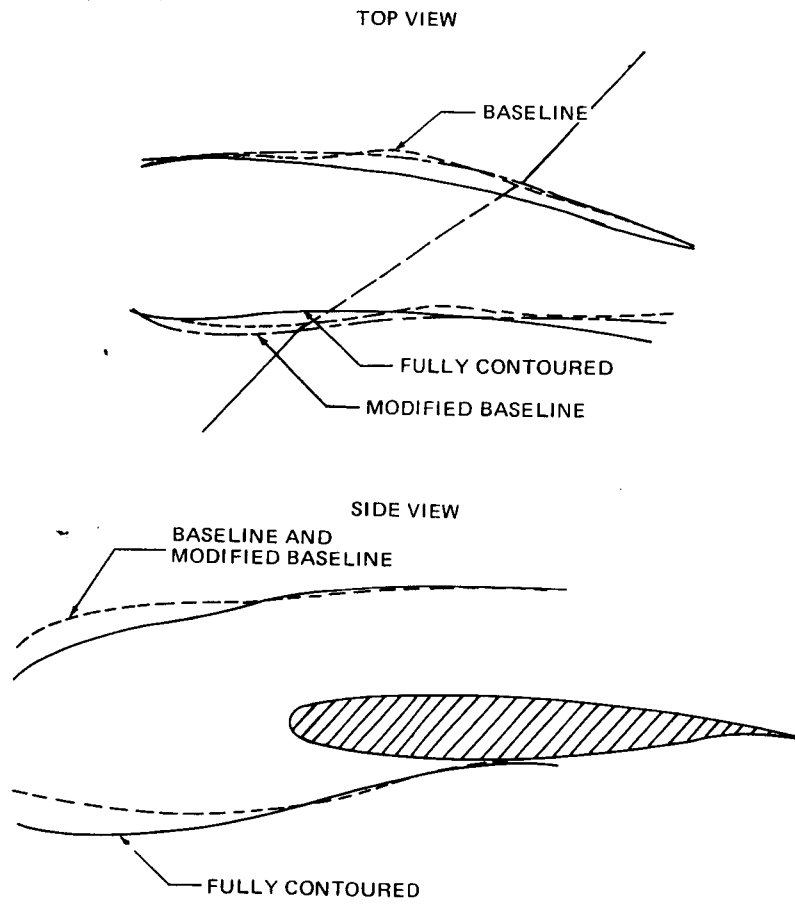


FIGURE 64. OVERWING CONTOURED NACELLE MODIFICATIONS, GEOMETRY COMPARISON

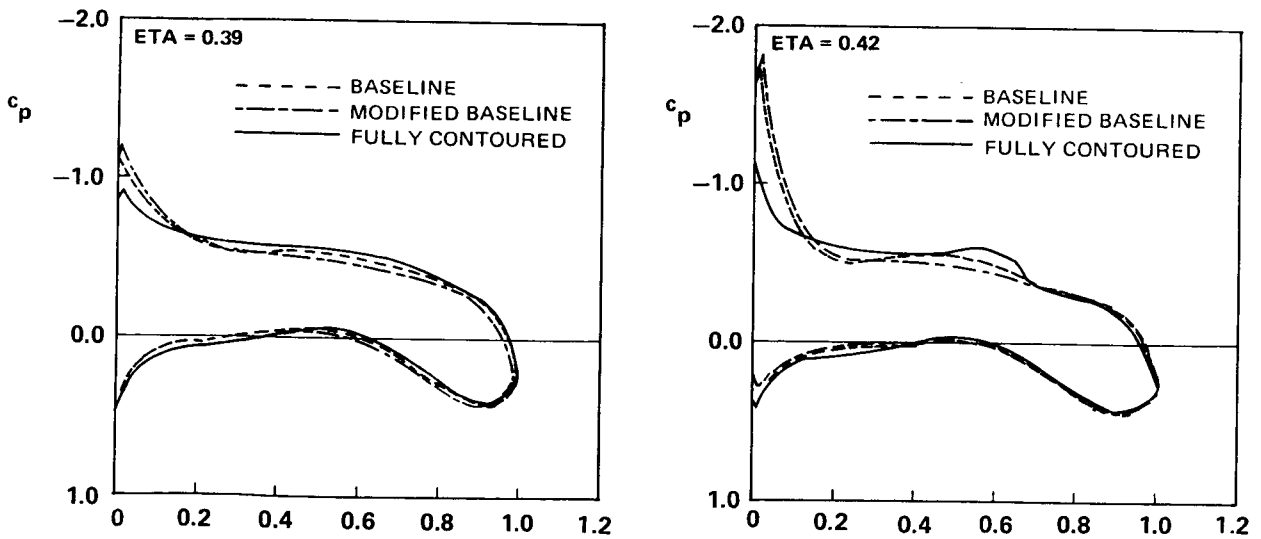
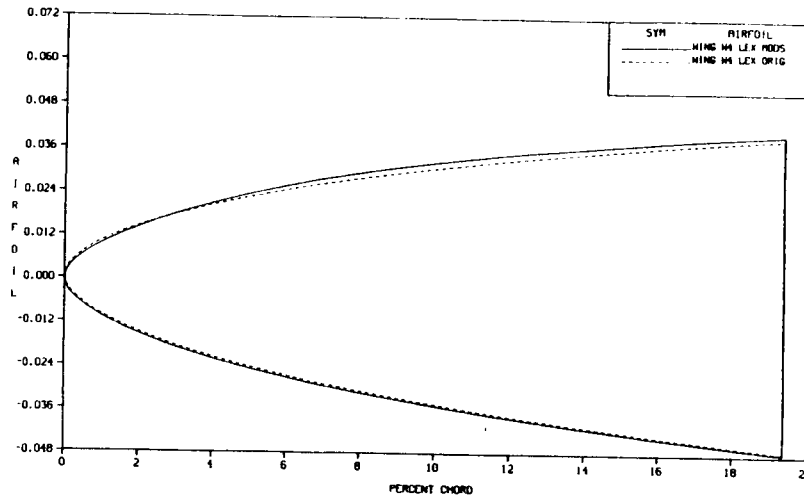


FIGURE 65. OVERWING CONTOURED NACELLE MODIFICATIONS, NEUMANN CHORDWISE PRESSURE COMPARISONS

ORIGINAL PAGE IS
OF POOR QUALITY

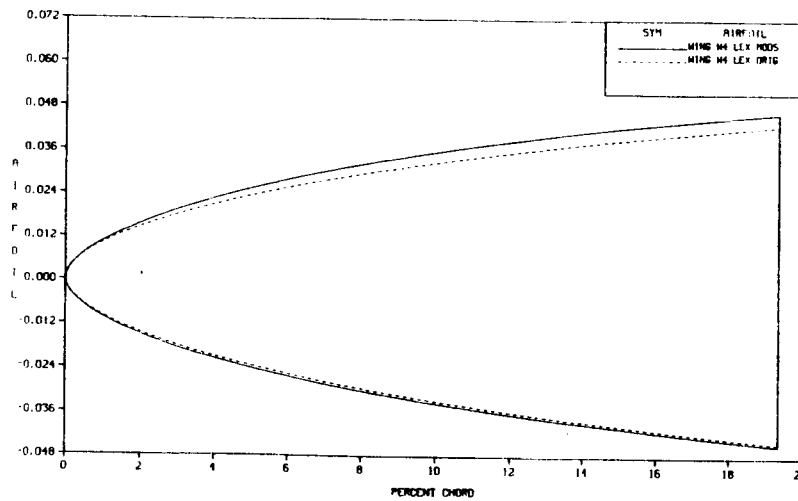
WING H4 LEX MODS ETA = .378

AIRFOIL GEOMETRY



WING H4 LEX MODS ETA = .42

AIRFOIL GEOMETRY



— MODIFIED
- - - BASELINE

FIGURE 66. OVERWING CONTOURED NACELLE LEX MODIFICATIONS, GEOMETRY COMPARISONS

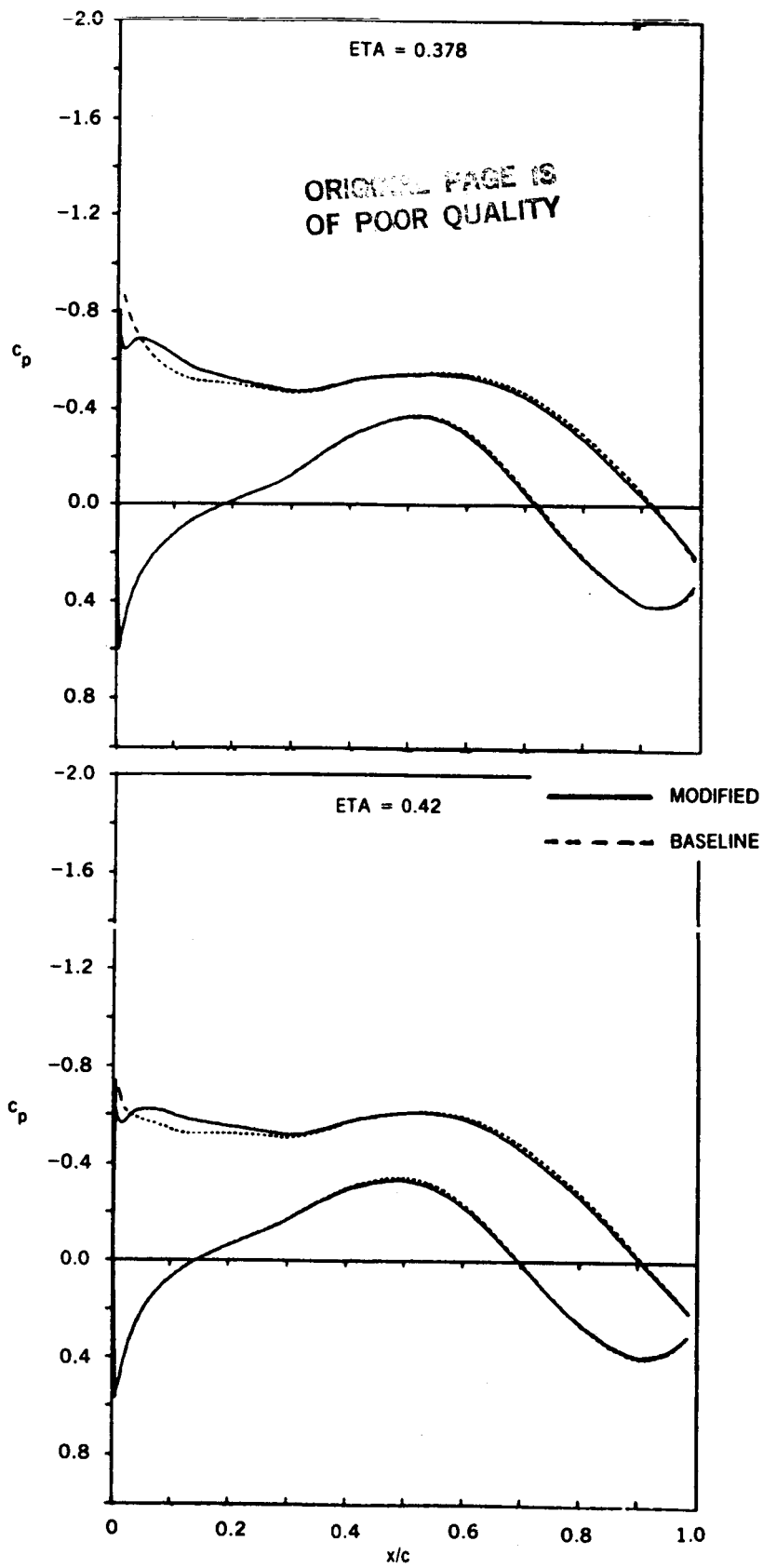


FIGURE 67. OVERWING CONTOURED NACELLE LEX MODIFICATIONS, JAMESON CHORDWISE PRESSURE COMPARISONS

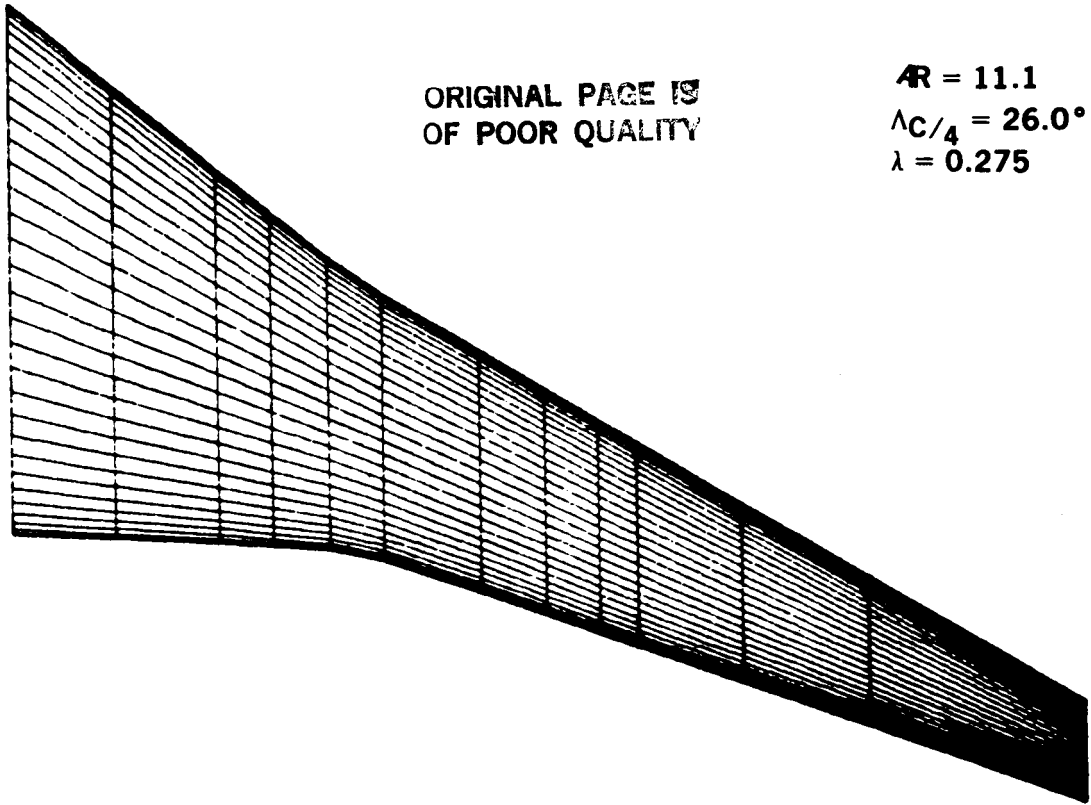


FIGURE 68. BASELINE WING W1 GEOMETRY

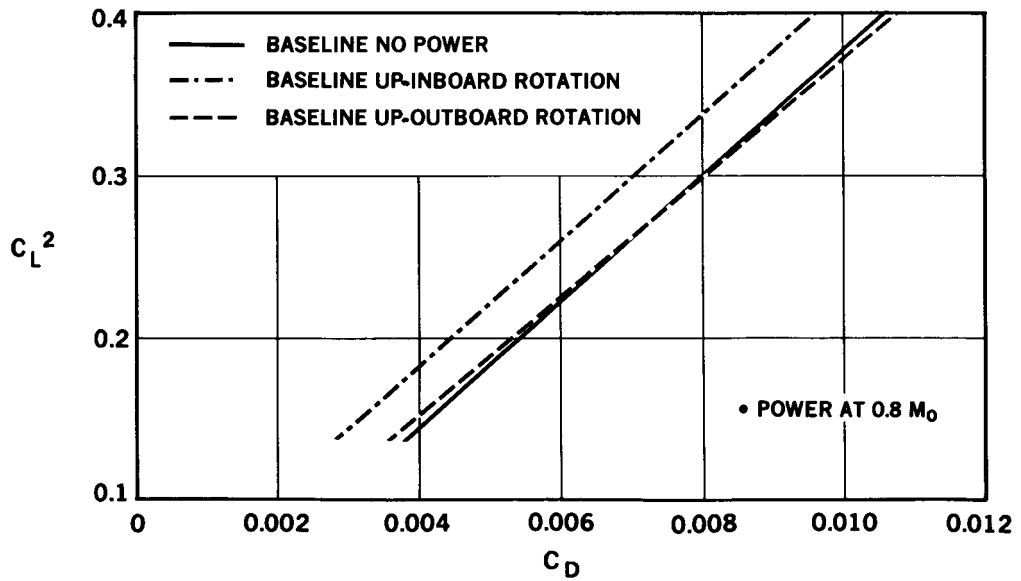


FIGURE 69. LIFTING LINE INDUCED DRAG POLARS, BASELINE WING

ORIGINAL PAGE IS
OF POOR QUALITY

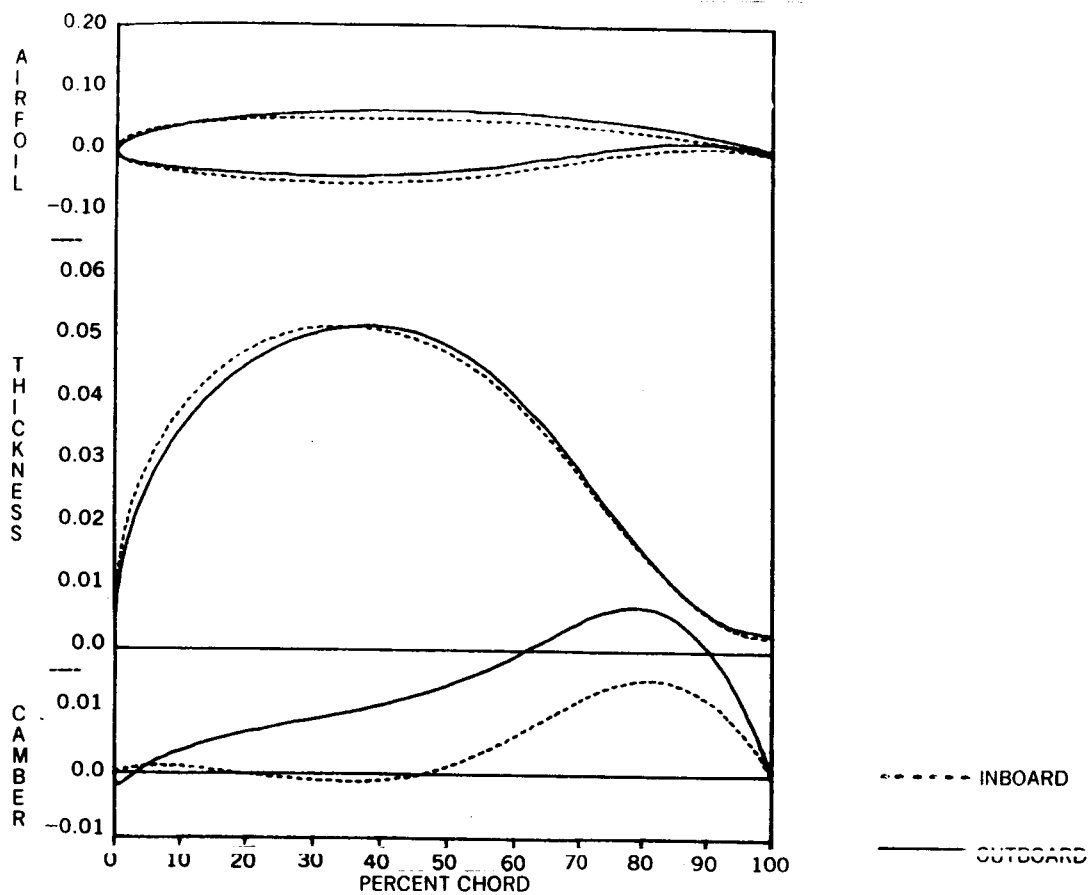


FIGURE 70. COMPARISON OF AIRFOIL GEOMETRIES FOR UP-OUTBOARD PROP ROTATION WING AT 70% PROP BLADE RADIUS

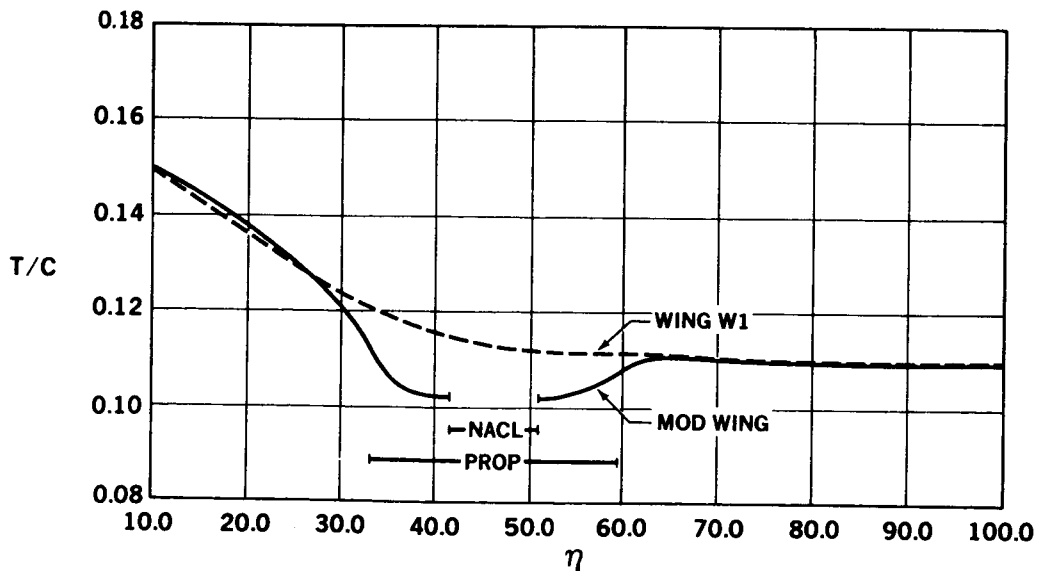


FIGURE 71. COMPARISON OF WING W1 AND MODIFIED WING THICKNESS DISTRIBUTIONS

ORIGINAL PAGE IS
OF POOR QUALITY

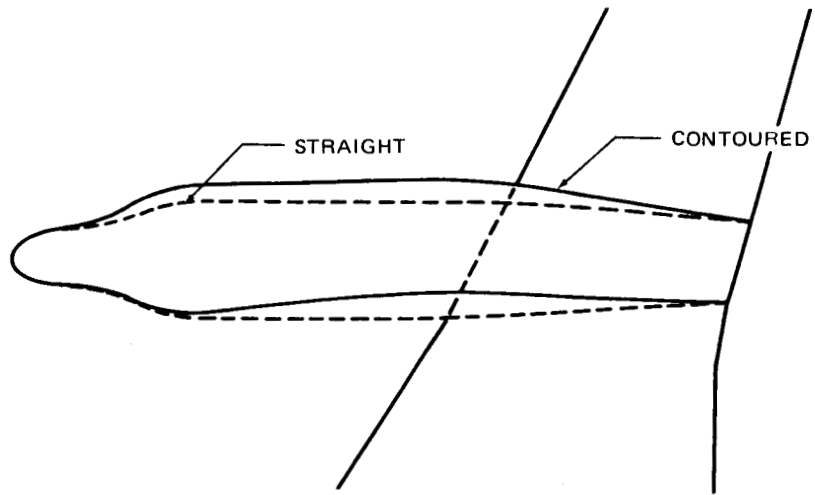


FIGURE 72. COMPARISON OF STRAIGHT AND CONTOURED OVERWING NACELLE SHAPES – TOP VIEW

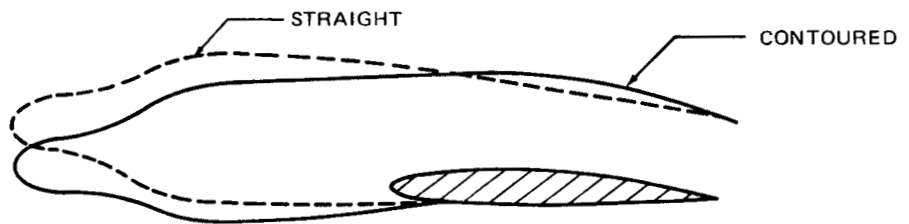


FIGURE 73. COMPARISON OF STRAIGHT AND CONTOURED OVERWING NACELLE SHAPES – SIDE VIEW

ORIGINAL PAGE IS
OF POOR QUALITY

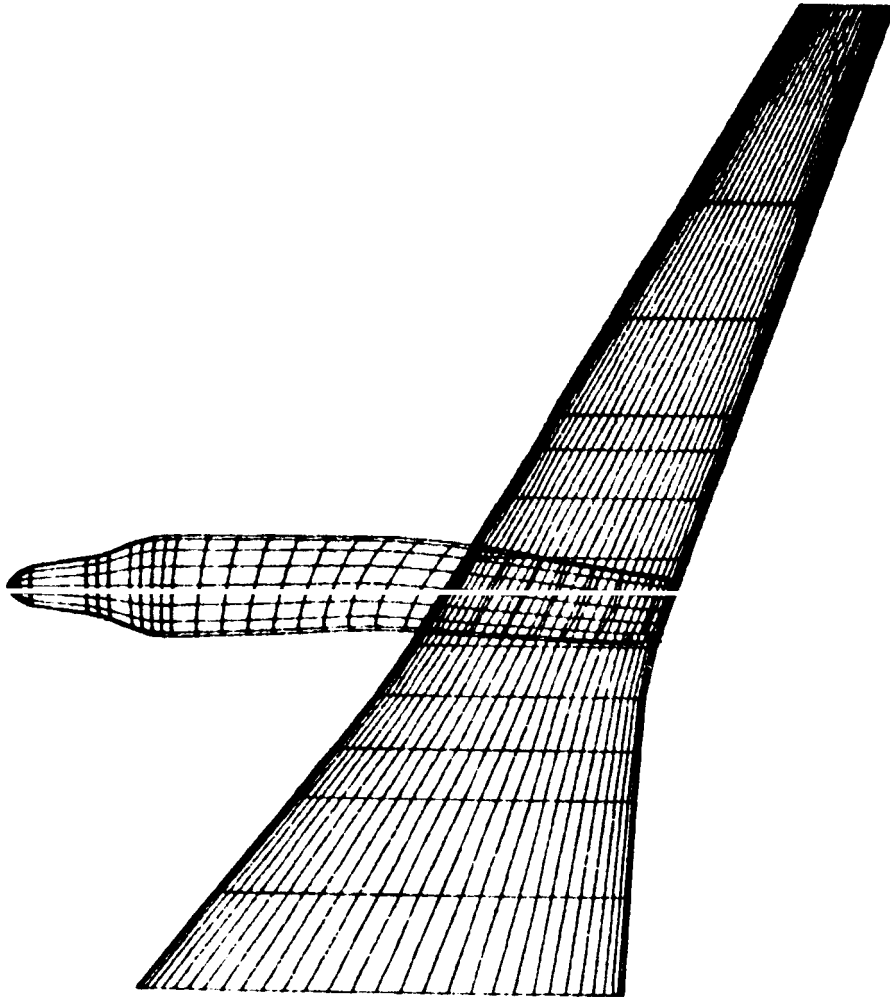


FIGURE 74. MODIFIED WING AND CONTOURED NACELLE GEOMETRY, TOP VIEW

ORIGINAL PAGE IS
OF POOR QUALITY

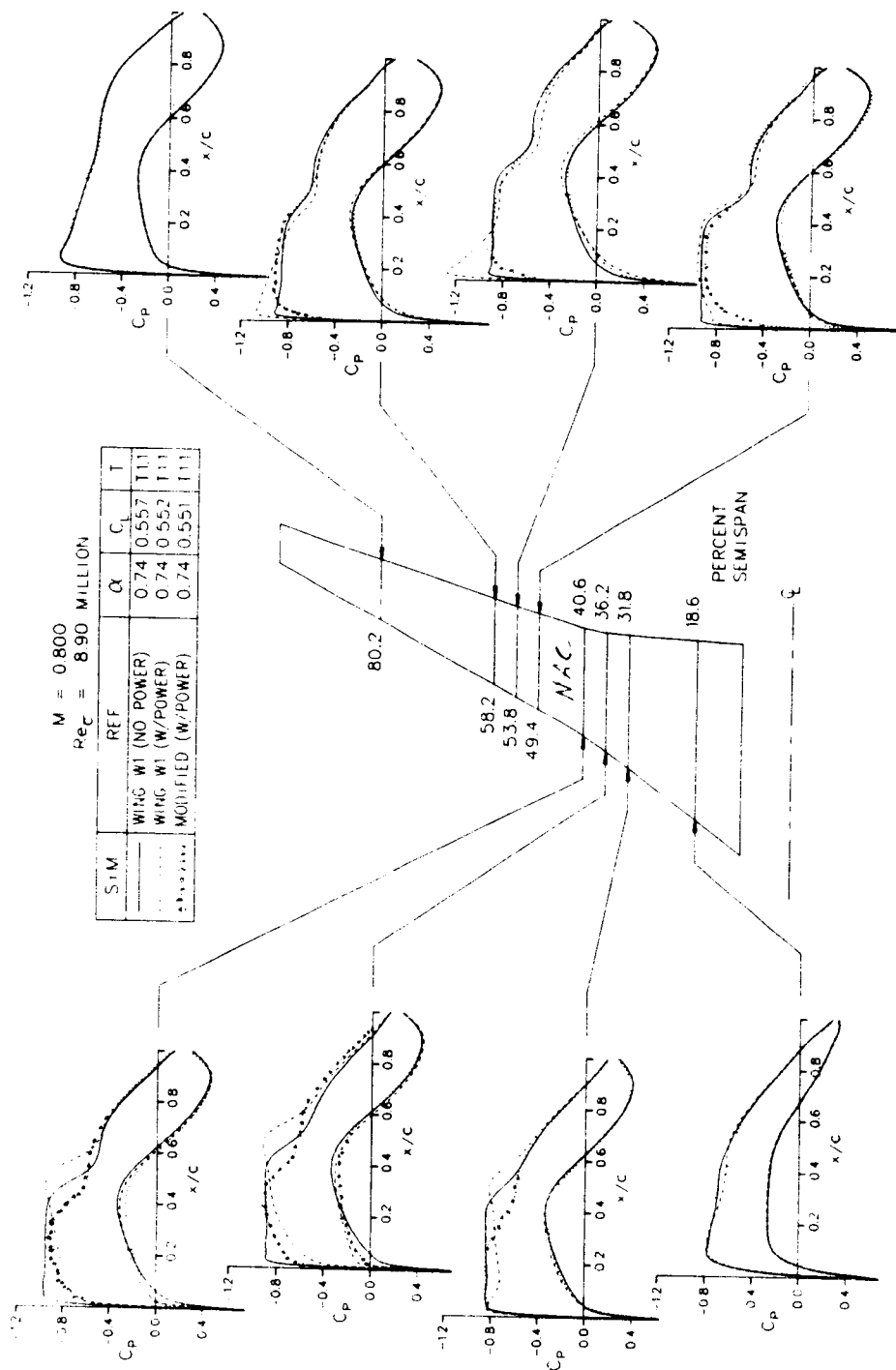


FIGURE 75. CHORDWISE PRESSURE DISTRIBUTIONS FOR MODIFIED AND BASELINE WINGS

ORIGINAL PAGE IS
OF POOR QUALITY

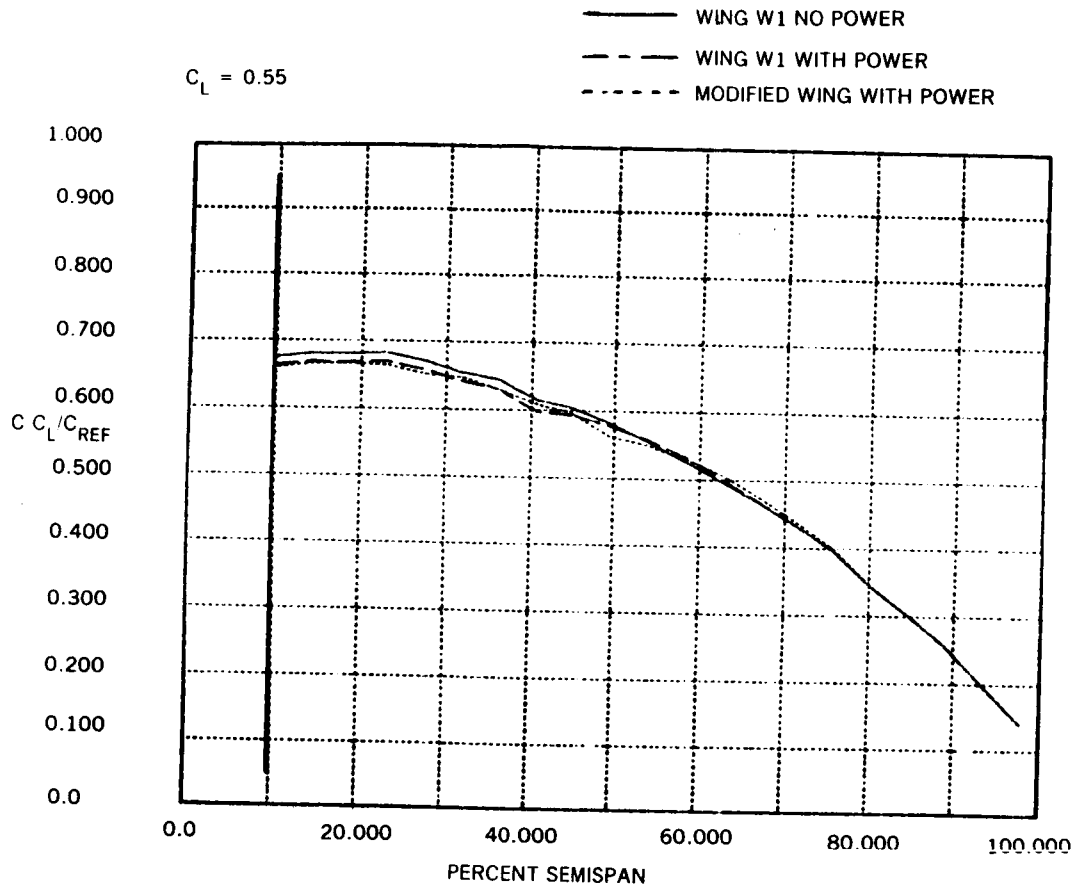


FIGURE 76. JAMESON SPAN LOADINGS FOR MODIFIED AND BASELINE WINGS

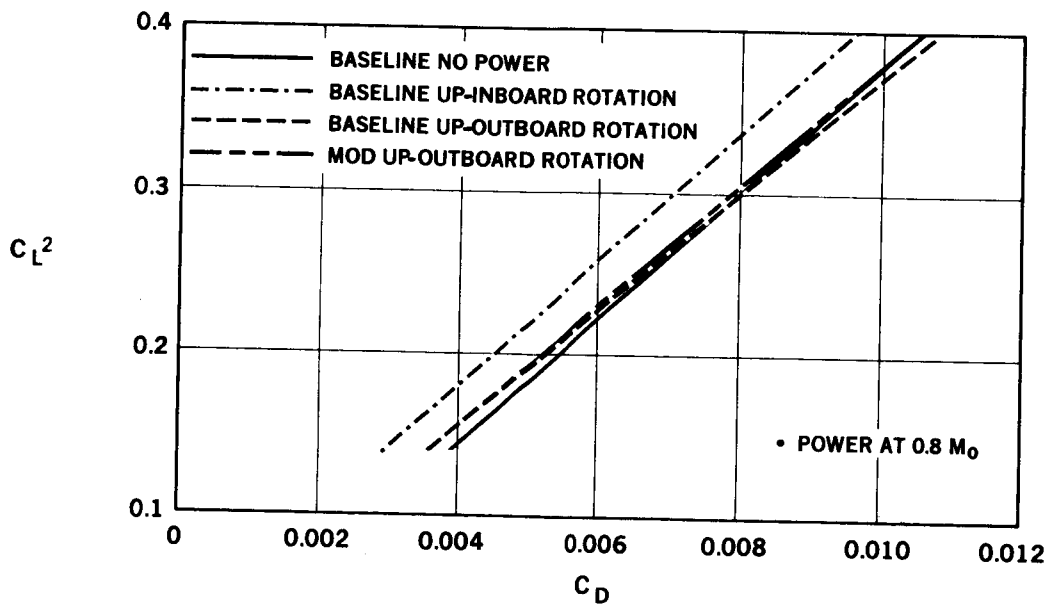


FIGURE 77. LIFTING LINE INDUCED DRAG POLARS, BASELINE AND MODIFIED WING

| | | | |
|--|--|--|----------------------------------|
| 1. Report No. NASA CR 166582 | 2. Government Accession No. | 3. Recipient's Catalog No. | |
| 4. Title and Subtitle Propfan Experimental Data Analysis | | 5. Report Date August 1984 | 6. Performing Organization Code |
| | | 8. Performing Organization Report No. ACEE-28-FR- | |
| 7. Author(s) David F. Vernon, Greg S. Page, H. Robert Welge | | 10. Work Unit No. | |
| 9. Performing Organization Name and Address Douglas Aircraft Company 3855 Lakewood Blvd. Long Beach, CA 90846 | | 11. Contract or Grant No. NAS2-11672 | |
| | | 13. Type of Report and Period Covered Contractor Report | |
| 12. Sponsoring Agency Name and Address National Aeronautics and Space Administration Ames Research Center Moffett Field, CA 94035 | | 14. Sponsoring Agency Code | |
| | | 15. Supplementary Notes Point of Contact: Alan D. Levin 227-6 Moffett Field, CA 94035 Commerical No. (415) 965-5858, FTS 448-5858 | |
| 16. Abstract A data reduction method, which is consistent with the performance prediction methods used for analysis of new aircraft designs, is defined and compared to the method currently employed by NASA using data obtained from an Ames Research Center 11-foot transonic wind tunnel test (316-3-11). Pressure and flow visualization data from The Ames test for both the powered straight underwing nacelle, and an unpowered contoured overwing nacelle installation is used to determine the flow phenomena present for a wing mounted turboprop installation. The test data is compared to analytic methods, showing the analytic methods to be suitable for design and analysis of new configurations. The data analysis indicated that designs with zero interference drag levels are achievable with proper wing and nacelle tailoring. A new overwing contoured nacelle design and a modification to the wing leading edge extension for the current wind tunnel model design are evaluated. Hardware constraints of the current model parts prevent obtaining any significant performance improvement due to a modified nacelle contouring. A new, aspect ratio 11 wing design for an up outboard rotation turboprop installation is defined, and an advanced contoured nacelle is provided. The design shows a slight drag reduction, compared to the unpowered clean wing, and maintains good pressure characteristics for the power-on case. | | | |
| 17. Key Words (Suggested by Author(s)) Transonic Design Turboprop Wing Design Propulsion Integration | | Release Date: June 1987 Star Category 05 | |
| 19. Security Classif. (of this report) Unclassified | 20. Security Classif. (of this page) Unclassified | 21. No. of Pages PAGE 126 | 22. Price INTENTIONALLY BLANK |

DOUGLAS AIRCRAFT COMPANY

3855 Lakewood Boulevard, Long Beach, California 90846 (213) 593-5511

MCDONNELL DOUGLAS



CORPORATION

PRINTED IN U.S.A. 9/84 TECH-1951